NOAA Technical Memorandum ERL NSSL-75

THUNDERSTORM-OUTFLOW KINEMATICS AND DYNAMICS

R. Craig Goff

Property of
NWC Library
University of Oklahoma

National Severe Storms Laboratory
Norman, Oklahoma
December 1975

UNITED STATES
DEPARTMENT OF COMMERCE
Rogers C.B. Morton, Secretary

NATIONAL OCEANIC AND
ATMOSPHERIC ADMINISTRATION
Robert M. White, Administrator

Environmental Research
Laboratories
Wilmot N. Hess, Director

9.302

CONTENTS

	Page
LIST OF FIGURES	iv
LIST OF TABLES	iv
ABSTRACT	v
1. INTRODUCTION AND REVIEW OF THE LITERATURE	1
2. SENSOR TOOLS	2
3. DATA PROCESSING AND OBJECTIVE ANALYSIS	2
4. THUNDERSTORM-OUTFLOW KINEMATICS	3
4.1 Grouping of Frontal Cases	3
4.2 Frontal Speed and Orientation	4
4.3 Spacing between Gust Fronts and Precipitation Onset	6
4.4 Pre-Gust Front Vertical Motion	8
4.5 Shape of the Front	9
4.6 Relationship between Wind, Potential Temperature, Wet-Bulb Potential Temperature and Pressure Discontinuities	10
4.7 Multiple Surges in Cold Air Outflow	11
4.8 Horizontal and Vertical Wind Shear	13
5. THUNDERSTORM-OUTFLOW DYNAMICS	15
6. SUMMARY AND CONCLUSIONS	17
7. ACKNOWLEDGMENTS	19
8. REFERENCES	19
APPENDIX	23

LIST OF FIGURES

Figure		Page
1	Schematic diagram of thunderstorm outflow.	9

LIST OF TABLES

Table		Page
1	General quantitative information about outflow cases.	5
2	Comparison of true frontal speed to computed speeds using various formulae.	7
3	Relationship between pressure (mb), potential temperature (°C) and wind (m s^{-1}) discontinuities and rainfall onset.	12
4a	Maximum absolute shear for 13 cases.	14
4b	Average maximum absolute shear for 13 cases.	14

ABSTRACT

Tall tower and conventional radar sensors at the National Severe Storms Laboratory detected twenty cases of cold air outflow from thunderstorms during 1971 through 1974. Tower data have resolved many small details of thunderstorm outflow not previously observed.

The data were objectively analyzed, each case plotted in 10 min, 450 m deep time-height sections and the cases arranged in an evolutionary sequence based on outflow and storm intensity criteria. Four stages of cold air outflow were established and variations in outflow character were discussed in terms of these stages. Most outflow observations were associated with solid or broken squall lines; two parent thunderstorms were of the supercell type and two others were left-moving cells following a thunderstorm split.

The data show that strong updrafts precede the leading edge of the outflow (the gust front). The gust front is a zone of sharp contrasts in wind, temperature, pressure, and moisture.

Gust fronts often move far ahead of associated precipitation. Secondary cold air surges are observed in about half the cases, confirming earlier observations of mature thunderstorm pulsation. Gust front shape, pre-gust front vertical motion and strength of frontal discontinuities appear to be functions of storm age.

For most of the outflow life history, a near balance is apparent between pressure gradient forces and drag forces but toward the end of the life cycle, Coriolis forces may be significant.

THUNDERSTORM-OUTFLOW KINEMATICS AND DYNAMICS

R. Craig Goff

1. INTRODUCTION AND REVIEW OF THE LITERATURE

Cold air outflow, produced by dry mid-tropospheric entrainment and subsidence resulting from negative buoyancy, is an important aspect of developing or well-developed thunderstorms. Some of this high-density air is left in a shallow layer near the earth's surface in the thunderstorm wake, but much is diverted to the front of the advancing storm due to conservation of horizontal momentum (Byers and Braham, 1949). Byers and Braham term this outflow the "cold-air dome". It also fits the general term "gravity current" (Charba, 1974). One might expect few differences in the leading edge of thunderstorm outflow, cold fronts, or seabreeze fronts. However, there appear to be important differences between each of these in terms of scale, life cycle and forcing mechanisms.

Several authors have described the two-dimensional (x,z) gross features of thunderstorm gust fronts (Charba, 1974; Ragette, 1973; Colmer, 1971; Byers and Braham, 1949), haboobs (Lawson, 1971; Idso, et al., 1972), cold fronts (Browning, 1971; Browning and Harold, 1970; Clarke, 1961; Berson, 1958; and Prandtl, 1952) and seabreeze fronts (Clarke, 1961 and Wallington, 1959). Most of these have been case studies of individual events.

There have been a number of laboratory studies of interest. Simpson (1972, 1969), Middleton (1966) and Keulegan (1958, 1957) developed laboratory gravity current models using liquids. Middleton and Keulegan concentrated on the hydraulic engineering aspects of gravity current flow and dealt with dynamical similarity problems. Keulegan first recognized the general shape and individuality of gravity current fronts and Simpson described the small features of the nose and head. Simpson (1969) relates his laboratory models to atmospheric prototypes and determines effects of the surface boundary layer on shape of leading edge substructure (Simpson, 1972).

Frontal theory was not developed much beyond ideal fluid flow until a few years ago. Ball (1960) and Eliassen (1959) show that surface friction acts on baroclinic motions to change a diffuse frontal zone into a sharp discontinuity in the planetary boundary layer. Daly and Pracht (1968) successfully modelled incompressible non-turbulent fluids for application to density current flow in channel locks and dam breaks. Recently, hydrostatic, quasi-steady, viscous models of cold fronts have been developed by Rao (1971) and Williams (1974). A non-hydrostatic fine-resolution model for thunderstorm outflow using the primitive equations has been developed by Mitchell (1975). Mitchell's model includes surface friction by employing a bulk aerodynamic drag term. The cold front models use a relatively coarse grid in the horizontal, while comparison of these two models show distinctly different characteristics (e.g., flow patterns, slope of front and intensity) between cold fronts and thunderstorm outflow.

Data from 20 thunderstorm-outflow cases have been gathered for this study. The paper has several objectives. First, the general kinematical outflow characteristics are established showing how the outflow develops then dissipates. Small details of the outflow leading edge are included in the investigation. The main data source, a tall meteorological tower in Oklahoma, is equipped with both horizontal and vertical velocity sensors. Direct sensing of vertical motion through a deep layer near the ground has not previously been reported, and it is a principle objective to discuss this important parameter's behavior. Lastly, a qualitative dynamical interpretation of the analysis will be undertaken. Kinematical results provide implicit information about forcing mechanisms. The kinematics and dynamics will be discussed in terms of outflow evolution stages.

2. SENSOR TOOLS

Data were obtained from two sources: the WKY-TV/NSSL 481 m meteorological tower and the NSSL WSR-57 conventional 10 cm radar with signal integration and range normalization.

The tall tower was equipped at seven levels (in 1971 and 1972) with horizontal wind and temperature sensors and at three levels with vertical wind and wet-bulb sensors.[1] Rainfall and pressure sensors were located at the surface. In 1973 and 1974 the tower was operated with wind, temperature, and moisture sensors at only three levels. Carter (1970) and Goff and Zittel (1974) provide additional information about tower equipment and its operation.

Radar data is available on film at two frames per minute. Signal integration provides echo intensity contours depicted by light and dark shading on radar film (see Appendix). Echo intensity values (dBz) for different shading vary slightly through the period. Range marks are at 20 n mi intervals in 1971-1973, and at 40 km intervals in 1974. Times are Central Standard Time. The PPI is range normalized by sensitivity time control (STC). Wilk and Kessler (1970) provide additional details on the radar sensor.

3. DATA PROCESSING AND OBJECTIVE ANALYSIS

Digital tower data, recorded at 10-second intervals on magnetic tape, were used for objective analysis schemes. Routine quality control procedures were run in advance. Sensors were not evenly spaced on the tower and to simplify programming for objective analyses, the data were fit to a regular array (z,t) for time-height and streamline analyses. For the z-direction, values at ten evenly spaced grid points (50 m intervals) were determined by linear interpolation and extrapolation from the seven levels of horizontal wind and temperature and three levels of wet-bulb temperature (1972 data) and vertical velocity (1971 and 1972 data). For 1973 and 1974 data, values at ten evenly spaced grid points were determined from only three levels of wind and temperature. Loss of fidelity in the objective analysis is expected in the later two years.

---

[1] There was no reliable moisture data in 1971.

For each tower cross section (see Appendix), 10 min of data is used. Thus, each section is a plot of a (60, 10) array. A time-to-space conversion (Galilean transformation) is used in which time derivatives are changed to space derivatives by $\partial/\partial t = c\partial/\partial x$, where c is gust front speed. Distortion in horizontal space with respect to the vertical is reduced by proper x-spacing after the time-to-space conversion. Distortion is a function of the speed of features as they pass the tower. The ratio of x:z varies from 1:3.3 to 1:0.8 and averages about 1:2.

A right-handed natural coordinate system was used where positive x points in the direction of frontal motion and y is parallel to the frontal axis. The axes represent the u and v wind components, respectively; u-component values are relative to the front.

Before plotting time-height sections, each array was filtered with three passes of a simple Shuman filter (see Haltiner, 1971, p. 270). This filter, with a cutoff at $2\Delta t$ and a response of 81% at $12\Delta t$ (=2 min), smooths unwanted high wave-number fluctuations and makes the data from instruments of differing response times more compatible.

4. THUNDERSTORM-OUTFLOW KINEMATICS

4.1 Grouping of Frontal Cases

Gust front cases were grouped as follows (number of cases in parentheses):

I. Gust fronts associated with intensifying storms or accelerating outflow (4).

II. Gust fronts associated with mature intense storms or strong outflow (8).

III. Gust fronts associated with dissipating storms or outflow decelerating with respect to the storm (4).

IV. Gust fronts in the final stage of life cycle (4).[2]

The 20 cases represent most events that occured during the two to three month annual observation period of the National Severe Storms Laboratory (NSSL). A few cases were excluded because radar and/or tower data were lacking. The groups have a statistically small sample size therefore, generalizations may require some later refinement.

Each of the 20 gust front cases was assigned to the gust front evolution-intensity categories based on storm age and storm gust front intensity criteria determined from tower and radar data. Outflow intensity criteria were more

---

[2]These four types roughly correspond to the mature and dissipating thunderstorm stages of Byers and Braham (1949); Types I and II to the mature stage and Types III and IV to the dissipation stage.

heavily weighted than frontal "age" when arranging cases. It was difficult to fit some cases into the life-cycle scheme when there were two or more outflow surges in advance of a thunderstorm (see Ward and Arnett, 1962). In these cases the oldest outflow surge often weakens and dissipates after moving far ahead of the storm's leading edge. Such dissipation sometimes occurs even though the parent storm remains intense.

4.2 Frontal Speed and Orientation

Speed and orientation of each front must be determined with some accuracy because objective analyses (such as the streamline analysis) are quite sensitive to these factors. Speed and orientation were determined from radar film. Two problems were encountered. First, the leading edge of thunderstorm outflow is often associated with dry convection (if far in advance of the main echo) and is sometimes not sensed by radar. Fortunately, there were data without intensity range normalization (STC). Such data make the radar sensitive enough at close range to detect the leading edge of outflow as a thin or fine line (Ligda and Bigler, 1958). When data without STC were not available when needed, the accuracy of frontal speed and orientation was reduced. Such cases will be identified. Second, in some storm types, speed and orientation of the outflow's leading edge were not conserved during the computation period. These cases, few in number, will be appropriately identified.

Radar diagrams and time-height sections are presented in the Appendix. Each case is given a letter designation (A through T) based on the life-cycle arrangement described in Section 4.1. The Appendix gives additional pertinent storm information. Some quantitative data is summarized in Table 1.

There appears to be a relationship between frontal speed and gust front maturity according to Table 1. Fronts associated with intensifying storms and accelerating outflow (Type I) tend to move slowly whereas systems nearing final dissipation (Type IV) tend to move more rapidly (however, with respect to the parent storm the outflow is moving more slowly). There are certain exceptions (e.g., Case D).

The frontal axis orientation in Table 1 refers to the azimuthal direction of the storm's (cell or squall line) left flank with respect to the cold air outflow.[3] Orientation shows no relation to storm evolution, except that Oklahoma thunderstorm gust fronts are generally oriented northeast to southwest or north to south. Exceptions are left moving storms (storms moving to the left of the mean tropospheric flow) whose leading edges are usually oriented west to east (Cases F and R).

Several authors have attempted to determine an expression for frontal speed using mean wind values ahead of and behind the front. Prandtl (1952) used the relationship

$$c_1 = \frac{1}{2}(u_1 + u_2) \tag{1}$$

[3]For example, if the front axis orientation was east-west and the outflow was moving south, the orientation would be 90°.

TABLE 1: General quantitative information about outflow cases.

Date	Case	Speed ($m\ s^{-1}$)	Orient. (°)	A Time of Frontal Passage	B Time of Onset of Precip.	Δt (min) B-A	Δx (km) $\Delta x = c\Delta t$ $\Delta t = t_B - t_A$	Smoothed 444 m max w ($m\ s^{-1}$)	Type of Front
14 May 74	A	6.1	67	0448	None	----	----	4.6	I
2 Jul 72	B	5.0	70	1318	1324	5.6	1.7	5.0	I
6 May 72	C	8.6	50	1734	1801	26.6	13.8	4.6	I
27 May 72	D	11.6	30	1503	1510	6.2	7.2	5.8	I
31 May 71	E	16.7	17	1927	1940	12.8	12.8	6.3	II
27 Jun 72	F	11.0	290	1936	1940	3.9	2.5	6.7	II Left Moving
7 Jun 71	G	11.8	50	1945	2009	24.3	17.2	5.1	II
23 May 74A	H	8.5	70	1716	None	----	----	6.3	II
16 Jun 73	I	11.5	22	1509	1515	6.5	4.5	5.3	II
10 Jun 71	J	13.1	5	2209	2249	39.6	31.1	6.3	II
2 Jun 71	K	12.4	70	2121	2126	5.3	4.1	3.5	II
4 Jun 73	L	5.5	60	1803	1834	31.7	10.5	4.0	II
14 Jun 72	M	9.6	0	0215	0217	1.5	0.9	5.9	III
12 Jun 71	N	8.0	0	0113	None	----	----	3.8	III
23 May 72	O	11.4	50	0440	None	----	----	3.8	III
12 May 72	P	6.9	10	0024	0030	5.7	2.4	3.5	III
23 May 74B	Q	17.5	50	1844	1836	*	*	2.5	IV
19 Apr 72	R	25.0	290	1656	None	----	----	2.6	IV Left Moving
26 May 71	S	11.0	120	1906	1942	36.1	23.8	3.9	IV
21 Apr 72	T	19.9	5	0034	0033	*	*	1.0	IV

*Precipitation onset precedes the gust front.

where u_1 and u_2 refer to velocity components in the cold and warm air, respectively. Clarke (1961) found that Prandtl's expression underestimated the frontal speed (u_2 is negative, usually) for cold fronts in Australia. Clarke's results were substantiated for Oklahoma thunderstorms gust fronts (Table 2). We find a more adequate expression for thunderstorm gust fronts is

$$c_2 = 0.7u_1 + 0.3u_2 , \tag{2}$$

where the warm air influence is small compared to the cold air influence. This appears logical since the warm air is typically pushed up over the cold air outflow. Table 2 shows the resultant error by comparing speeds determined from (2) to actual speeds (tower layer smoothed maxima). Only the first three frontal types were included in the table; however, Case Q was included from Type IV. Most Type IV fronts appear to propagate by some other mechanism in addition to mechanical forcing.[4] The average error for the 17 analysis cases is only -0.30 m s^{-1}. There is a tendency for (2) to overestimate speed when the front is in early stages and to underestimate speed when the front is dissipating.

Clarke's conclusion that u_1 adequately predicted frontal speed was also supported here since the magnitude of the second term in (2) was much smaller than the first. The expression

$$c_3 = 0.67u_1 \tag{3}$$

predicts the frontal speed with 0.26 m s^{-1} average error. Table 2 gives individual error values for c_3. Mean error and error variance is similar for both (2) and (3). The average actual speed for front Types I-III (including Case Q from Type IV) is 10.42 m s^{-1}. Values computed by (1) deviate most from observed values when lower-level wind speeds are used.

4.3 Spacing Between Gust Fronts and Precipitation Onset

Two columns in Table 1 pertain to spacing between gust fronts and the leading edge of measureable precipitation. Both were determined from digital tower data. Δt in Table 1 refers to time in minutes between frontal passage and precipitation onset and Δx is the time-to-space converted distance (km) between the features. During all but the mature stage of thunderstorm life cycle, the gust front passage is either dry or the onset of precipitation is almost coincident with the gust front passage. Exceptions are Cases C and S. For Case C, which is 30 to 40 min old but intensifying, the gust front has moved far ahead of the precipitation. This agrees with Byers and Braham (1949) who found the discontinuity could travel 10 to 12 km from the cell center in 15 to 20 min.

Greatest spacing between the wind shift and precipitation occurs for mature storms. These results confirm those of Ragette (1973) for Alberta

---

[4]The Byers and Braham (1949) phenomenon of frontal progression by downward transported thrusts was not observed in Cases R and S but may be a factor in Case T.

TABLE 2: Comparison of true frontal speed to computed speeds using various formulae.

Date	Case Designation	Front Speed (m s^{-1})	Error (m s^{-1}) $c_1 = 0.5u_1 + 0.5u_2$	Error (m s^{-1}) $c_2 = 0.7u_1 + 0.3u_2$	Error (m s^{-1}) $c_3 = 0.67u_2$
14 May 74	A	6.1	-1.7	-1.3	-0.4
2 July 72	B	5.0	-2.2	0.6	1.6
6 May 72	C	8.6	-1.6	1.1	0.6
27 May 72	D	11.6	-4.7	0.1	0
31 May 71	E	16.7	-3.4	2.3	1.6
27 Jun 72	F	11.0	-4.6	-0.4	0.2
7 Jun 71	G	11.8	-4.3	3.5	4.7
23 May 74A	H	8.5	-6.4	-2.8	-1.2
16 Jun 73	I	11.5	-2.6	1.9	2.0
10 Jun 71	J	13.1	-4.4	-1.4	-1.1
2 Jun 71	K	12.4	-6.4	-2.3	-1.4
4 Jun 73	L	5.5	-4.9	-1.5	0.6
14 Jun 72	M	9.6	-3.1	-0.1	-0.3
12 Jun 71	N	8.0	-3.5	0	-0.2
23 May 72	O	11.4	-6.6	-1.8	-1.1
12 May 72	Q	6.9	-3.9	-1.5	-0.8
23 May 74B	P	17.5	-6.2	-1.7	-2.3
Average		10.42	-4.15	-0.30	0.26

hailstorms, but generally disagree with findings of Colmer (1971), who believed greatest spacing occurred with decaying storms. The two features have the greatest separation in Case J (31.1 km). Several other cases indicate separation in excess of 10 km. Barclay and Wilk (1970) observed that rain began up to 54 min after the windshift in two apparently mature squall line cases. Variability observed from case to case for similar types may be due to inherent outflow differences between continuous squall lines and single cells.

In Case Q the precipitation occurred 8 min ahead of the gust front. A similar case was observed by Ragette who postulated that such a sequence implied the formative stage of the gust front. However, in this case it is more likely that the gust front has been overrun by precipitation. Gust front movement was retarded by the low-level outflow cold air and capping inversion left behind by the Case H storm. In this respect Case Q resembles Case T and was considered to be in the final stage of evolution.

4.4 Pre-gust Front Vertical Motion

A common feature of all gust fronts is the updraft observed just ahead of and extending slightly behind the cold air outflow (Fig. 1). Vertical motion (w) is, of course, attributed to the lifting of warm (less dense) air over the frontal boundary.

Updraft concentrations ($w \geq 1$ m s^{-1}) occur in a thin band (1 to 1.5 km in width) along the gust front. Maximum updrafts occur generally 1 km or less ahead of the gust front. These and other observations do not agree with those of Ragette (1973) and Rao (1971). They found small updrafts in a broad band commencing 25 km and 40 km, respectively, ahead of the front. Maximum values in both the Ragette and Rao studies occurred about 10 km ahead of the cold air edge, a much greater distance than any of the cases in this paper; however, observations in this paper agree well with those of Browning (1971) for a cold front in England.

The w values shown in Table 1 were extracted from digital data obtained from the 444 m level of the tower. The 10-second data has been smoothed and maximum value noted for each case. Vertical velocity time-height sections in the Appendix show that maximum updraft occurs very close to the 450 m grid level, although in no case is there a closed contour within the tower layer. Table 1 shows that updrafts generally increase with frontal strength (increasing slope), then decrease as the front dissipates (shallower slope). The vertical velocity values agree with those observed by several other authors. The maximum value in Table 1 is 6.7 m s^{-1} (Case F), compared with an updraft in excess of 8 m s^{-1} at 1.2 km for a cold front in England (Browning and Harold, 1970), 10 m s^{-1} for another cold front in England reported by Browning (1971) and 8 m s^{-1} for a sea breeze front (Wallington, 1959). The Case F maximum value does not represent the absolute maximum higher up since contours are open at 450 m. Rao's (1971) model computes values of w two orders of magnitude smaller partially because of the modelled front's very shallow slope. Ragette (1973) finds maximum values of about 1 m s^{-1} using the same technique with observed winds. It is apparent that vertical velocities obtained by integrating the continuity equation (using horizontal wind data from either a model or actual observations over a coarse grid) such as in the Rao and Ragette studies, yield excessively low values.

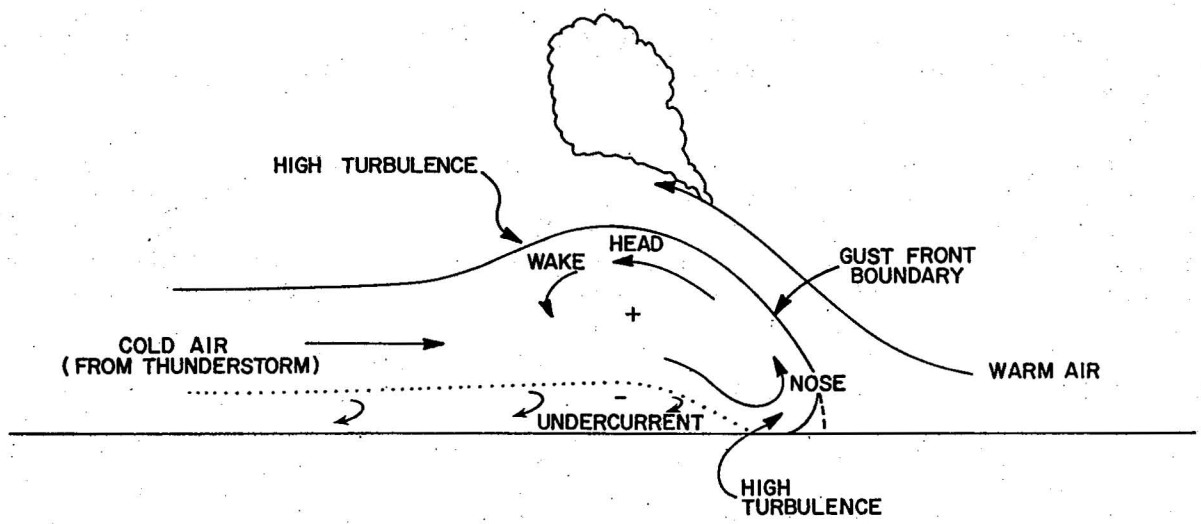

Fig. 1. Schematic diagram of thunderstorm outflow.

4.5 Shape of the Gust Front

Streamline analyses illustrated in the Appendix show the outflow boundary in mature cases assumes a fairly general shape (Fig. 1). This paper addresses only the boundary's lower 450 m since the tower detected the entire vertical extent of the outflow only for Case S. Other authors who described the atmospheric frontal boundary (Berson, 1958; Charba, 1974) and the laboratory gravity current (Middleton, 1966; Simpson, 1969 and 1972) used terminology we will follow. The nose (the protruding leading edge of the cold air outflow) is illustrated schematically in Fig. 1; the undercurrent is the low-level reverse flow (relative to the front) under the cold air. The term gust front or gust frontal zone is defined as the boundary separating flow originating from a cold source from that originating from a warm source. This boundary follows the zero contour in the u-component of the horizontal wind (bottom panel in the time-height sections of the Appendix) and is well defined in the streamline analysis.

Gust frontal zone shape varies as the storm (and, thus, the associated front) intensifies and dissipates. In formative stages the nose appears close to the ground and there is little undercurrent (Cases A, B and C). In contrast to mature fronts, accelerating gust fronts do not show surface drag effects and are not bowed back near the ground (as is the case in, say, Case E). Case A closely resembles Fujita's (1960) "back-current front", formed when the surface flow is unable to overcome the counter pressure-gradient force.

Case D is atypical of Type I fronts. The undercurrent has erroded the outflow base quite severely. The reader will note, however, that this gust front is preceded by a rather sharp but shallow inversion. It appears that

cold air outflow has difficulty dislodging this dense air resulting in the unusual frontal shape. Other than Case D, Type I gust fronts have slopes of about 45°.

Type II fronts have slopes generally between 45° and 75° in the layer from 100 m to the tower top. Surface drag appears to affect the low-level portion of the mature front (Type II), bending it back into the cold air (Mitchell, 1975). Warm air is entrained under the cold air and enhances the nose feature. In addition, cross-isentropic flow above 100 m produces a direct solenoidal circulation, hence a more pronounced bulge in cold air (Fig. 1). Some cases show little evidence of a nose (Case G). This may be attributed to cold air in the nose collapsing into the warm air. Collapse occurs when the cold air bulge has extended too far into the warm air. Our data imply that the lapse rate exceeds the autoconvective lapse ($\partial\theta/\partial z \leq -2.4°C\ 100\ m^{-1}$ at 1000 mb) in these cases. Overturning appears to enhance low-level downdrafts just behind the front (Case G). Since the collapse implies considerable turbulence, there should be an adverse effect on take-off and landing of aircraft. In Cases H, I and L there is also little evidence of a nose but the data is too coarse (see Section 3) to resolve this feature (or lack of it).

Charba (1974) inferred that the nose can extend 1.3 km into the warm air,[5] but we find that in none of the 20 cases does the nose extend more than 200 m into the warm air. Mitchell (1975) finds in his numerical model that for large values of surface drag in mature fronts, the nose maintains its configuration; i.e., fails to show the cyclic tendency to collapse and reform. This apparent deficiency arises because his model achieves a steady state balance between pressure forces and drag forces.

Dissipating fronts (Type III) have some characteristics similar to Type II fronts; e.g., undercurrents are usually present, but frontal slopes appear smaller once again, typical of those in intensifying fronts. This is due in part to the outflow becoming shallow rather than a result of low-level accelerations related to pressure forces as in Type I fronts. If the gust front propagates far from the rain-cooled downdraft, the cold air is gradually warmed by entrainment and mixing unless warming is counteracted by a fresh supply of cold air from the storm. However, vertical mixing in the baroclinic frontal zone decreases as the thermal gradient decreases implying a reduced frontal slope. A similar physical sequence is described by Williams (1974).

4.6 Relationship Between Wind, Potential Temperature, Wet-Bulb Potential Temperature and Pressure Discontinuities

Closely space tower data make possible detailed analysis of wind, potential temperature, moisture and pressure discontinuities. Fujita (1963), Barclay and Wilk (1970) and Charba (1974) have discussed the relative positions of these features. Their results are essentially verified here.

---

[5] Charba also found that the nose was located 750 m above the ground. The average height of the nose in the 17 cases which show the feature is around 100 m, sometimes even lower.

Frontal discontinuities of wind, potential temperature and pressure are not coincident. However, for the 11 cases in which wet-bulb temperature data was available, potential temperature (θ) and wet-bulb potential temperature (θ_w) discontinuities generally coincided. The above authors observed that a pressure jump occurred first followed by a windshift then a temperature (θ or θ_w) discontinuity. The same general results were found in these 20 cases except that the gust fronts were usually preceded by a gradual rise in pressure rather than a strong rise (pressure jump) observed by Charba and Fujita. The sharpest pressure gradient generally coincided with the ~~potential temperature~~ horizontal wind discontinuity. Table 3 shows that the gradual pressure rise commences up to 45 min (only three cases exceed 30 min) prior to cold air arrival, but there is considerable time variation from case to case.

When strong horizontal wind gradients occur in the frontal zone, both sharp temperature gradients and sharp pressure gradients are implied and observed, in agreement with Clarke (1961). In mature cases, the gust frontal windshift was quite obvious in the u-component but hardly noticeable in the v-component. Therefore, Table 3 gives only the u-component changes (Δu). While u-component changes appear to be the rule in Type II gust fronts, the principal change occurs in the v-component in Type I situations. Both components are roughly of equal importance in Type III gust fronts whereas windshifts are not well defined in Type IV fronts. Large windshifts usually precede the θ or θ_w discontinuity by only a minute or two, although the wind actually begins subtle changes as soon as the pressure begins to rise.

4.7 Multiple Surges in Cold Air Outflow

Ward and Arnett (1962) observed multiple cold air surges from a single thunderstorm using data from a large surface station mesonetwork. The authors attribute this to thunderstorm pulsation. Byers and Braham (1949) found multiple surges where new development occurred above the outflow but downwind of the parent cell. Lemon (1974) found several frontal discontinuities in a surface analysis of motions in a severe thunderstorm. Several multiple surge examples were observed in this study also. Sometimes secondary surges[6] are manifest only by a temperature discontinuity and sometimes only by a windshift. Occasionally both occur simultaneously. Cases F and I have obvious double surges; Cases B, E, F, G, H, K, N and S are also multiple surge types but the secondary discontinuities appear off the plots (and are not shown) far behind the outflow's leading edge (in Case K a second gust front is barely discernable). The second cold air surge in Case F (at about 1940 CST) is associated with precipitation onset. There is no noticeable windshift. A secondary windshift and temperature discontinuity are observed at 1512 CST in Case I.

We see that the secondary surge is sometimes associated with the leading edge of precipitation--the leading edge of the outflow being dry. This is not always true, however, as in Cases E, I, J and N both surges are dry. The precipitation onset in Cases E, I and J is a tranquil transition. There is no precipitation in Case N.

---

[6]The primary surge is the onset of cold air or the gust front.

TABLE 3. Relationship between pressure (mb), potential temperature (°C) and wind (m s^{-1}) discontinuities and rainfall onset

Case	Onset of ~~PJMP~~ PRESSURE RISE*	Onset of WSHFT*	θ or θ_w Discontinuity*	Onset of Rainfall*	Δp	Δu	$\Delta\theta$
A	0435	0447	0447	-	1.2	6	4.0
B	1312	1314	1320	1324	1.3	14	1.0
C	1728	1732	1735	1801	1.1	8	4.5
D	1451	1501	1502	1510	3.0	16	6.5
E	1911	1926	1927	1940	3.0	16	6.5
F	1849	1934	1935	1940	2.5	14	5.0
G	1918	1943	1945	2009	5.2	20	7.0
H	1700	1711	1716	-	2.2	14	5.0
I	1505	1508	1508	1515	2.8	14	8.5
J	2145	2207	2208	2249	2.1	17	3.0
K	2052	2116	2120	2126	6.6	16	7.0
L	1721	1759	1802	1834	2.8	10	7.0
M	0206	0214	0214	0217	1.2	7	3.0
N	0107	0110	0111	-	1.2	12	1.0
O	0430	0437	0438	-	1.9	16	2.5
P	2354	0022	0023	0030	2.3	4	3.0
Q	1816	1838	-	1836	3.9	18	-
R	1643	-	1656	-	0.8	-	4.5
S	1819	1900	1904	1942	1.9	16	6.5
T	0028	0028	-	0033	3.0	18	-

*Times are local standard time

The second gust front in Case S is associated with precipitation onset at the tower facility but at the NSSL mesonetwork site, 40 km south, a double gust front phenomenon is observed in the dry air. Apparently the second east-west frontal boundary moves out ahead of the precipitation south of the tower site. Thereafter, a third gust front is likely associated with the precipitation onset. Case G is the only other observed case of three outflow surges.

Multiple surges, most prevalent in mature storms (Type II), also infrequently occur with Types I, III and IV. Mature storms are believed most likely to pulsate, indicating that these types of storms are not steady state, at least with respect to outflow.

4.8 Horizontal and Vertical Wind Shear

Strong winds often observed in thunderstorm outflow result in large vertical and horizontal shears. Vertical shear is experienced both near the surface and at the outflow upper boundary; however, this boundary is typically above the tower top. Large horizontal shear occurs at the outflow's leading edge and may also be strong along secondary outflow boundaries (multiple outflow surge cases). Knowledge of shear values in echo-free air some distance from the parent thunderstorm is important for pilots and air traffic controllers because it cannot be readily detected by operational remote sensors.

Values of six shear terms $\partial u/\partial x$, $\partial v/\partial x$, $\partial w/\partial x$, $\partial u/\partial z$, $\partial v/\partial z$, $\partial w/\partial z$ were determined for high resolution data (13 cases from 1971 and 1972). The same procedure was followed as in plotting the time-height sections: wind component values were determined at grid points of a regular array (x,z:60,10). Data were smoothed using one pass of a 9-point operator ($2\Delta t$ cutoff filter with 93% response at $12\Delta t$). A time-to-space conversion was used for horizontal shear computations; e.g., $\partial u/\partial x = (1/c)\partial u/\partial t$, where c is gust front speed. Errors in gust front speed determination are, of course, manifest in these shears.

Table 4 is a summary of shear information determined from the smoothed wind field. Explanation of the table is simplified by considering only one shear, say, $\partial u/\partial x$. A $\partial u/\partial x$ frequency distribution was compiled for each case and maximum values isolated. The largest absolute maximum ($|\partial u/\partial x|_{max}$) for the 13 cases in which the distribution was tabulated was then found and appears in Table 4a (likewise for the other five shears). Table 4b is simply the average absolute maximum $\partial u/\partial x$ for 13 cases.

In Table 4 the grid levels 1 through 10 refer to 50 m vertical grid levels (grid level 1 = surface, grid level 2 = 50 m height, etc.) for $\partial/\partial x$ gradients. Grid layers 1 through 9 refer to 50 m thick layers (grid layer 1 = 0 to 50 m layer, grid layer 2 = 50 to 100 m layer, etc.) for $\partial/\partial z$ gradients. All shears are in units m s^{-1} 100 m^{-1}.

The table shows that shears of horizontal wind ($\partial u/\partial x$, $\partial v/\partial x$, $\partial u/\partial z$, $\partial v/\partial z$) are generally larger than shears of vertical wind ($\partial w/\partial x$, $\partial w/\partial z$). Gradients of the horizontal motion component normal to the front (u) are slightly greater than components parallel to the front (v). Shears of horizontal wind are greatest near the ground, show a minimum at roughly 200 m,

TABLE 4a: Maximum Absolute Shear (13 cases) [m s^{-1} 100 m^{-1}]

Grid level or layer of gradient:

	1	2	3	4	5	6	7	8	9	10
$\partial u/\partial x$	11.1	5.0	4.9	5.4	4.7	4.1	4.8	5.3	4.5	4.6
$\partial v/\partial x$	7.0	3.2	3.4	3.8	3.4	3.7	4.0	4.8	4.8	7.8
$\partial w/\partial x$	0.0	1.2	2.2	3.4	3.8	3.4	2.6	2.8	3.3	3.8
$\partial u/\partial z$	16.2	8.4	8.7	9.6	9.4	8.6	10.8	6.5	10.6	---
$\partial v/\partial z$	26.1	10.2	6.9	5.6	8.2	6.4	6.4	6.3	9.7	---
$\partial w/\partial z$	3.8	2.1	2.3	2.0	2.6	3.1	3.1	3.1	3.1	---

TABLE 4b: Average Maximum Absolute Shear (13 cases) [m s^{-1} 100 m^{-1}]

Grid Level or layer of gradient:

	1	2	3	4	5	6	7	8	9	10
$\partial u/\partial x$	4.3	2.0	2.3	2.3	2.3	2.4	2.6	2.9	2.9	3.2
$\partial v/\partial x$	4.0	1.5	1.5	1.7	1.9	1.9	1.9	2.2	2.2	2.6
$\partial w/\partial x$	0.0	0.6	0.9	1.2	1.3	1.2	1.1	1.5	1.9	2.4
$\partial u/\partial z$	11.6	5.8	4.7	4.6	4.1	4.7	5.0	4.1	5.1	---
$\partial v/\partial z$	10.6	5.3	4.1	3.6	3.9	3.6	3.4	3.2	4.3	---
$\partial w/\partial z$	2.1	1.6	1.7	1.3	1.7	1.9	1.9	1.9	1.9	---

then increase slowly to 450 m. $\partial w/\partial x$ (assumed zero at $z = 0$) increases rapidly up to about 200 m then more slowly above. $\partial w/\partial z$ has similar values throughout the tower layer. Vertical derivatives are generally larger than horizontal derivatives, typical of boundary layer flows in unperturbed conditions.

Shears in Table 4 probably represent values greater than those observed in normal boundary layer stratifications in central Oklahoma, although little data is available for comparison when the boundary layer is unperturbed (especially lacking is comparison vertical velocity data). Crawford and Hudson (1970) cite horizontal wind data taken from the WKY-TV tower during the years of 1966 and 1967. Comparison of vertical shears in gust fronts and average conditions shows that shears near the ground are comparable, whereas, near the top of the tower, maximum absolute vertical shears in gust fronts exceed average vertical wind shears by about an order of magnitude.

This brief investigation of wind shear is not complete. Beran (1974) points out that "the problem of ideally depicting the shear for aircraft operations is far from the simple one of measuring gradients". One needs to know

$$\frac{\partial}{\partial x}\left(\frac{\partial \overline{V}}{\partial z}\right) = \frac{\partial^2 \overline{V}}{\partial x \partial z} \quad . \tag{4}$$

where $\overline{V}$ is the horizontal wind vector. While it is usually sufficient to assume horizontal homogeneity; i.e.,

$$\frac{\partial^2 \overline{V}}{\partial x \partial z} = 0 \quad , \tag{5}$$

such a condition is far from achieved in the study of outflows. Further, we have not discussed so-called "shear gusts" (deviations from the mean shear) which Beran feels are important in flight safety considerations. Such investigations await future studies.

5. THUNDERSTORM-OUTFLOW DYNAMICS

Surface drag, which affects frontal shape, is also partly responsible for observed low-level flow patterns in the cold air. Drag forces operating at low levels in the vicinity of the front induce warm air under the cold outflow by decelerating the cold air near the ground. As a result, many potential temperature sections (Types II and III) show a potentially colder air pocket elevated a few hundred meters above the surface rather than at ground level. Corresponding streamline analyses show numerous small scale eddies associated with the unstable layer below the cold pocket and a sudden shift from cold air flow toward the front to a reverse flow in the vertical cross sections (top to bottom). Vertical mixing is certainly enhanced when rolls are produced as in Case M, but apparently mixing does not entrain enough cold air at low levels to overcome the warm air undercurrent.

Charba (1974) ascribes low-level flow patterns close to the front to downward momentum transport from mixing in the wake of the head. However,

mechanisms responsible for flow patterns near the outflow leading edge are probably only weakly influenced by turbulence in the wake during most of the life-cycle (Clarke, 1961), since processes there are of small scale and do not diffuse large quantities of momentum or heat.

To understand what the flow pattern is, we introduce the circulation defined in the x,z plane as

$$C = \iint \left(\frac{\partial w}{\partial x} - \frac{\partial u}{\partial z}\right) dxdz \quad . \tag{6}$$

A positive (counterclockwise) circulation (positive integrand) is observed near the gust front because $\partial u/\partial z$ is negative and larger in magnitude than $\partial w/\partial x$. Potential energy has been converted to kinetic energy by the direct circulation created by solenoidal effects. (The solenoidal field itself has been created by differential advection.) Solenoidal effects are contained in an expression for the time rate of change of circulation. Before differentiating (6), it is put into line integral form

$$C = \oint \bar{V}\cdot d\bar{s} \tag{7}$$

where $\bar{V}$ is the 2-dimensional (x,z) velocity vector and $d\bar{s}$ is an increment of the position vector. Upon differentiating (7) we see that we can substitute the forcing terms in the vector equation of motion when the differential operator is brought inside the integral, such that

$$\frac{dC}{dt} = \oint \frac{d\bar{V}}{dt}\cdot d\bar{s} = -\oint \frac{1}{\rho} \nabla p\cdot d\bar{s} + \oint (2\bar{V} \times \bar{\omega})\cdot d\bar{s} + \oint \bar{g}\cdot d\bar{s} + \oint \bar{F}r\cdot d\bar{s} \tag{8}$$

where ρ is the density, p is the pressure, $\bar{\omega}$ is the angular velocity and $\bar{g}$ is the gravitational acceleration vector. Since the line integral of a single valued potential is zero the gravitational term in (8) vanishes. The remaining terms are the solenoidal term, the Coriolis term and the friction terms, respectively. To better understand the dynamics in terms of the objective analyses in the Appendix, the solenoidal term is changed to

$$-\iint_A \hat{n}\cdot(\nabla\alpha \times \nabla p)\, dxdz \tag{9}$$

using Stokes Theorem, and hence to

$$-R \iint \hat{n}\cdot(T\nabla \ln\theta \times \nabla \ln p)\, dxdz \tag{10}$$

using the equation of state and Poisson's equation. Here, α is the specific volume, R is the gas constant, T is the temperature, θ is the potential

temperature and $\hat{n}$ is the unit normal (positive direction into the page). (10) shows that solenoids are formed by intersecting surfaces of θ and p.

Since a potential temperature discontinuity lags the windshift, a large number of solenoids per unit area are generated just behind the gust front. Within the windshift zone a positive circulation fills the whole tower layer. In other words, pressure forces become very strong in the frontal zone, accelerating the flow, overwhelming drag forces and suppressing the undercurrent. These characteristics appear typical of frontal Types II and III. Cases E, J, M, N and O are good examples.

If the low-level isentropes are severely bent back into the cold air at the front, there will be fewer solenoids and a much smaller positive time rate of change of circulation. Since (6) is negative, we expect evidence of an undercurrent as in Case K. The stratification implies an unstable situation indicative of incipient overturning (collapsing of the nose).

Some distance behind the gust front, straight line flow exists above the undercurrent because $\partial u/\partial z$ and $\partial w/\partial x$ balance. Pressure gradient forces are dominant. Within the undercurrent, strong positive vertical shear implies a negative circulation produced by surface drag decelerations. If only solenoidal effects are considered, there is a small positive time rate of change of circulation. Surface friction changes the sign of the integral, however. The depth of the drag-dominated outflow boundary layer is inversely proportional to the pressure gradient force which weakens as the distance from the front increases.

Diffusion of momentum and heat in the wake and undercurrent become important in the final stage. Case S is an example. At low levels the negative circulation grows in vertical extent until it dominates the positive solenoidal accelerations in the frontal zone. This is assisted by what could be the growing influence of inertial forces (we presume that the outflow has persisted for sufficient time to allow Coriolis forces to increase in relative importance). As the pressure gradient between outflow onset and the ambient air is reduced, momentum decreases and the cold air becomes isolated from the thunderstorm. A large positively circulating roll develops in the wake eddy. Isolated cold pockets as in Case S are infrequently observed. We expect that decelerating (relative to the storm) outflow airmasses would normally be overrun by new surges of the parent thunderstorm. Evidence of the Coriolis influence is the large negative v-component values which grow at the expense of u. The effect is to tilt the plane of the circulation, increasing the vertical vorticity at the expense of the horizontal vorticity (see Hess, 1959, p. 246).

6. SUMMARY AND CONCLUSIONS

Twenty thunderstorm-outflow cases documented by the 481 m WKY-TV/NSSL tower and WSR-57 radar were described. It was possible to order the cases using outflow and storm intensity criteria. Four stages of outflow and gust front evolution were found. Thunderstorm-outflow characteristics were analyzed in terms of the four stages.

Gust front motion was found to be a strong function of cold air speed and a weak function of warm air speed. New expressions relating these speed values were derived. Frontal orientation was often northeast to southwest except in left-moving cells (west to east). Spacing between gust front and precipitation onset was generally greatest in older storms, but there were exceptions. Many cases were dry.

Positive vertical motion in advance of cold air outflow was an important frontal zone feature. Updraft values were highly correlated with frontal life cycle, showing a maximum in the mature stage. The strongest smoothed updraft was 6.7 m s^{-1} at 450 m although the objective analysis implied that stronger updrafts often occurred above the tower layer.

Frontal shape varied with outflow evolution. In early stages fronts had shallow slopes with little evidence of an undercurrent. As stronger circulations developed and flow was accelerated by solenoidal forces, the front became steeper near the top of the tower layer but surface drag forces also became significant decelerating flow near the ground. A nose was formed which showed a tendency to collapse and reform. The collapse, induced by unstable stratification, coincided with large low-level downdrafts. In dissipative stages fronts became shallower once again as solenoidal forces were reduced.

Frontal discontinuities of wind, potential temperature and pressure were not coincident. A pressure rise was observed first, followed by a windshift then a potential temperature discontinuity. A windshift preceding a thermal boundary is evidence that the atmosphere is adjusting to solenoidal accelerations in the frontal zone. Potential and wet-bulb potential temperature ~~discontinuities and a pressure jump were coincident.~~ generally coincided, as did pressure and wind discontinuities

About half the cases contained more than one cold air surge often associated with strong windshifts. Two cases had three discontinuities. Most observations of multiple fronts occurred near or at the mature stage of the storm.

Often attendant with thunderstorm outflow were strong winds and high horizontal and vertical shears. Vertical shears of the horizontal wind component normal to the fronts ($\partial u/\partial z$) usually had the largest values, although the largest shear observed was a $\partial v/\partial z$ exceeding 26 m s^{-1} 100 m^{-1}.

Three forces dominate thunderstorm outflow. In early and mature stages only the solenoidal forces and drag forces are important. Solenoidal forces create a positive circulation in the cold air near the front. Strong baroclinicity overwhelms the drag forces and the positive circulation often penetrates to the ground. Some distance from the front in the cold air, pressure gradient forces (or solenoidal forces) and frictional forces are also important, but apparently interact differently. Solenoids in the surface layer produce a weak positive time rate of change of circulation in a region of generally negative circulation where drag forces decelerate the flow. Above this layer straight line flow is produced by weak gradients of $\partial w/\partial x$ and $\partial u/\partial z$.

In final stage of the outflow gust fronts, Coriolis forces become important in some cases. The inertial force, surface drag and diffusion of warm

air in the wake of the current head are the principle dissipative mechanisms of the front.

A great deal remains to be learned about cold air outflow of the thunderstorm. NSSL storm intercept teams have seen numerous examples of tornadic vortices along these gust fronts. A study of such a phenomenon has not been addressed here. The 3-dimensional aspects of gust fronts must be understood before a study of gust front tornadoes can be pursued. Knowledge of the 3-dimensional gust front character also will assist pilots and aeronautical engineers since such information is critical to the response of aircraft and aerospace vehicles. Lastly, we need to know more about how the outflow affects the thunderstorm mesocyclone or the rotating updraft.

7. ACKNOWLEDGMENTS

The author appreciates the services of Messrs. W. David Zittel, meteorologist, and Leonard Johnson, electronic technician, who assisted in collecting this data set. The objective analyses were modified versions of schemes developed by Dr. Gary Achtemeier of the Illinois State Water Survey. The modifications were made by Mr. William Bumgarner of NSSL. The author thanks Drs. Ron Alberty and Joseph Schaefer who reviewed the manuscript and Mrs. Connie Hall who typed it.

8. REFERENCES

Ball, F. K., 1960: A theory of fronts in relation to surface stress. Quart. J. Roy. Meteor. Soc., 86, 51-66.

Barclay, P. A., and K. E. Wilk, 1970: Severe thunderstorm radar echo motion and related weather events hazardous to aviation operations. ESSA Tech. Memo. ERLTM-NSSL, No. 46, 63 pp.

Beran, D. W., 1974: Remote sensing wind and wind shear system, Report No. FAA-RD-74-3, Dept. of Transportation, Federal Aviation Administration.

Berson, F. A., 1958: Some measurements of undercutting cold air. Quart. J. Roy. Meteor. Soc., 84, 1-16.

Browning, K. A., and T. W. Harold, 1970: Air motion and precipitation growth at a cold front. Quart. J. Roy. Meteor. Soc., 96, 369-398.

Browning, K. A., 1971: Radar measurements of air motion near fronts. Weather, 26, 293-304.

Byers, H. R., and R. R. Braham, Jr., 1949: The Thunderstorm, U. S. Government Printing Office, Washington, D. C., 287 pp.

Carter, J. K., 1970: The meteorologically instrumented WKY-TV tower facility. NOAA Tech. Memo. ERLTM-NSSL, No. 50, 18 pp.

Charba, J., 1974: Application of gravity current model to analysis of squall-line gust front. Mon. Wea. Rev., 102, 140-156.

APPENDIX

FIGURE LEGEND

Left Pages:

Streamline analysis and time-height sections of vertical velocity (m s^{-1}), wet-bulb potential temperature (°K) (1971, 1972 only), potential temperature (°K), horizontal wind speed component parallel to gust front (v) and wind speed component normal and relative to the gust front (u) (m s^{-1}). Each objective analysis is 10 min long and 450 m thick; time increases from right to left. Date and start time of plot is in the upper left and time-to-space converted 1 km distance is indicated in the upper right.

Right Pages:

(Top) 10 cm WSR-57 conventional radar diagram with echo contouring. dBz values vary from year to year and case to case but shadings roughly represent powers (x) of 10^x mm^6 m^{-3} rainfall intensity. Time clock is in the upper right. Range marks are at 20 n mi intervals in 1971 and 1972 and at 40 km intervals in 1973 and 1974. The WKY-TV tower is located at the isolated ground clutter return at 358° and 20 n mi, best seen in the diagrams for Cases E and K. The radar was on 2° tilt in Case F, on 8° tilt in Case I. There is no radar diagram for Case N.

(Bottom) Quantitative remarks. Speed and orientation error subjectively determined. "Remarks" source is mostly from Storm Data (U. S. Dept. of Commerce) reports; some personal observations. Units correspond to radar range mark units or those used in Storm Data reports.

14MAY74 0446

1 KM

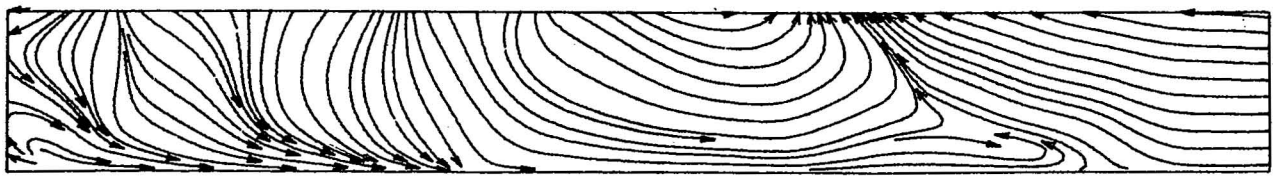

STREAMLINE ANALYSIS

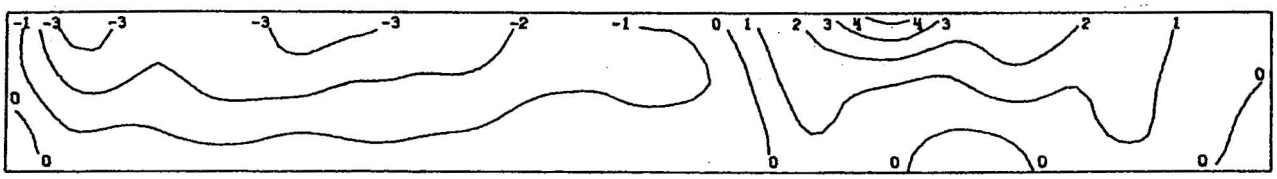

VERTICAL VELOCITY

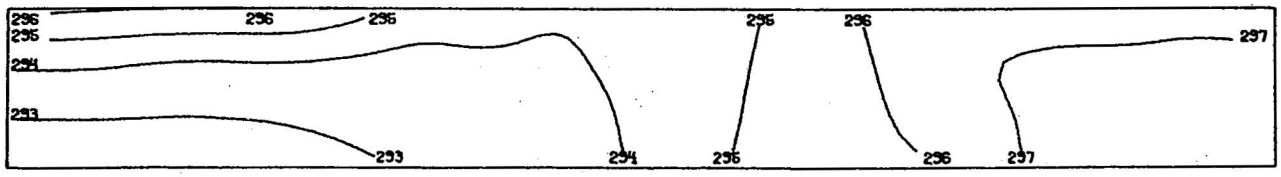

WET BULB POTENTIAL TEMPERATURE

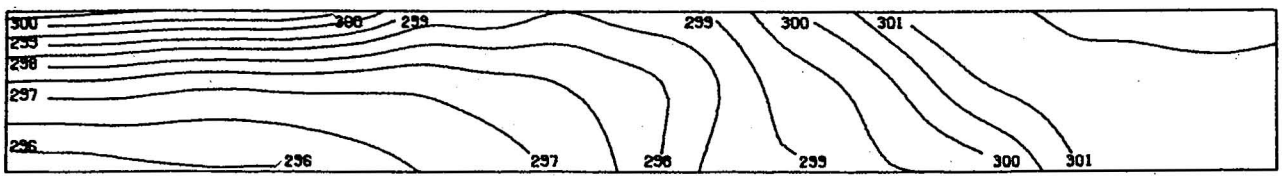

POTENTIAL TEMPERATURE

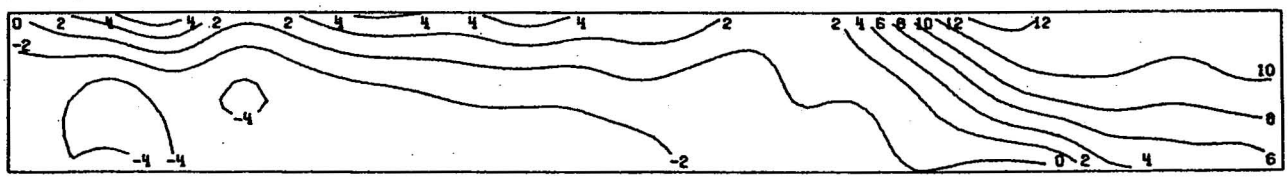

WIND SPEED PARALLEL TO FRONT

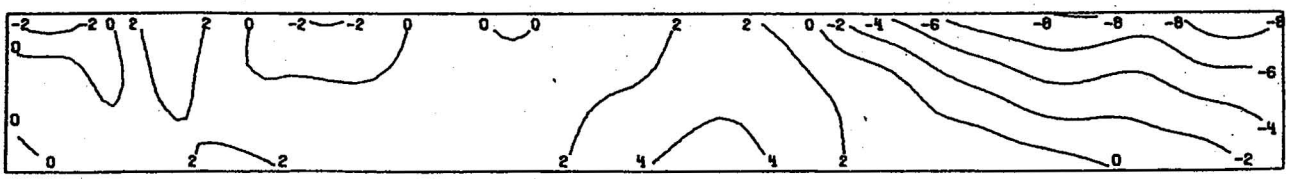

RELATIVE WIND SPEED, COMPONENT NORMAL TO FRONT

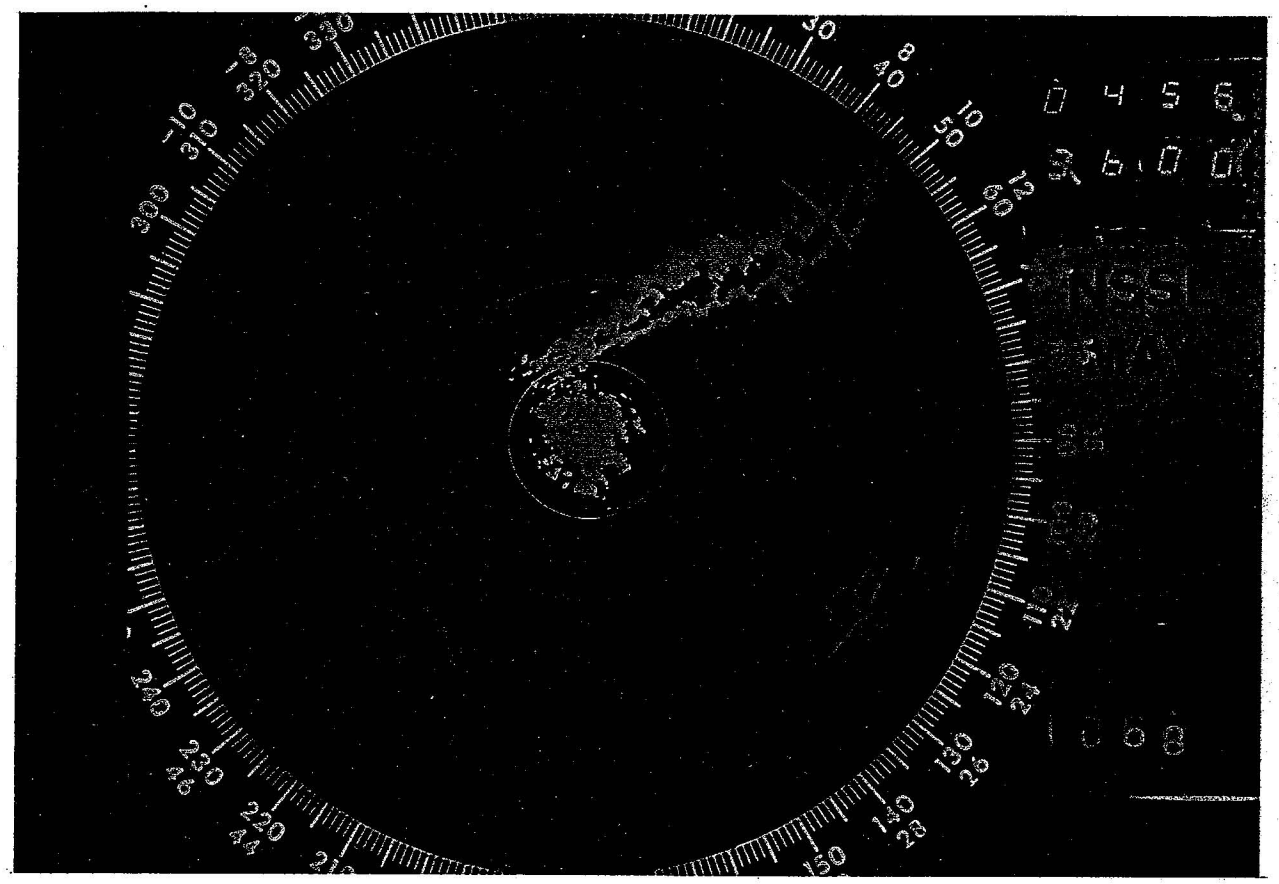

Case A

Date: 14 May 74 (date on radar diagram is incorrect)

Time of gust front: 0448 CST

Speed: 6.1 m s^{-1}

Orientation: 67°

Speed and orientation error less than 10%

Pressure jump: 1.2 mb 0435 - 9451 CST

Total rainfall: Trace

Remarks: Squall line dissipating generally but some new development on southwest end (gust front in formative stage); non-severe storm.

02JUL72 1314

1 KM

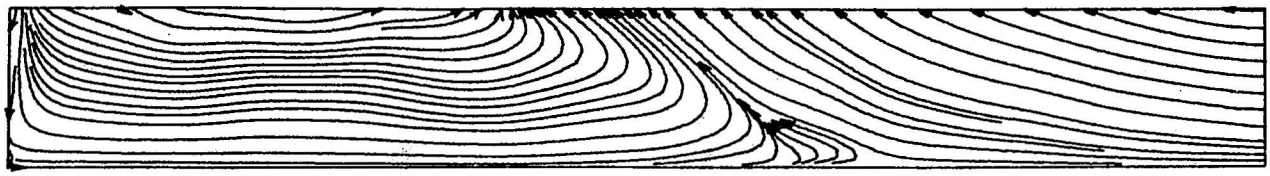

STREAMLINE ANALYSIS

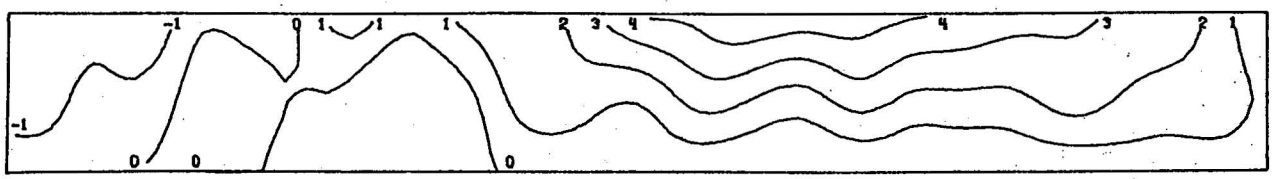

VERTICAL VELOCITY

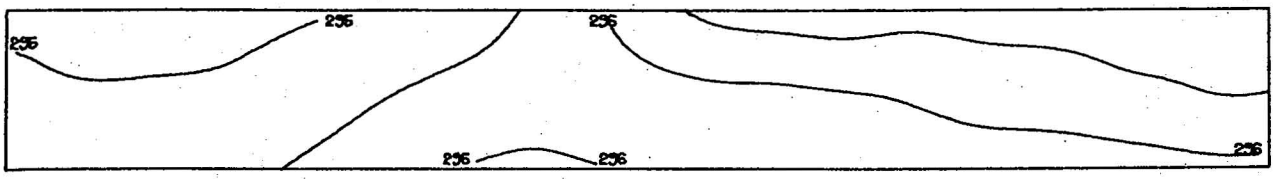

WET BULB POTENTIAL TEMPERATURE

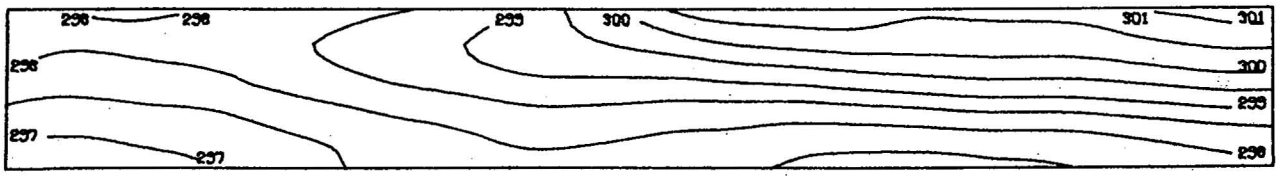

POTENTIAL TEMPERATURE

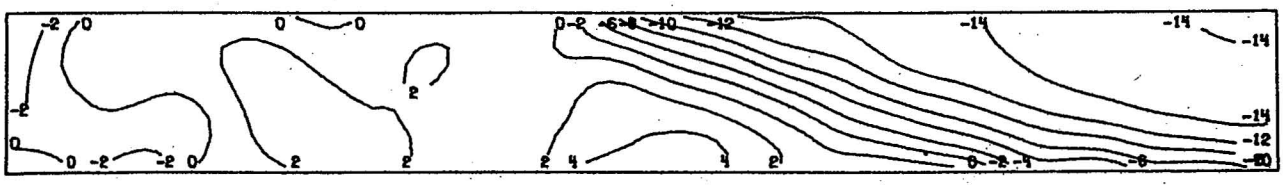

WIND SPEED PARALLEL TO FRONT

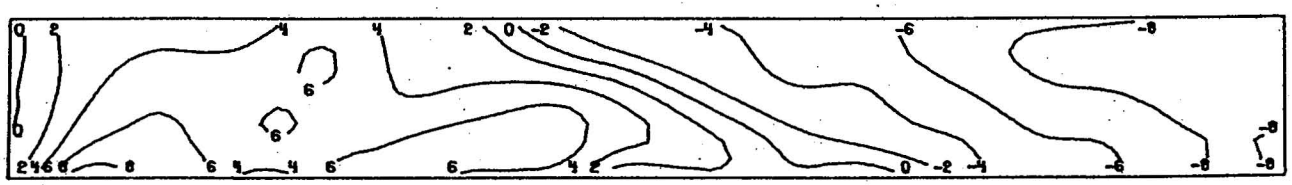

RELATIVE WIND SPEED, COMPONENT NORMAL TO FRONT

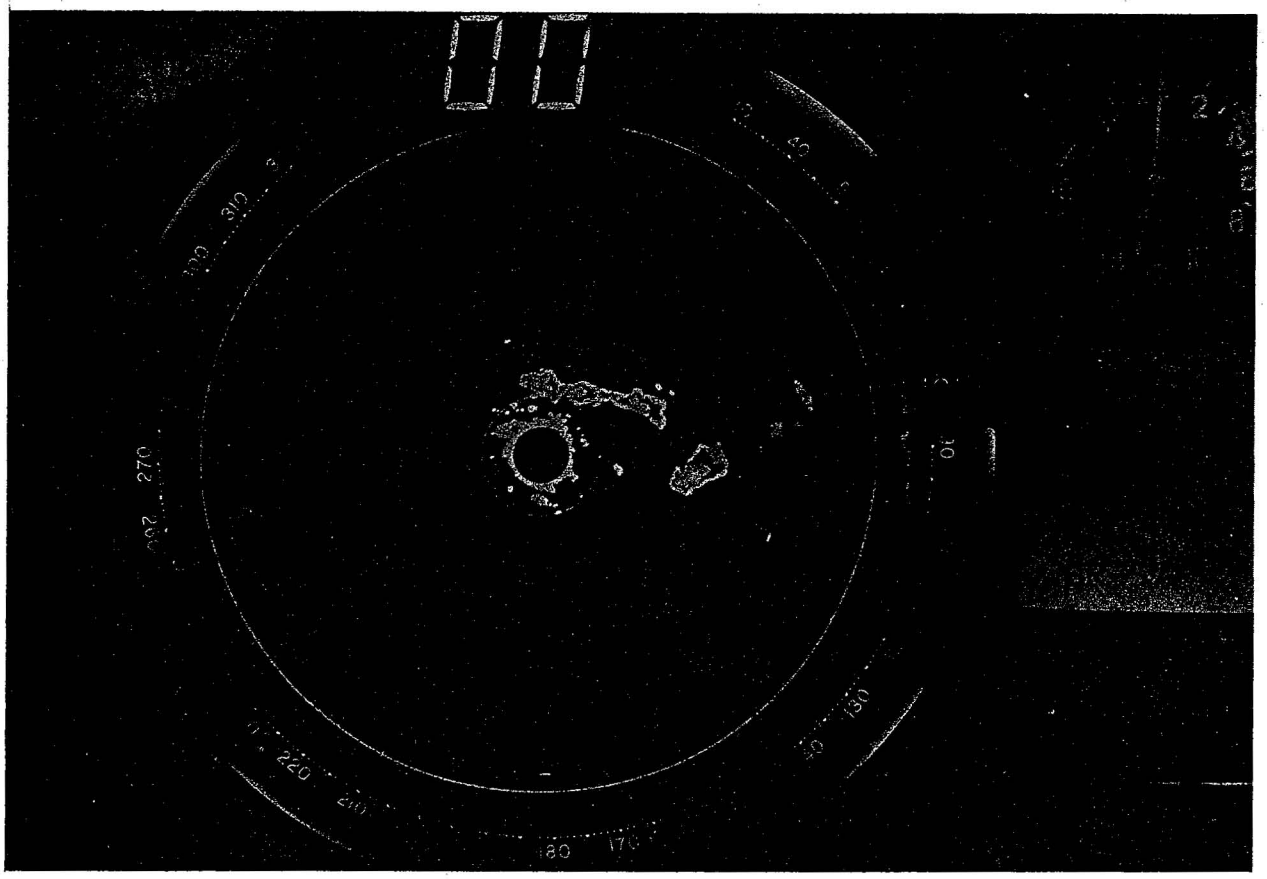

Case B

Date: 2 July 72

Time of gust front: 1318 CST

Speed: 5.0 m s^{-1}

Orientation: 70°

Speed and orientation errror greater than 10%

Pressure jump: 1.3 mb 1312 - 1327 CST

Rain began: 1324 CST ended: 1344 CST

Total rainfall: 0.96 in

Maximum intensity: 6.60 in hr^{-1} 1327 CST

Remarks: Well defined circulation visible on radar (4° tilt); 1 3/4 inch hail 5 n mi north of tower; later developing storms produced 2 3/4 inch hail and winds up to 100 mph in Oklahoma City - Norman area.

06MAY72 1731

1 KM

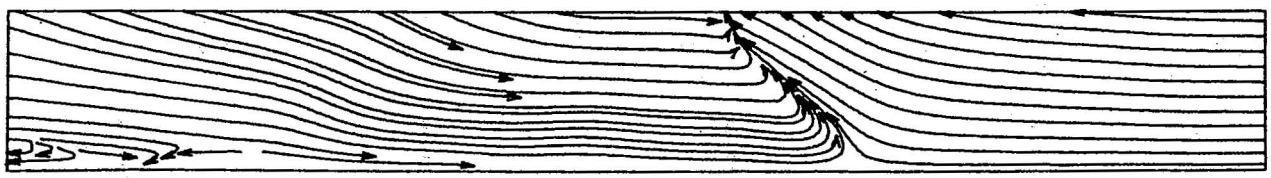

STREAMLINE ANALYSIS

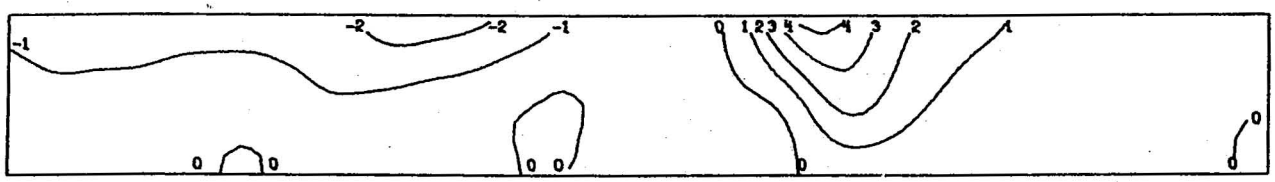

VERTICAL VELOCITY

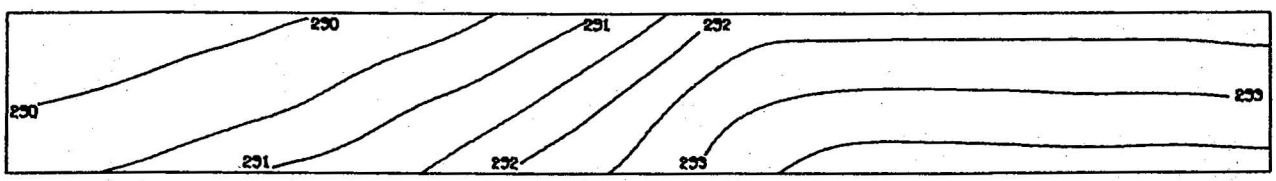

WET BULB POTENTIAL TEMPERATURE

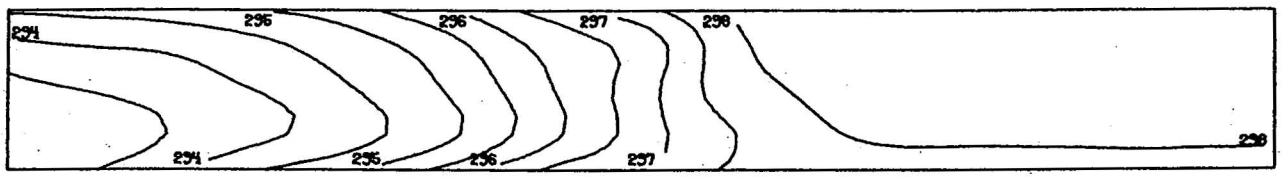

POTENTIAL TEMPERATURE

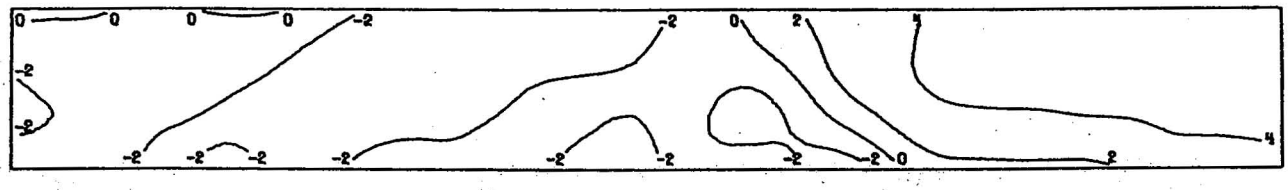

WIND SPEED PARALLEL TO FRONT

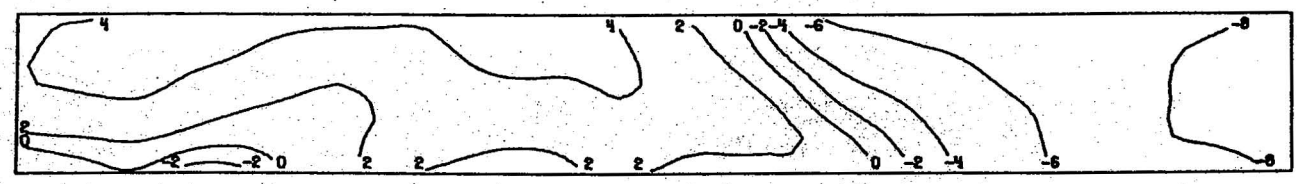

RELATIVE WIND SPEED, COMPONENT NORMAL TO FRONT

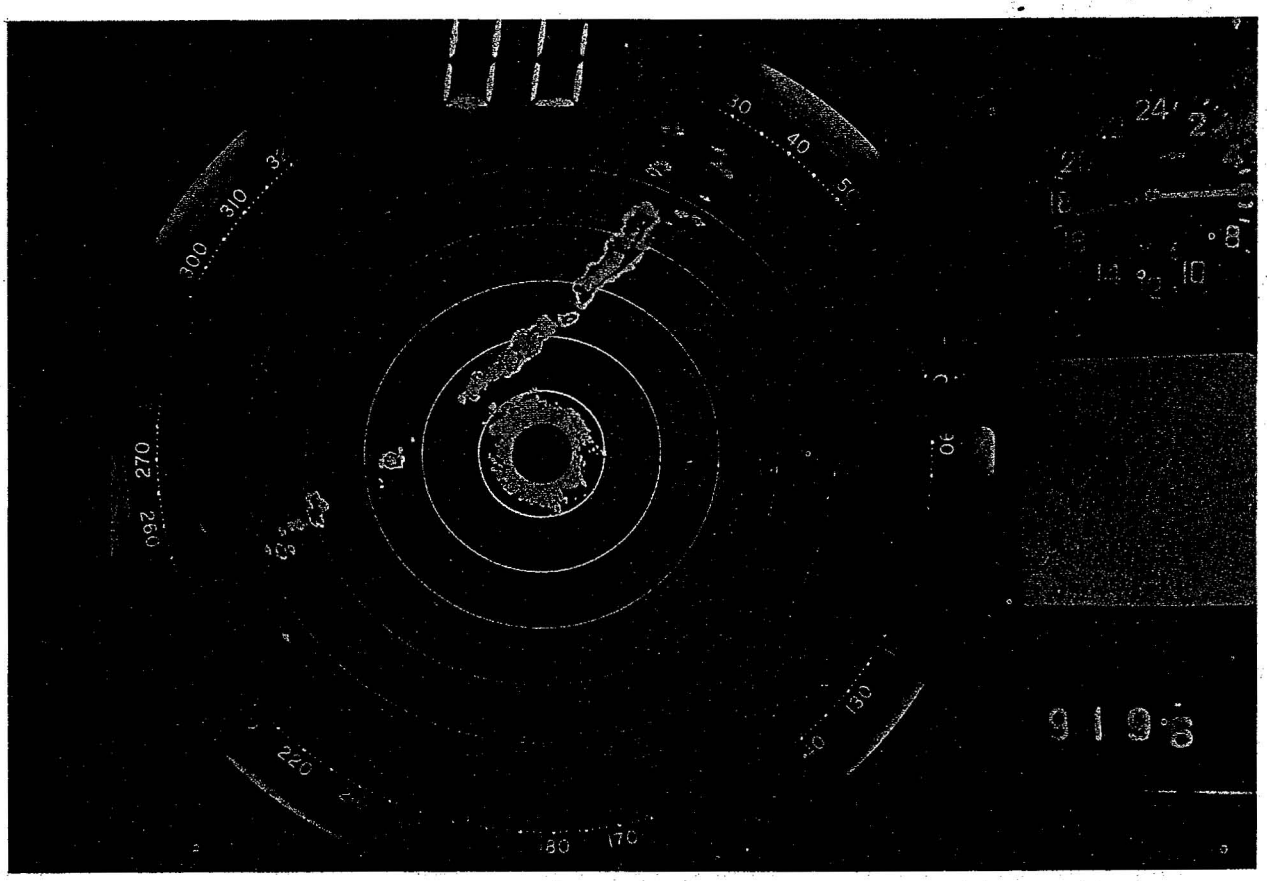

Case C

Date: 6 May 72

Time of gust front: 1734 CST

Speed: 8.6 m s^{-1}

Orientation: 50°

Speed and orientation error less than 10%

Pressure jump: 1.1 mb 1728 - 1742 CST

Rain began: 1801 CST ended: 1837 CST

Total rainfall: 0.43 in

Maximum intensity: 2.40 in hr^{-1} 1811 CST

Remarks: No severe weather

27MAY72 1459

1 KM

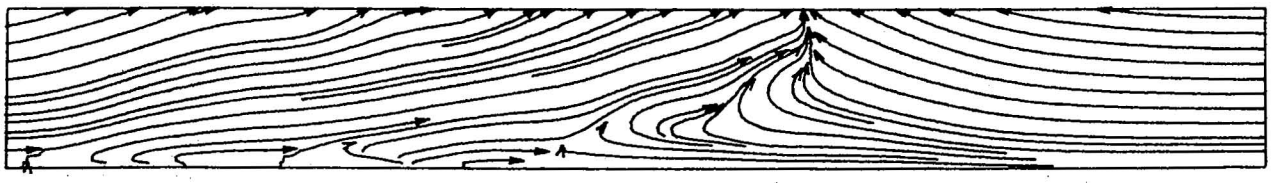

STREAMLINE ANALYSIS

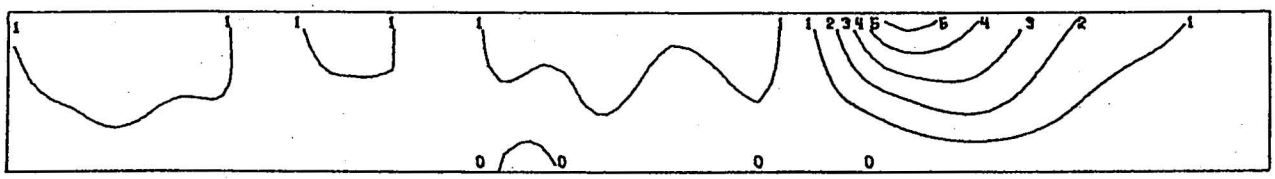

VERTICAL VELOCITY

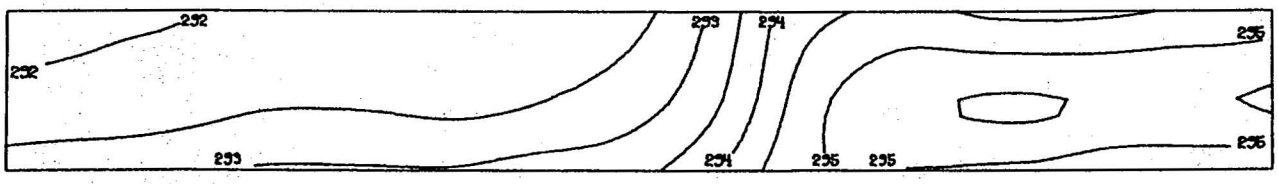

WET BULB POTENTIAL TEMPERATURE

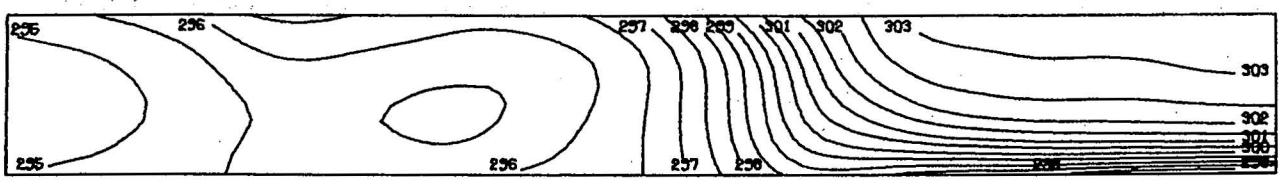

POTENTIAL TEMPERATURE

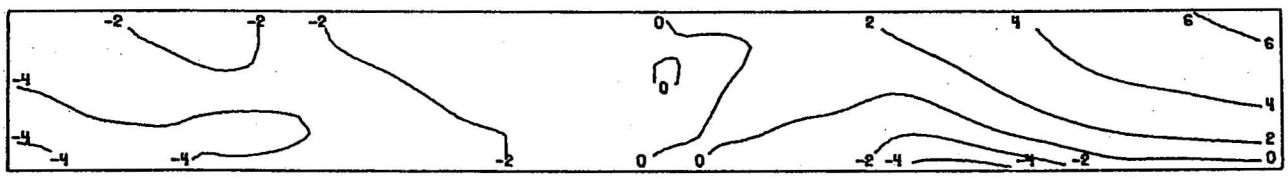

WIND SPEED PARALLEL TO FRONT

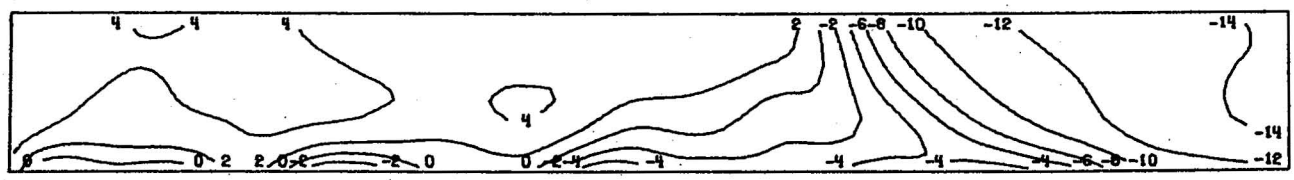

RELATIVE WIND SPEED, COMPONENT NORMAL TO FRONT

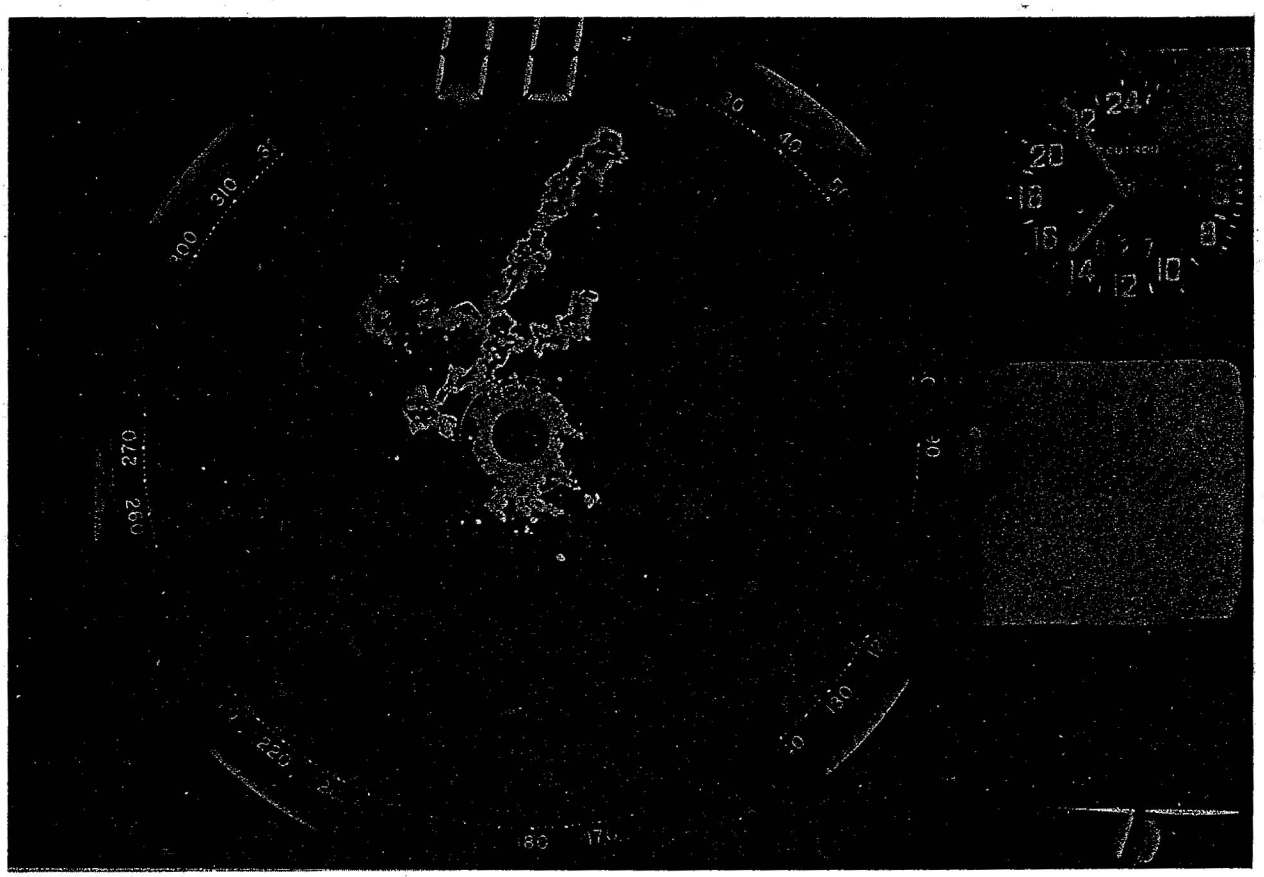

Case D

Date: 27 May 72

Time of gust front: 1503 CST

Speed: 11.6 m s^{-1}

Orientation: 30°

Speed and orientation error about 10%

Pressure jump: 3.0 mb 1451 - 1522 CST

Rain began: 1510 CST ended: unknown

Total rainfall: 1.00 in by 1528 CST

Maximum intensity: 5.40 in hr^{-1}

Remarks: Data collection interrupted at 1528 CST; precipitation records incomplete; 3/4 inch hail 10 n mi west of Norman and 1 3/4 inch hail 10 n mi north of Norman.

31MAY71 1924

1 KM

STREAMLINE ANALYSIS

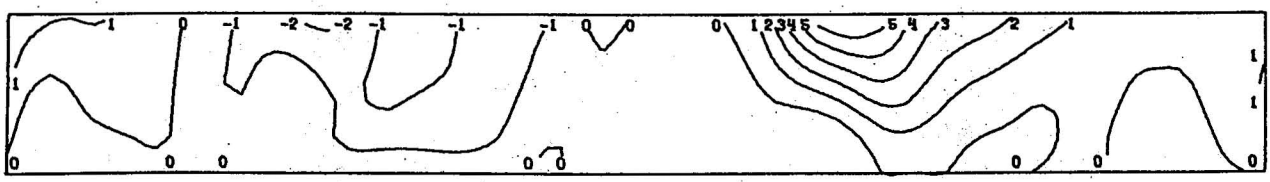

VERTICAL VELOCITY

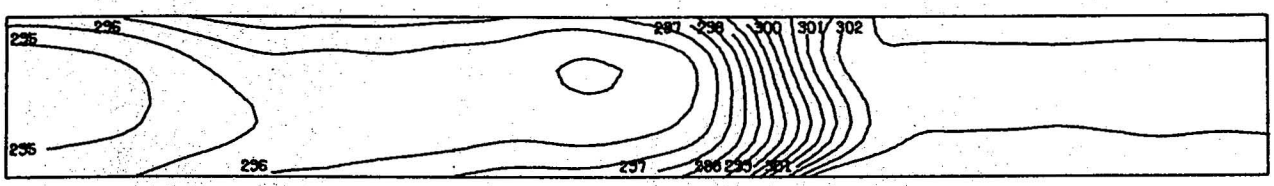

POTENTIAL TEMPERATURE

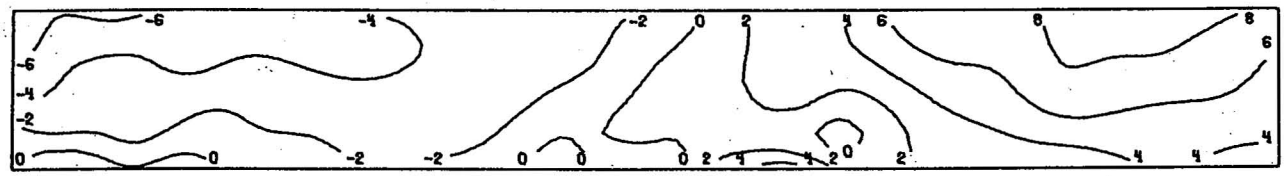

WIND SPEED PARALLEL TO FRONT

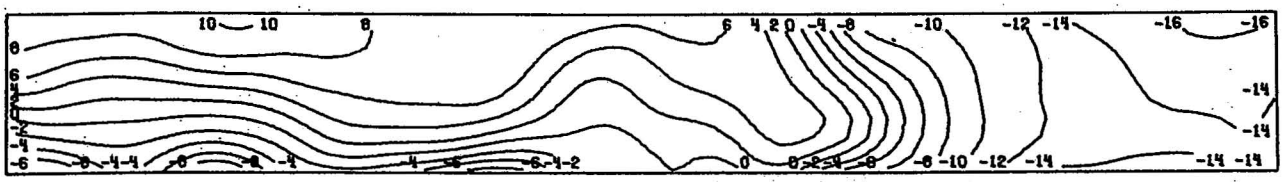

RELATIVE WIND SPEED, COMPONENT NORMAL TO FRONT

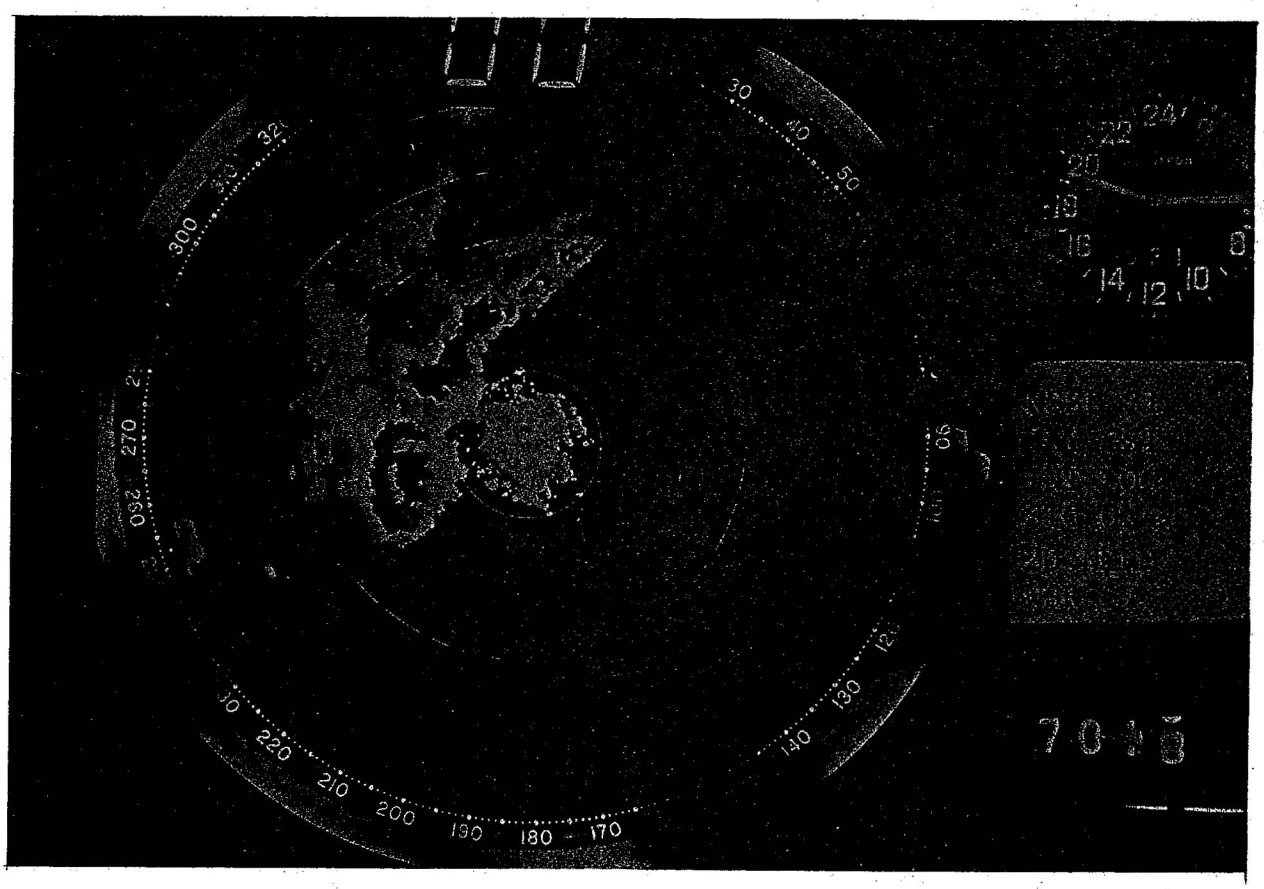

Case E

Date: 31 May 71

Time of gust front: 1927 CST

Speed: 16.7 m s^{-1}

Orientation: 17°

Speed and orientation error about 10%

Pressure jump: 3.9 mb 1911 - 1939 CST

Rain Began: 1940 CST ended: 2000 CST

Total rainfall: unknown

Remarks: Precipitation data noisy, cannot determine rainfall intensity; wind damage 10 n mi south of tower; no tornadoes.

27JUN72 1933

1 KM

STREAMLINE ANALYSIS

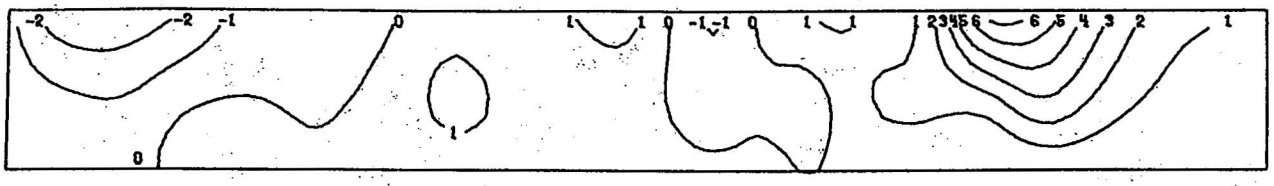

VERTICAL VELOCITY

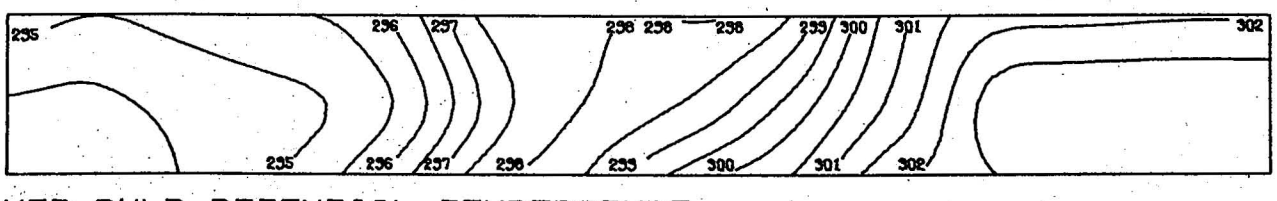

WET BULB POTENTIAL TEMPERATURE

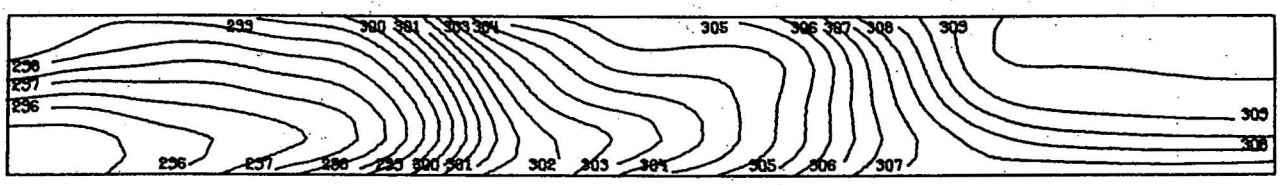

POTENTIAL TEMPERATURE

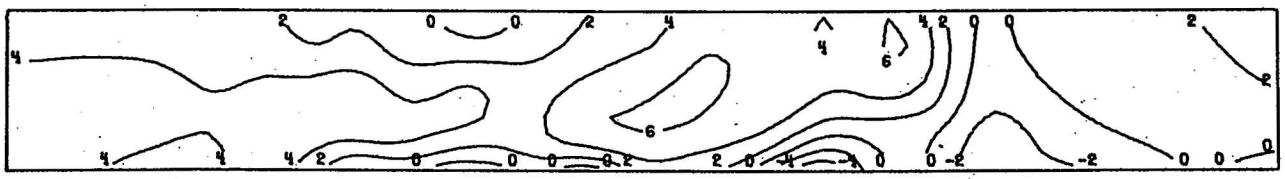

WIND SPEED PARALLEL TO FRONT

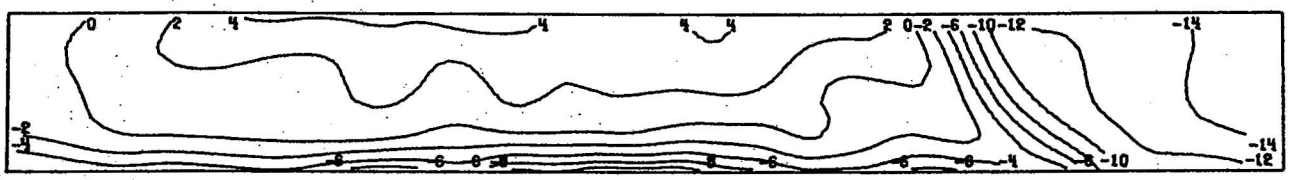

RELATIVE WIND SPEED, COMPONENT NORMAL TO FRONT

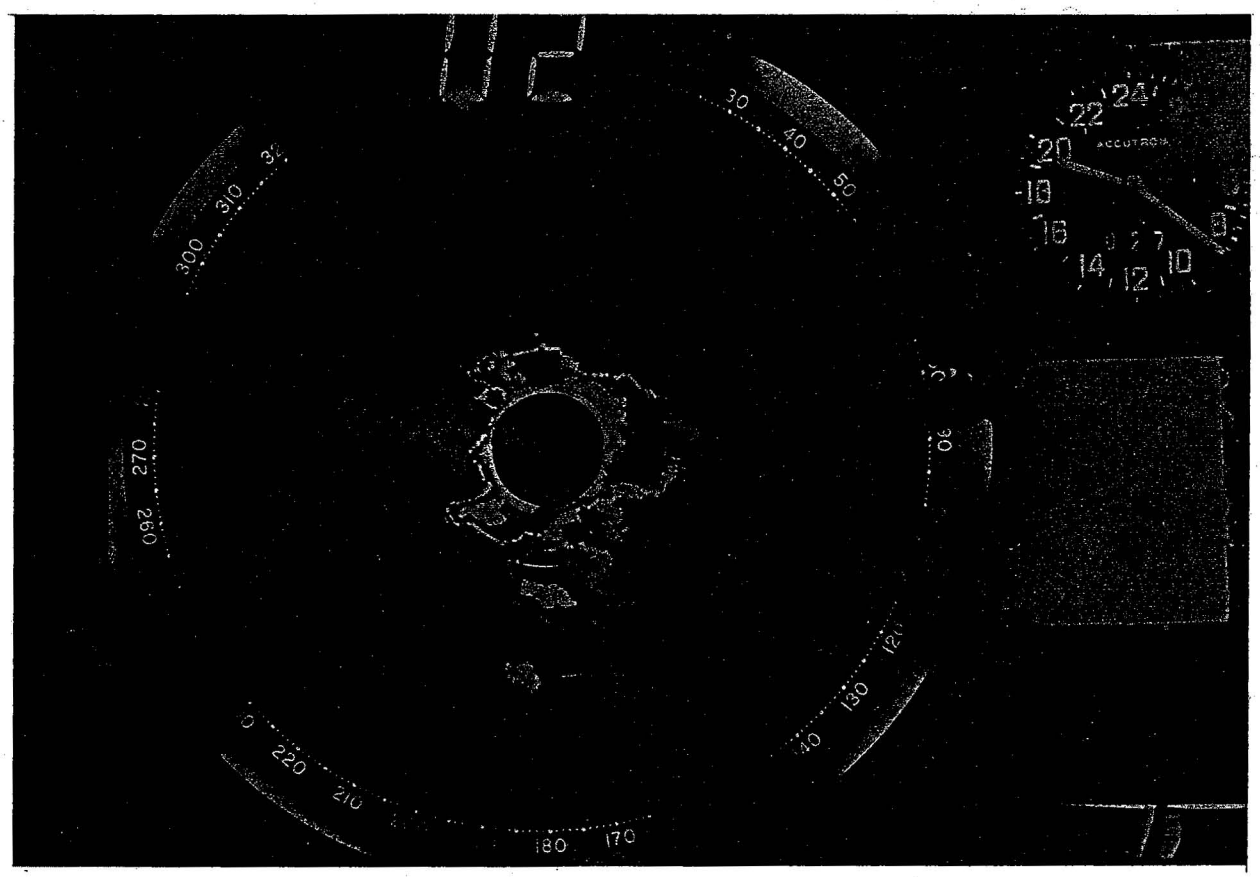

Case F

Date: 27 Jun 72

Time of gust front: 1936 CST

Speed: 11.0 m s^{-1}

Orientation: 290°

Speed and orientation error less than 10%

Pressure jump: 2.5 mb 1849 - 1942 CST

Rain Began: 1940 CST ended: 1944 CST

Total rainfall: 0.09 in

Maximum intensity: 2.40 in hr^{-1} 1941 CST

Remarks: Radar on 2° tilt; left moving cell passes over tower, 3/4 inch hail at Norman. Funnel 10 n mi north of Norman associated with adjacent cell.

07JUN71 1942

1 KM

STREAMLINE ANALYSIS

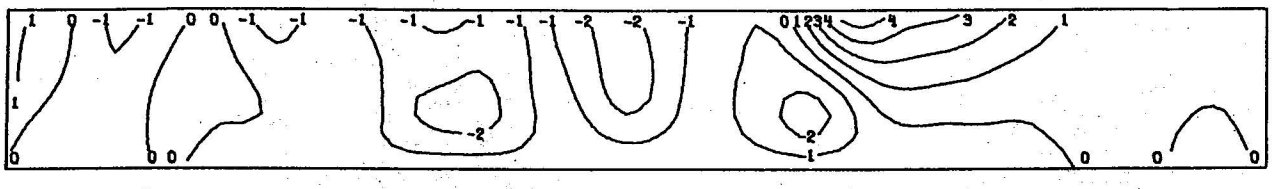

VERTICAL VELOCITY

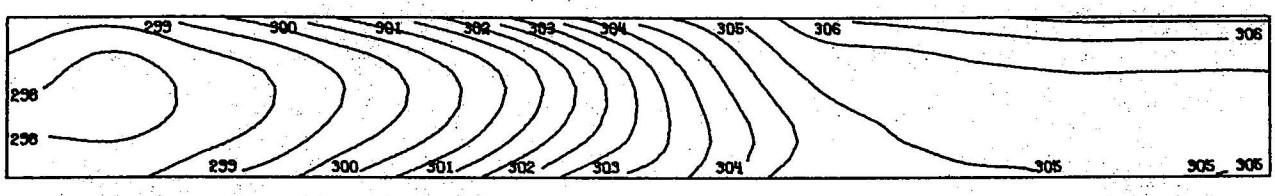

POTENTIAL TEMPERATURE

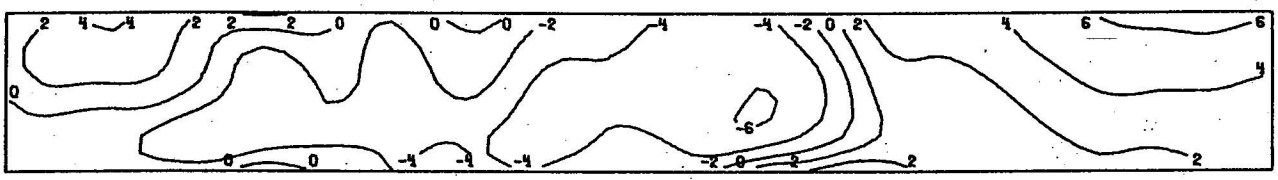

WIND SPEED PARALLEL TO FRONT

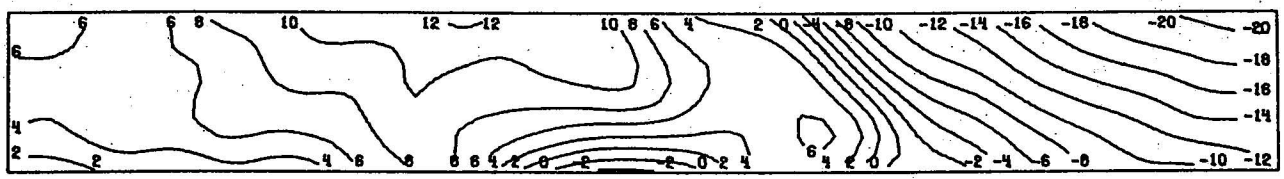

RELATIVE WIND SPEED, COMPONENT NORMAL TO FRONT

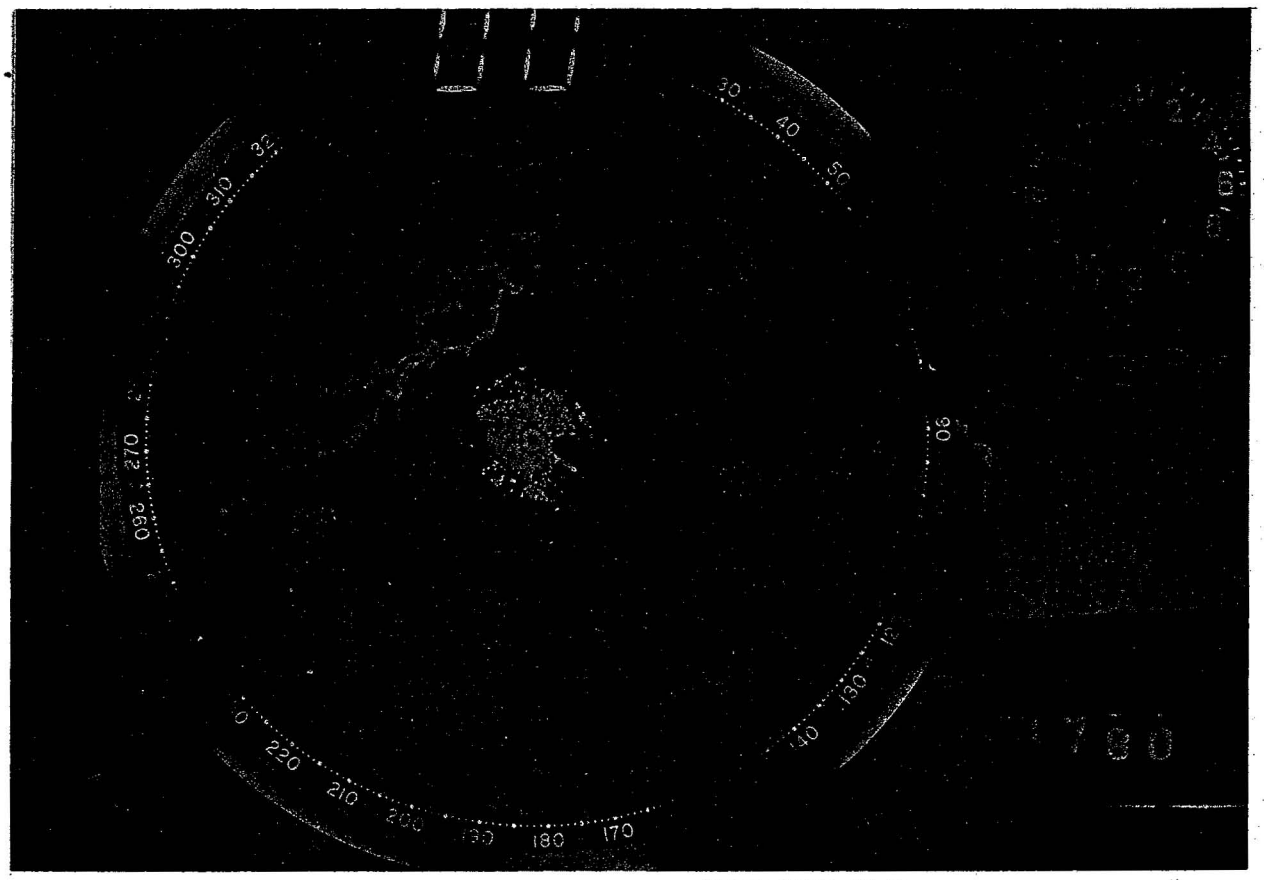

Case G

Date: 7 Jun 71

Time of gust front: 1945 CST

Speed: 1.8 m s^{-1}

Orientation: 50°

Speed and orientation error about 10%

Pressure jump: 5.2 mb 1918 - 2003 CST

Rain began: 2209 CST ended: 2322 CST

Total rainfall: 0.34 in

Maximum intensity: unknown

Remarks: Rainfall data noisy; winds to 65 mph in Oklahoma City, 66 mph at NSSL and 60 mph at Stillwater (30 n mi northeast of tower); no tornadoes.

23MAY74 1712

1 KM

STREAMLINE ANALYSIS

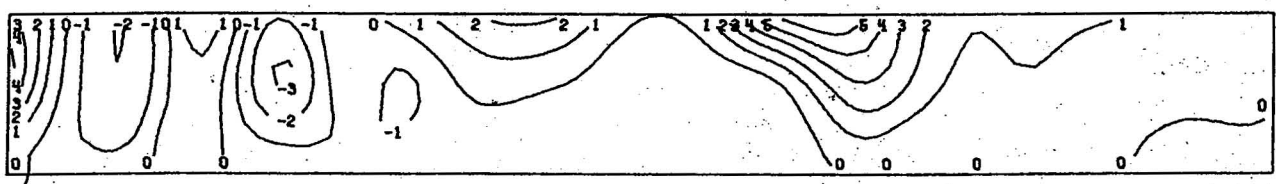

VERTICAL VELOCITY

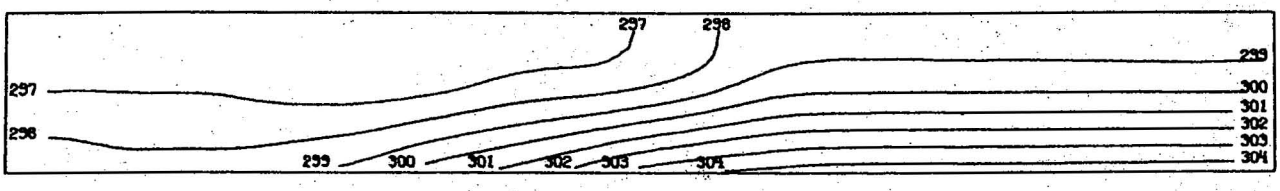

WET BULB POTENTIAL TEMPERATURE

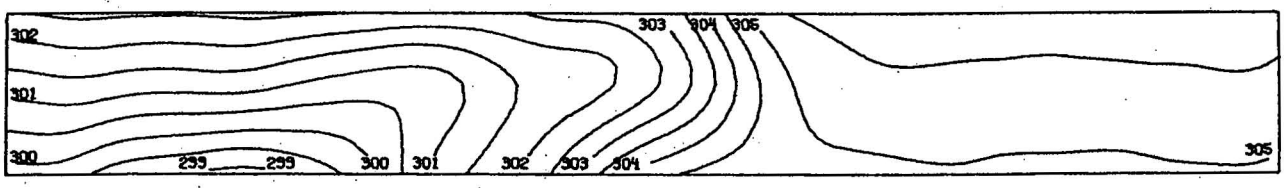

POTENTIAL TEMPERATURE

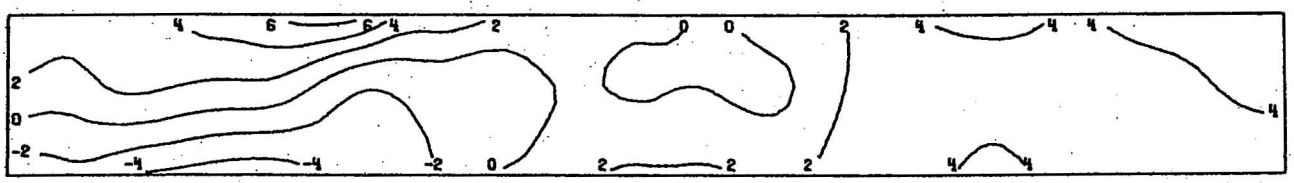

WIND SPEED PARALLEL TO FRONT

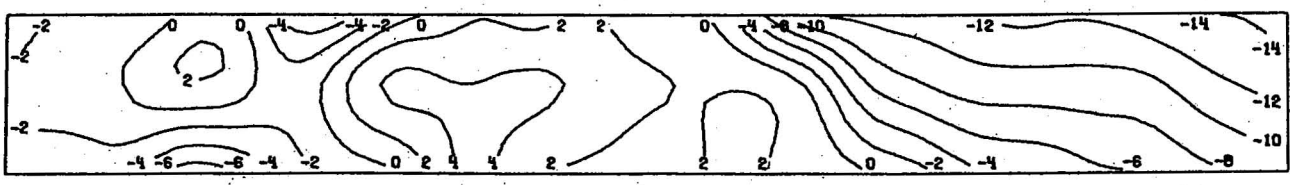

RELATIVE WIND SPEED, COMPONENT NORMAL TO FRONT

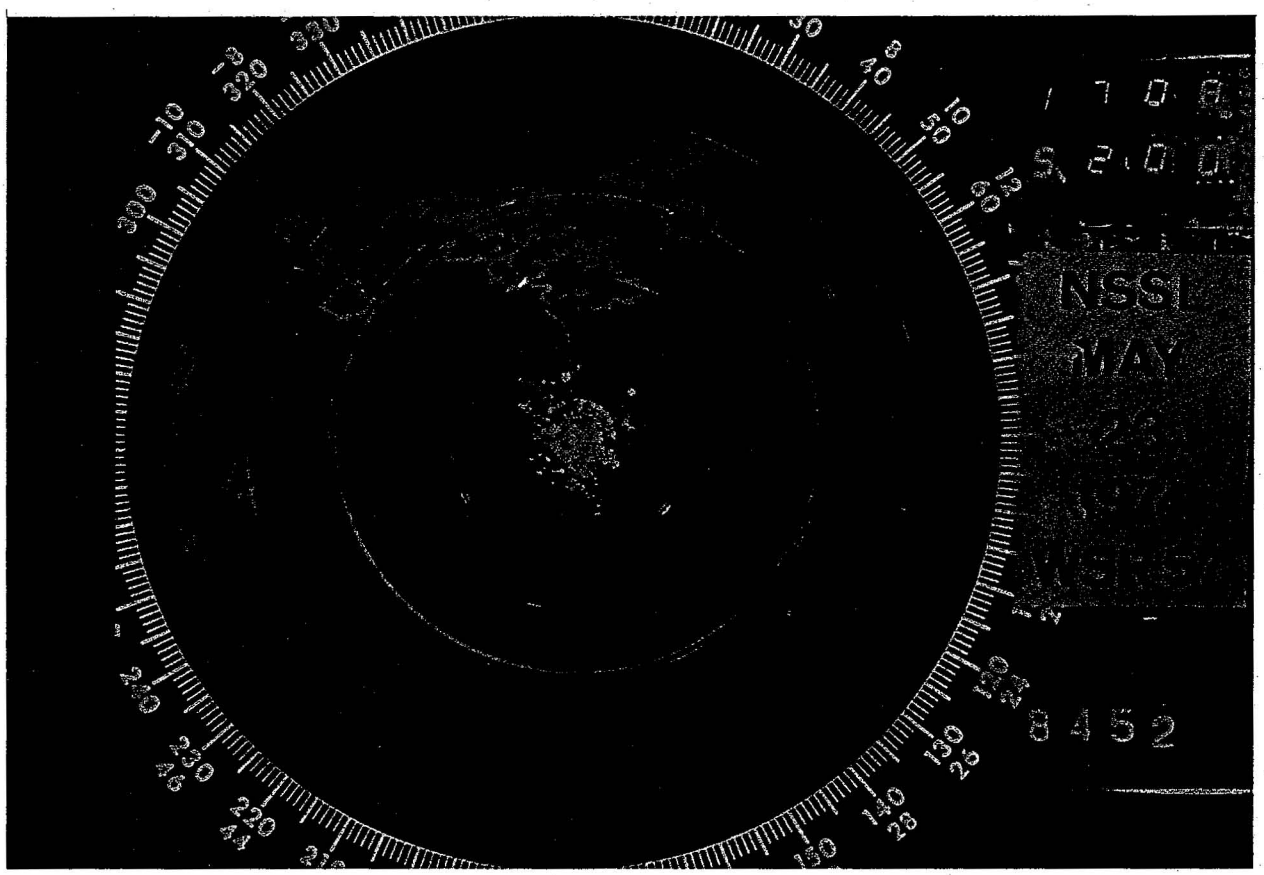

Case H

Date: 23 May 74 A

Time of gust front: 1716 CST

Speed: 8.5 m s^{-1}

Orientation: 70°

Speed and orientation error greater than 10%

Pressure jump: 2.2 mb 1700 - 1717 CST

Total rainfall: None

Remarks: Funnel and 2 inch hail at Kingfisher (40 km northwest of tower).

10JUN71 2206

1 KM

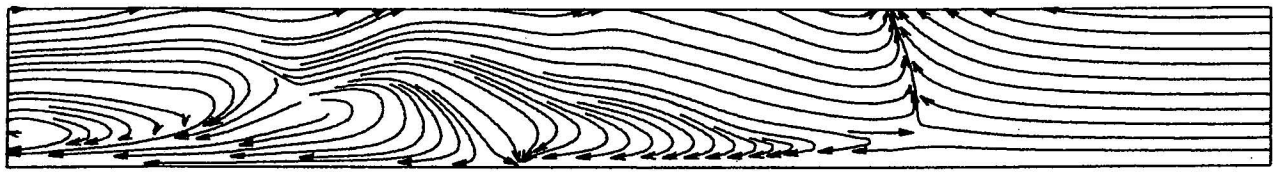

STREAMLINE ANALYSIS

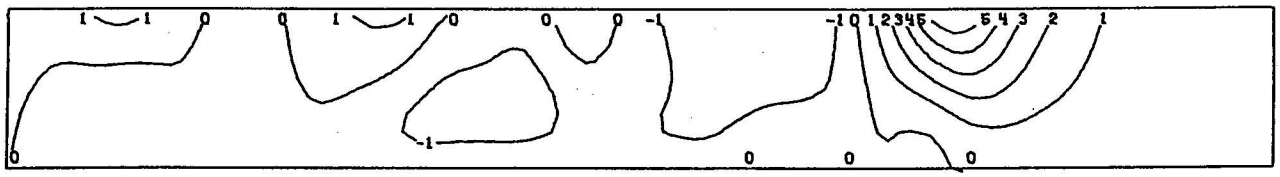

VERTICAL VELOCITY

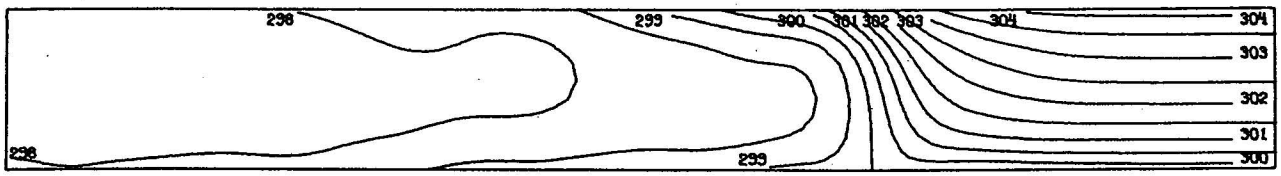

POTENTIAL TEMPERATURE

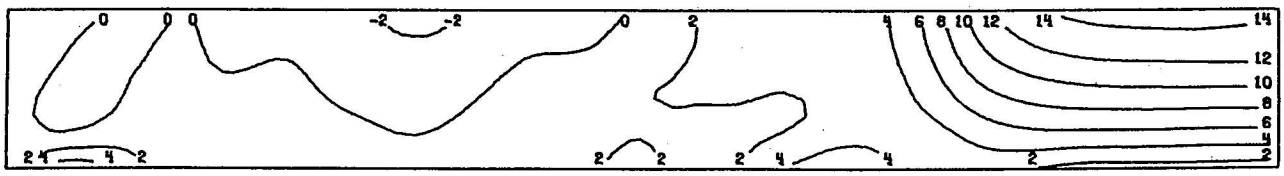

WIND SPEED PARALLEL TO FRONT

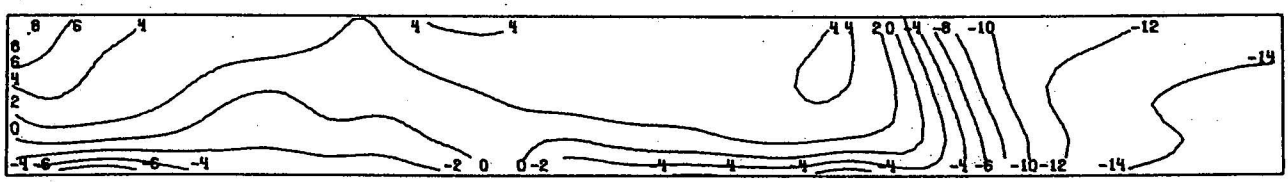

RELATIVE WIND SPEED, COMPONENT NORMAL TO FRONT

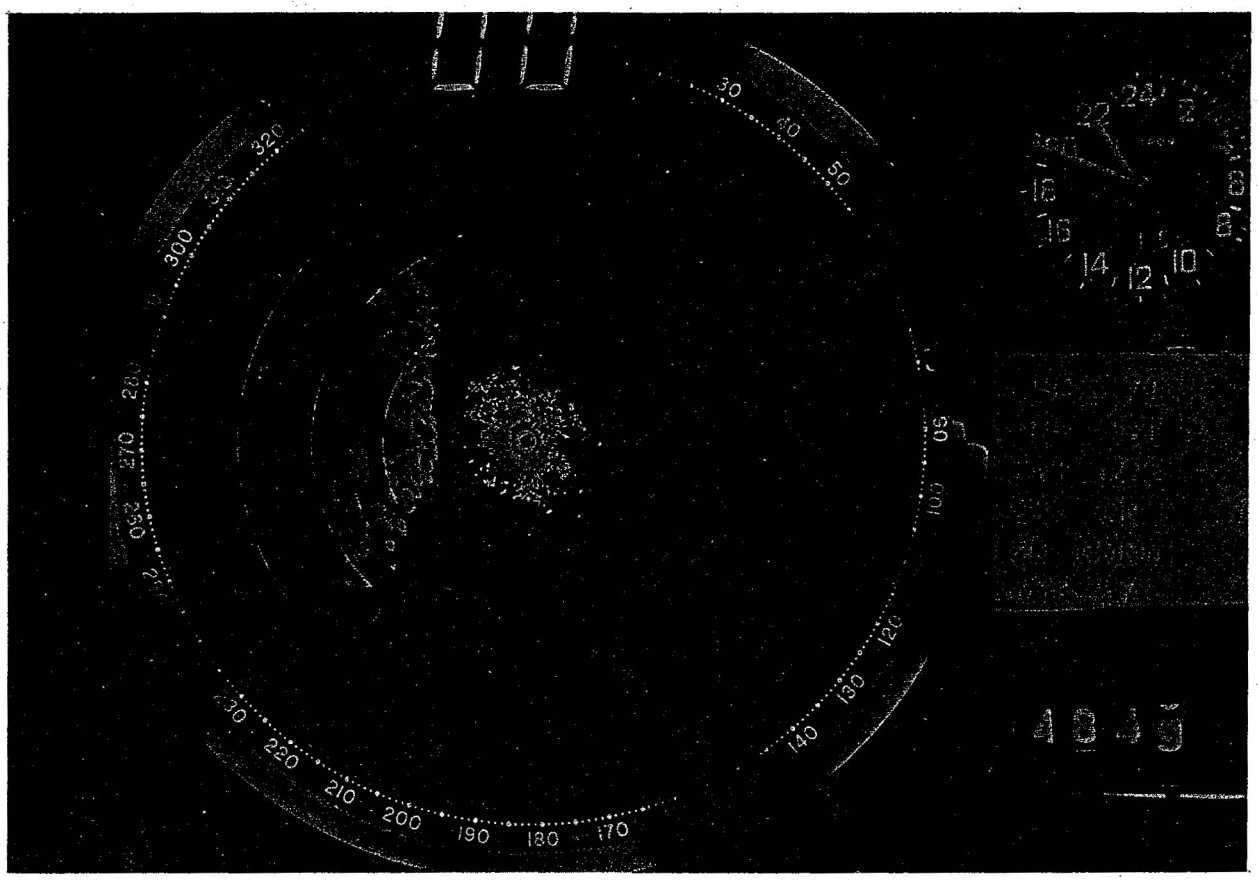

Case J

Date: 10 Jun 71

Time of gust front: 2209 CST

Speed: 13.1 m s^{-1}

Orientation: 5°

Speed and orientation error less than 10%

Pressure jump: 2.1 mb 2145 - 2213 CST

Rain began: 2249 CST ended: 2304 CST

Total rainfall: 0.08 in

Maximum intensity: unknown

Remarks: Rainfall data noisy; no severe weather.

02JUN71 2118

1 KM

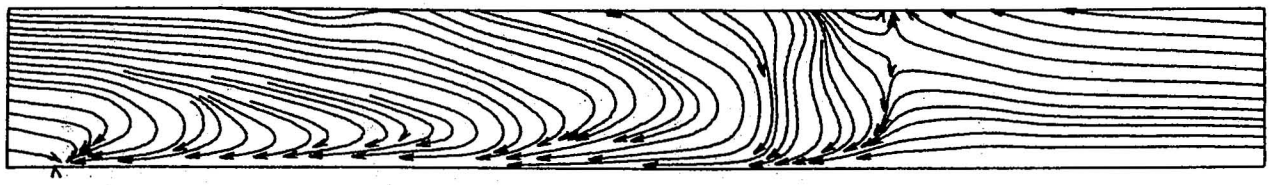

STREAMLINE ANALYSIS

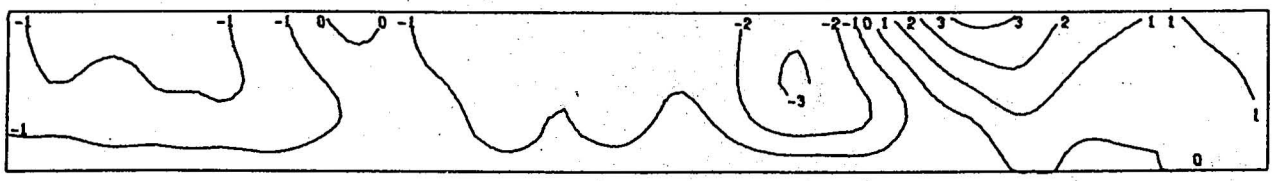

VERTICAL VELOCITY

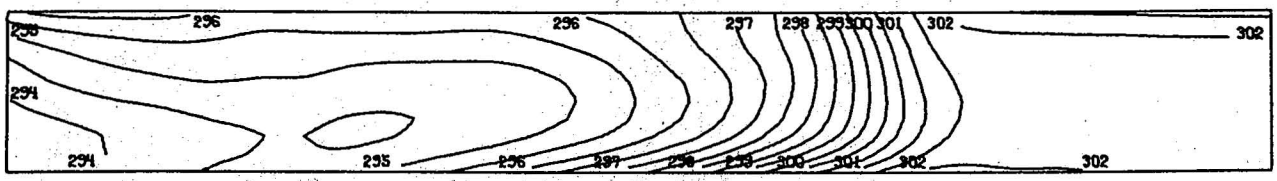

POTENTIAL TEMPERATURE

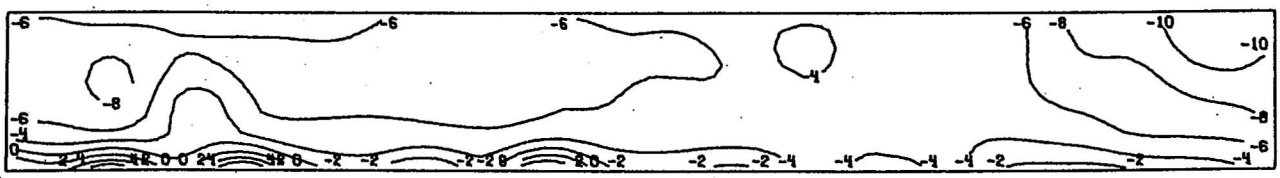

WIND SPEED PARALLEL TO FRONT

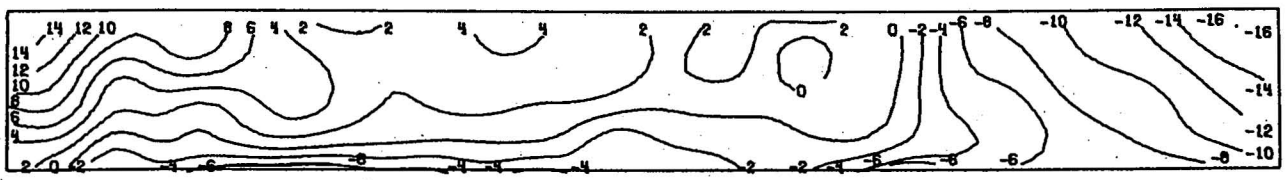

RELATIVE WIND SPEED, COMPONENT NORMAL TO FRONT

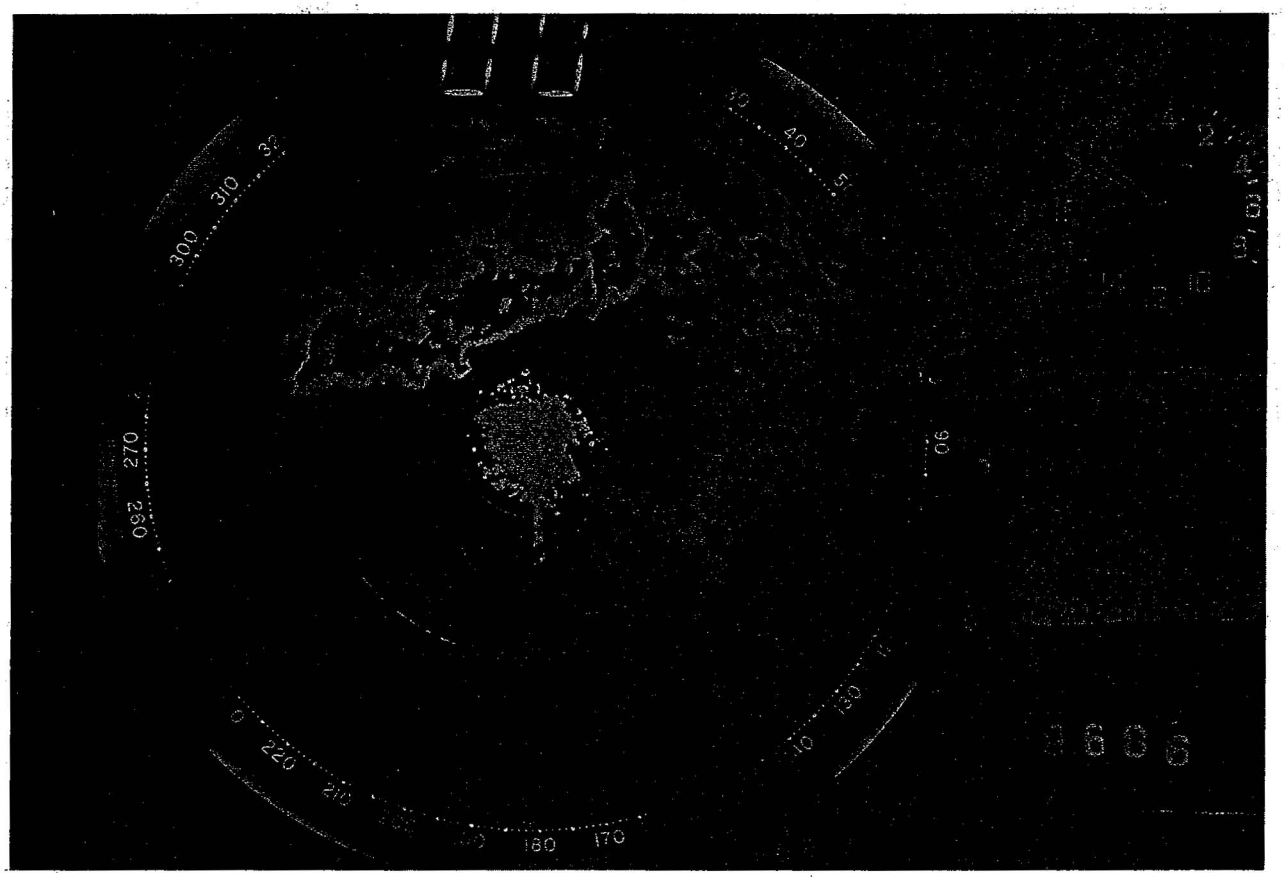

Case K

Date: 2 Jun 71

Time of gust front: 2121 CST

Speed: 12.4 m s^{-1}

Orientation: 70°

Speed and orientation error about 10%

Pressure jump: 6.6 mb 2052 - 2137 CST

Rain began: 2126 CST ended: 2300 CST

Total rainfall: 2.05 in

Maximum intensity: 8.40 in hr^{-1} 2133 CST

Remarks: Gusts to 100 mph recorded at Stillwater 30 n mi northeast of tower; funnel northwest of Guthrie, 20 n mi north to tower; funnel 5 n mi north Yukon, 15 n mi west of tower; winds to 70 mph in Oklahoma City; 3/4 inch hail at airport.

04JUN73 1759

1 KM

STREAMLINE ANALYSIS

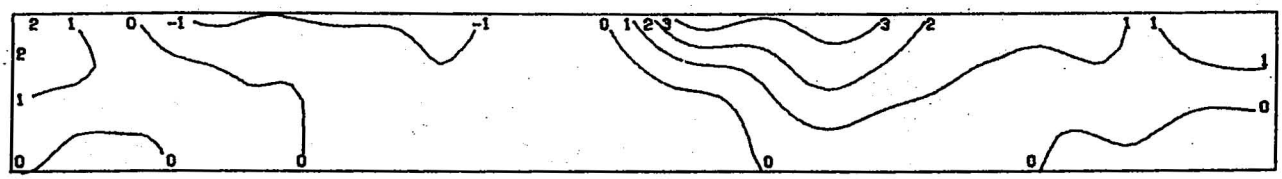

VERTICAL VELOCITY

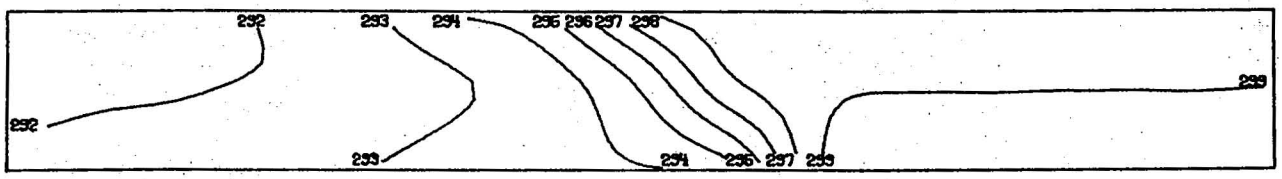

WET BULB POTENTIAL TEMPERATURE

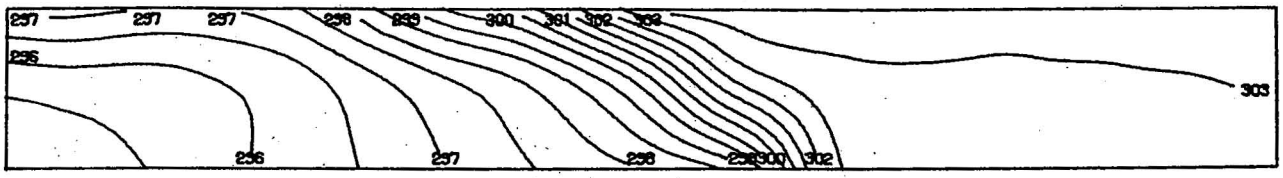

POTENTIAL TEMPERATURE

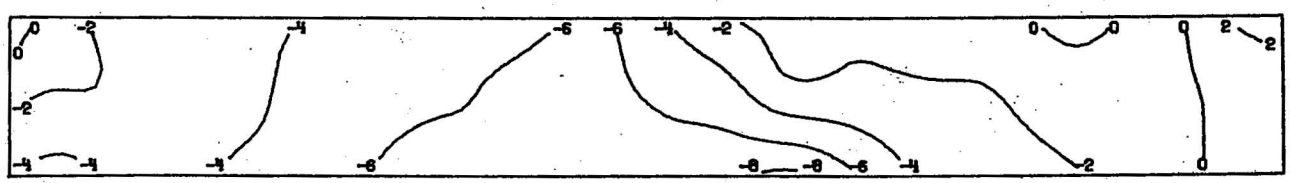

WIND SPEED PARALLEL TO FRONT

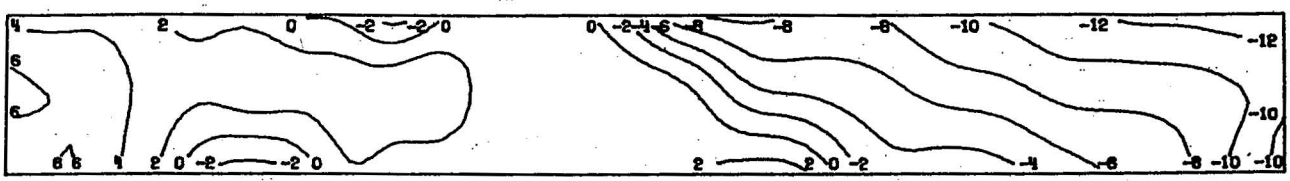

RELATIVE WIND SPEED, COMPONENT NORMAL TO FRONT

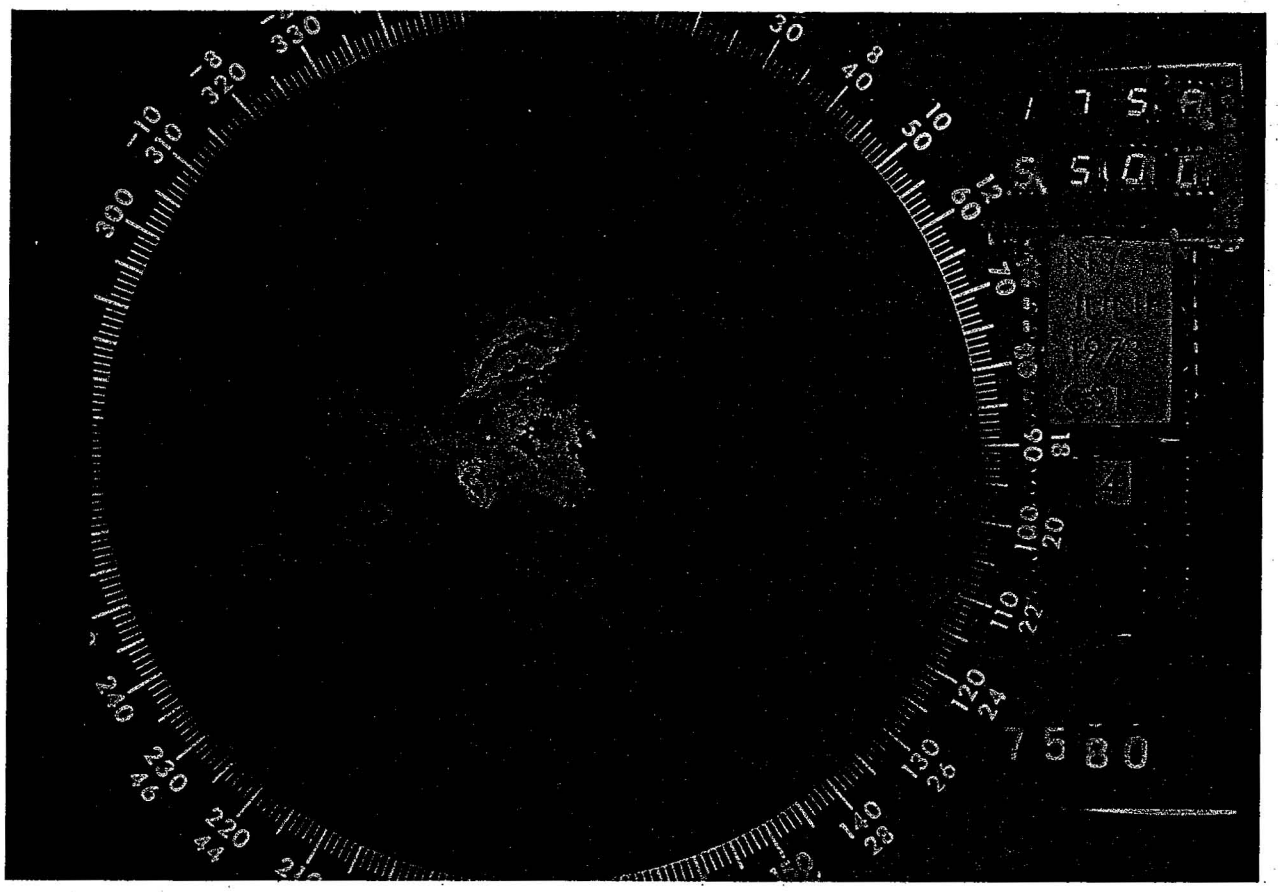

Case L

Date: 4 Jun 73

Time of gust front: 1803 CST

Speed: 5.5 m s^{-1}

Orientation: 60°

Speed and orientation error about 10%

Pressure jump: 2.8 mb 1721 - 1802 CST

Rain Began: 1834 CST ended: 2150 CST

Total rainfall: 1.52 in

Maximum intensity: 4.20 in hr^{-1} 1838 CST

Remarks: Hail damage 40 km northwest of tower; wind damage, funnel in Stillwater 60 km northeast of tower; baseball sized hail, 2 funnels in Moore 20 km south of tower; wind damage, funnel and tornado damage at Yukon 30 km west of tower; hail, wind damage and 2 funnels in Oklahoma City; hail, tornado observed at NSSL.

14JUN72 0211

1 KM

STREAMLINE ANALYSIS

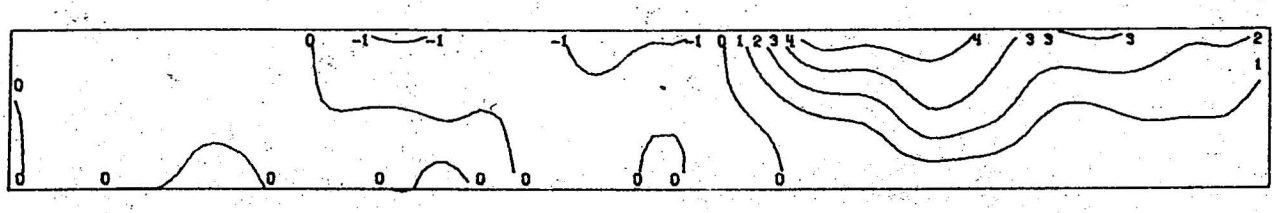

VERTICAL VELOCITY

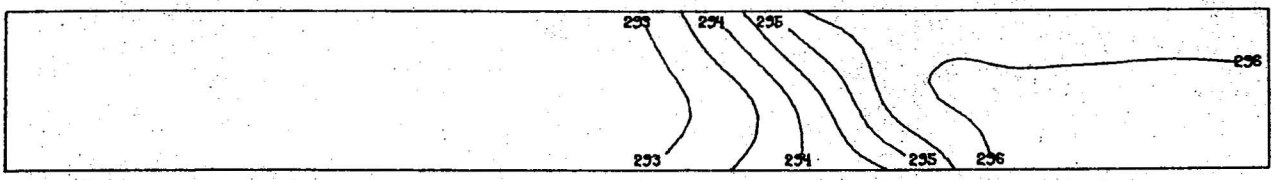

WET BULB POTENTIAL TEMPERATURE

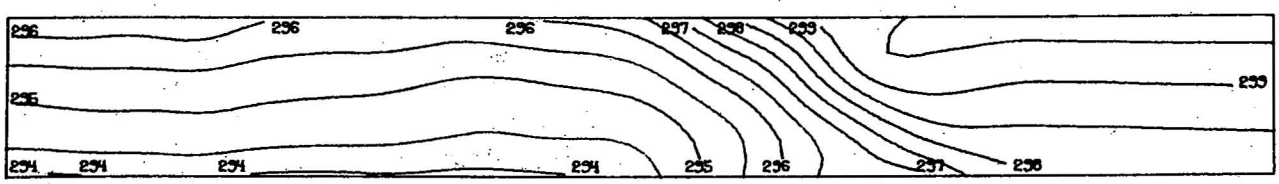

POTENTIAL TEMPERATURE

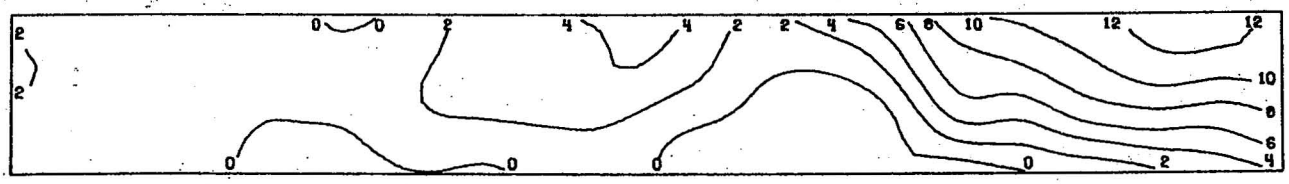

WIND SPEED PARALLEL TO FRONT

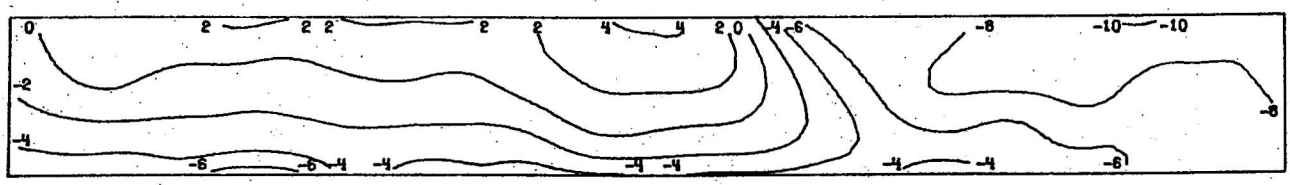

RELATIVE WIND SPEED, COMPONENT NORMAL TO FRONT

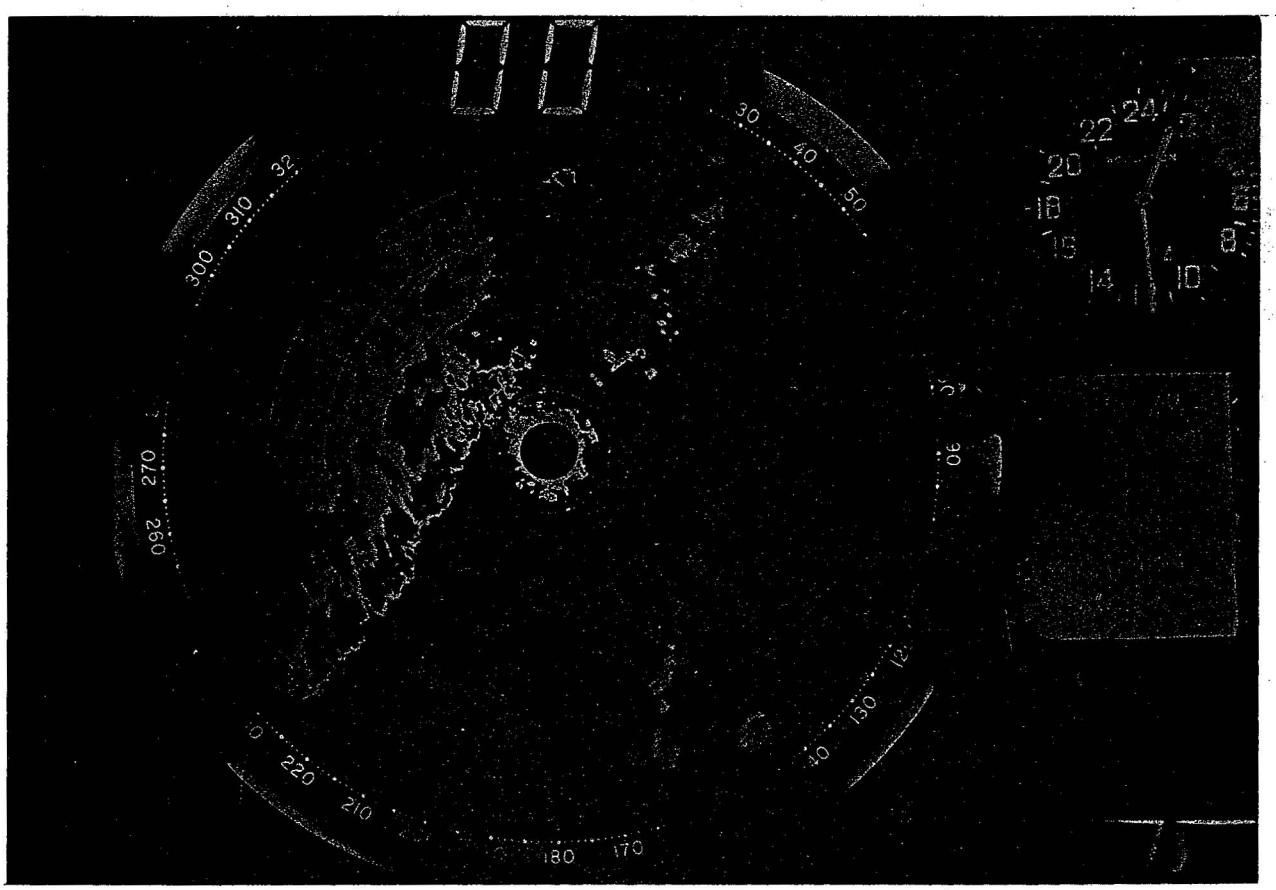

Case M

Date: 14 Jun 72

Time of gust front: 0215 CST

Speed: 9.6 m s^{-1}

Orientation: 0°

Speed and orientation error less than 10%

Pressure jump: 1.2 mb 0206 - 0227 CST

Rain began: 0217 CST ended: 0242 CST

Total rainfall: 0.34 in

Maximum intensity: 1.80 in hr^{-1} 0230 CST

Remarks: Shear-gravity waves observed after squall line (0310 CST); no severe weather.

12JUN71 0109

1 KM

STREAMLINE ANALYSIS

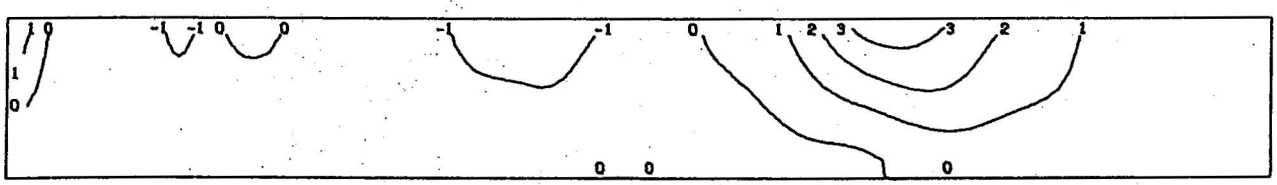

VERTICAL VELOCITY

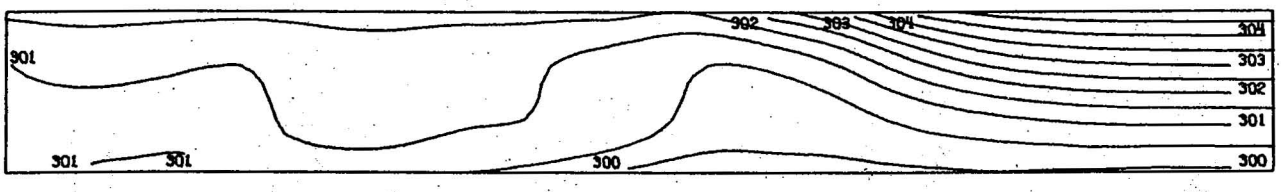

POTENTIAL TEMPERATURE

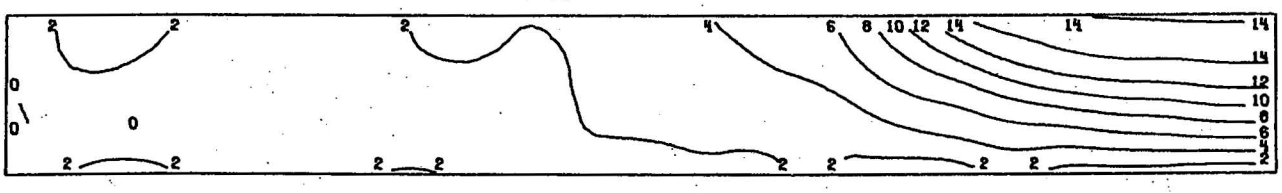

WIND SPEED PARALLEL TO FRONT

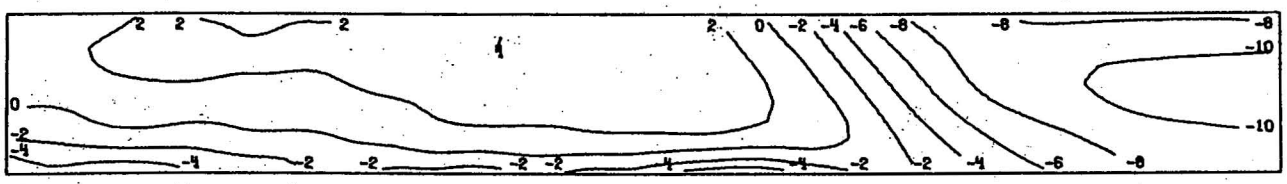

RELATIVE WIND SPEED, COMPONENT NORMAL TO FRONT

(No NSSL radar data available)

Case N

Date: 12 Jun 71

Time of gust front: 0113 CST

Speed: 8.0 m s^{-1}

Orientation: 0°

Speed and orientation error about 10%

Pressure jump: 1.2 mb 0107 - 0130 CST

Total rainfall: None

Remarks: No severe weather.

23MAY72 0436

1 KM

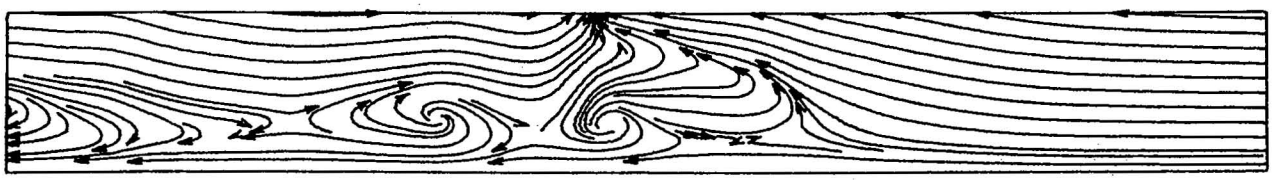

STREAMLINE ANALYSIS

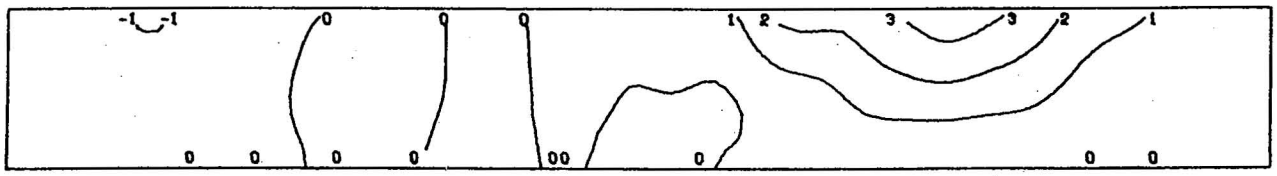

VERTICAL VELOCITY

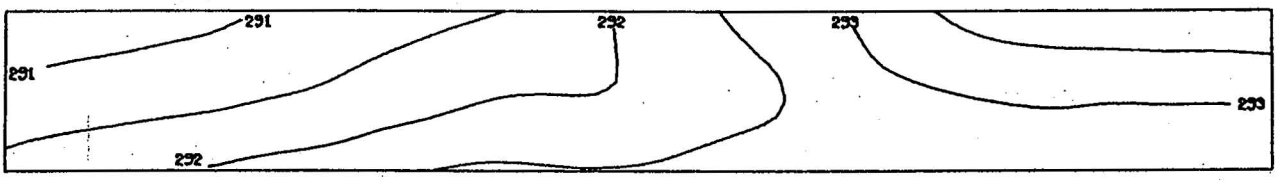

WET BULB POTENTIAL TEMPERATURE

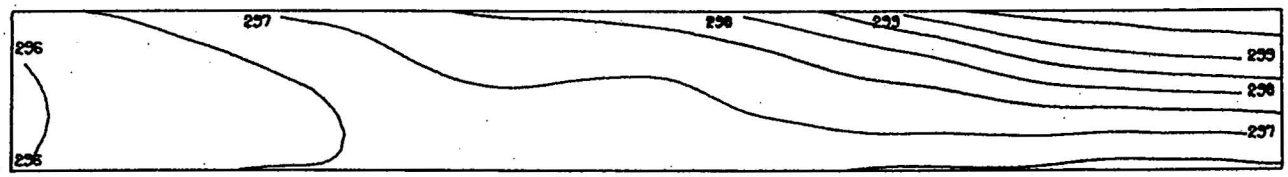

POTENTIAL TEMPERATURE

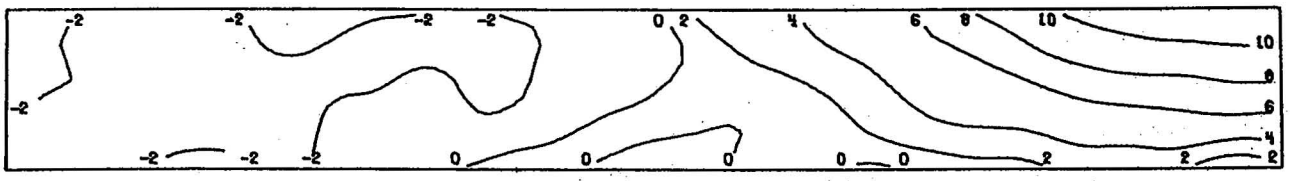

WIND SPEED PARALLEL TO FRONT

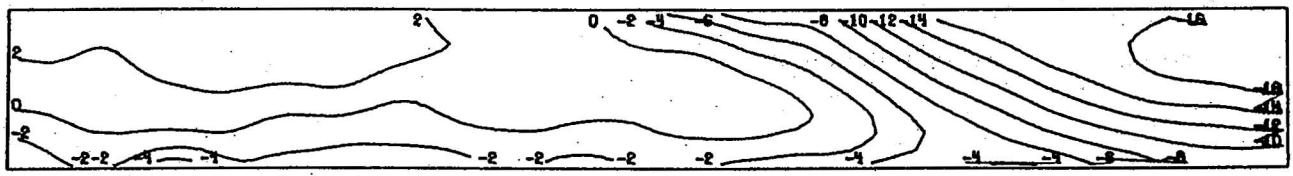

RELATIVE WIND SPEED, COMPONENT NORMAL TO FRONT

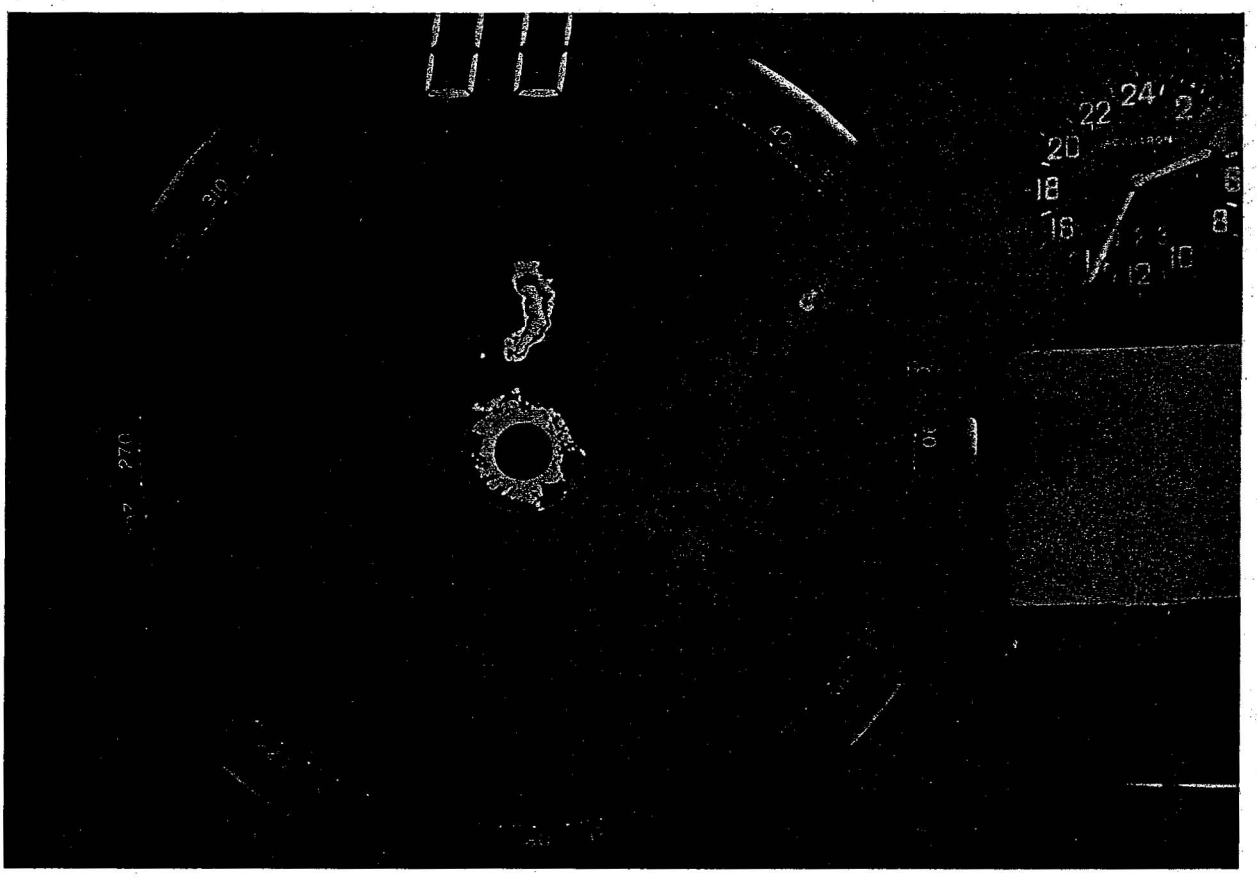

Case O

Date: 23 May 72

Time of gust front: 0440 CST

Speed: 11.4 m s^{-1}

Orientation: 50°

Speed and orientation error about 10%

Pressure jump: 1.9 mb 0430 - 0445 CST

Total rainfall: None

Remarks: No severe weather.

12MAY72 0020

1 KM

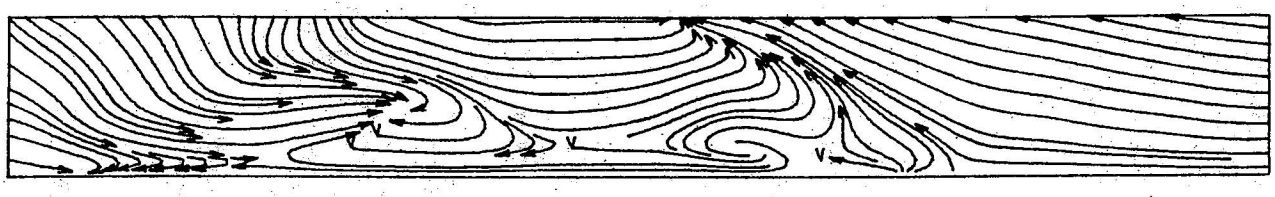

STREAMLINE ANALYSIS

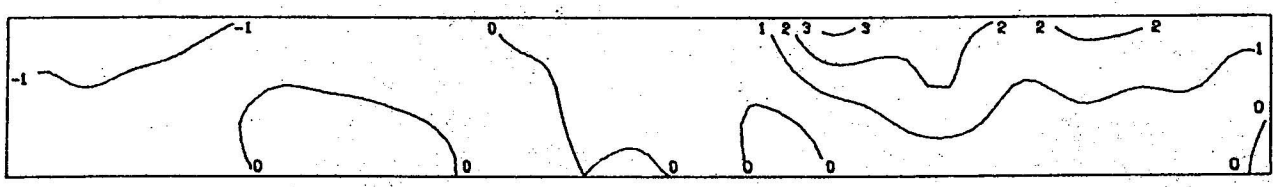

VERTICAL VELOCITY

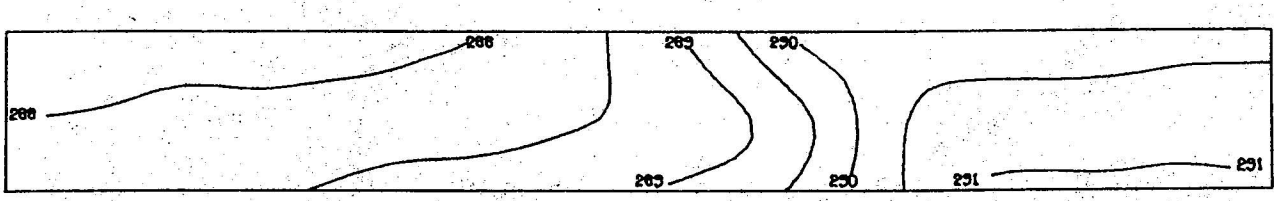

WET BULB POTENTIAL TEMPERATURE

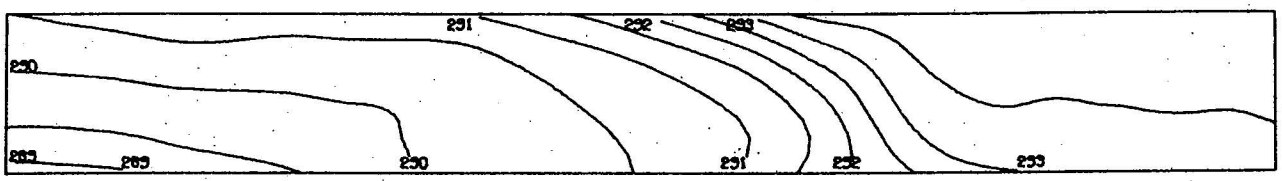

POTENTIAL TEMPERATURE

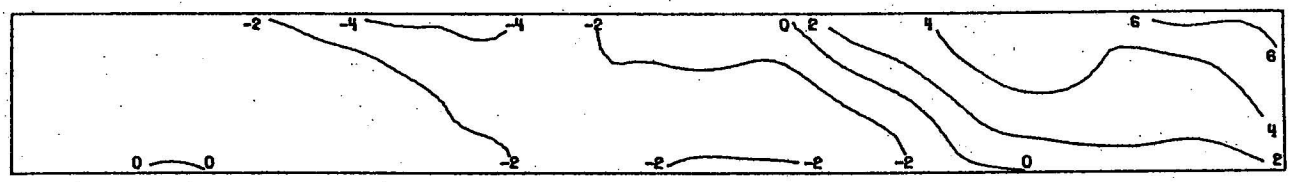

WIND SPEED PARALLEL TO FRONT

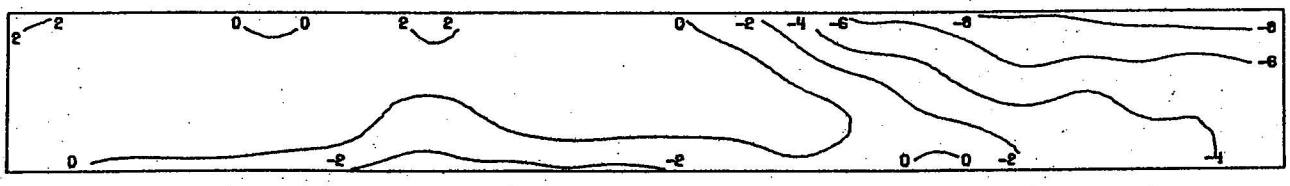

RELATIVE WIND SPEED, COMPONENT NORMAL TO FRONT

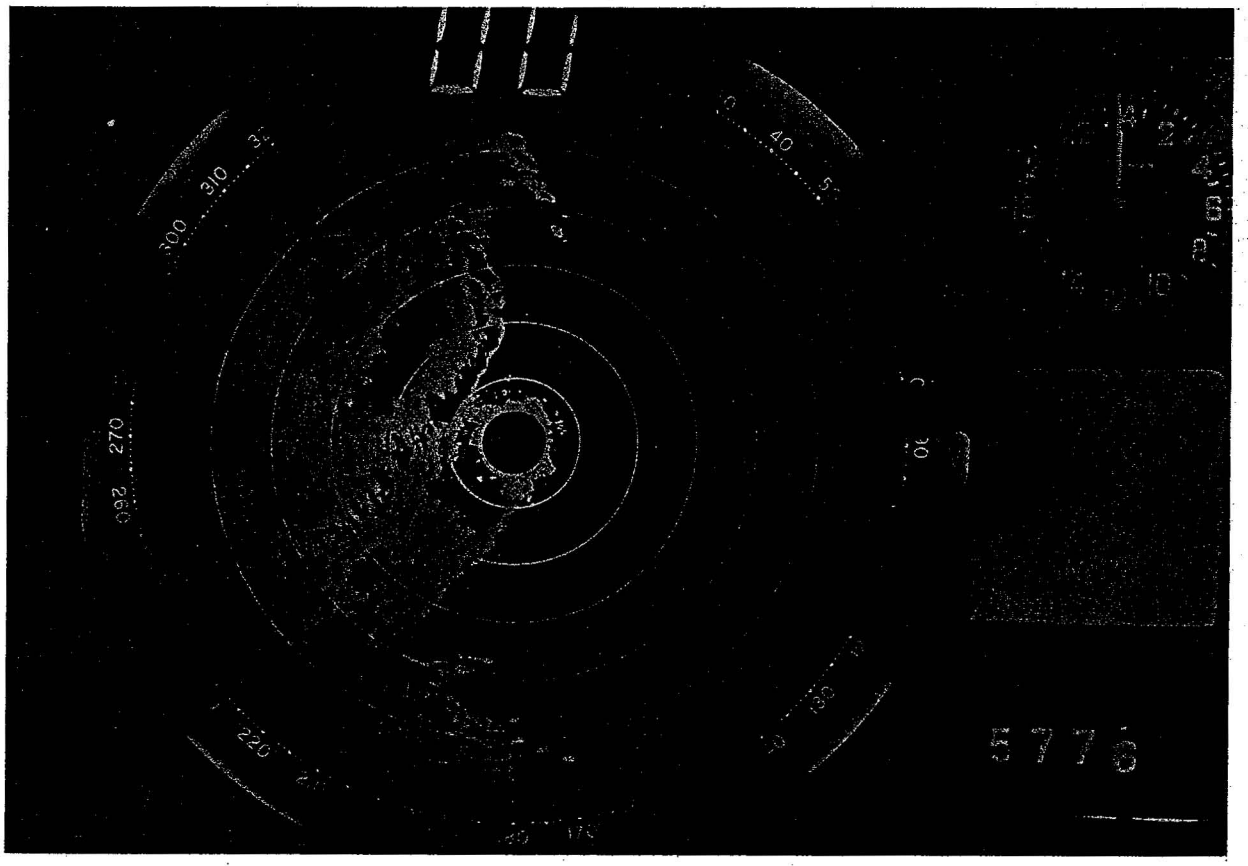

Case P

Date: 12 May 72 (date incorrect on time clock)

Time of gust front: 0024 CST

Speed: 6.9 m s^{-1}

Orientation: 10°

Speed and orientation error less than 10%

Pressure jump: 2.3 mb 2354 (11 May) - 0044 (12 May) CST

Rain began: 0030 CST ended: 0612 CST

Total rainfall: 2.07 in

Maximum intensity: 3.60 in hr^{-1} 0045 CST

Remarks: No severe weather.

23MAY74 1837

1 KM

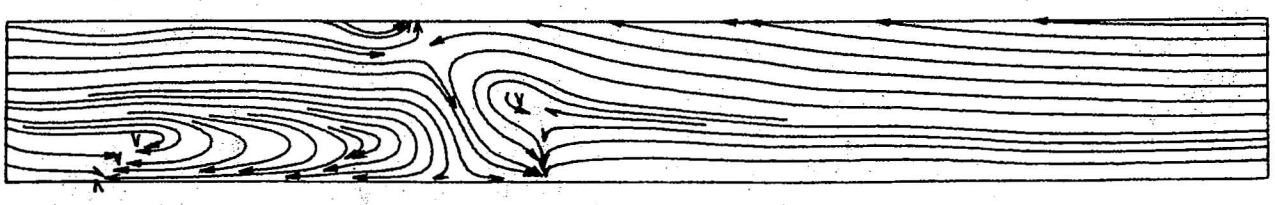

STREAMLINE ANALYSIS

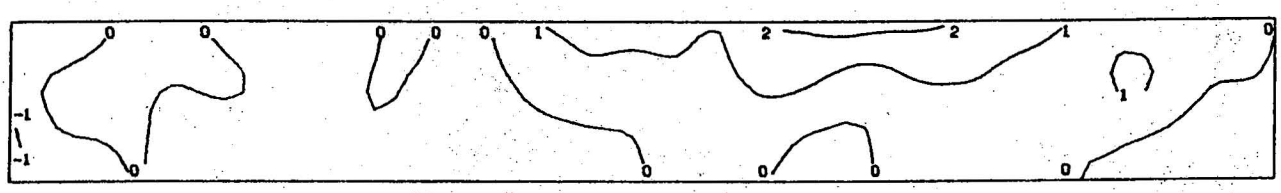

VERTICAL VELOCITY

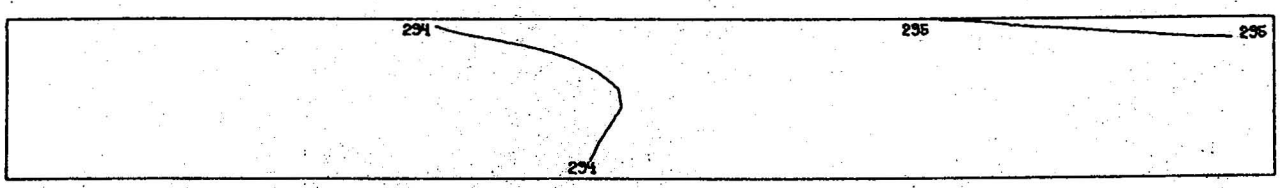

WET BULB POTENTIAL TEMPERATURE

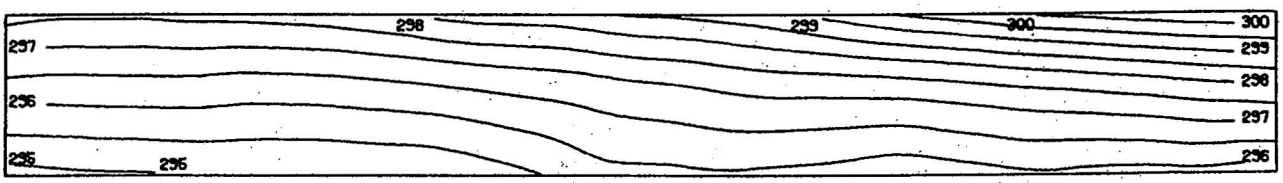

POTENTIAL TEMPERATURE

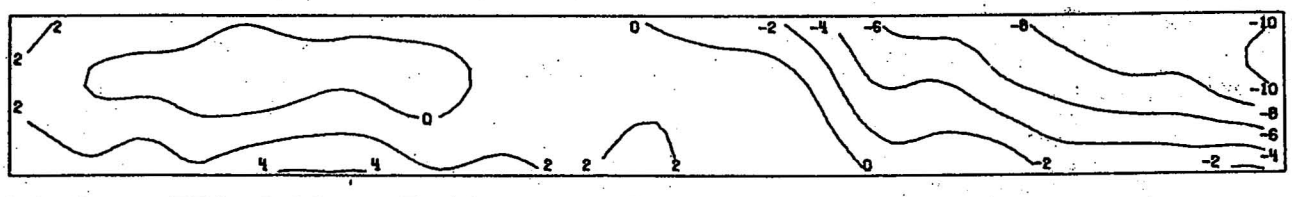

WIND SPEED PARALLEL TO FRONT

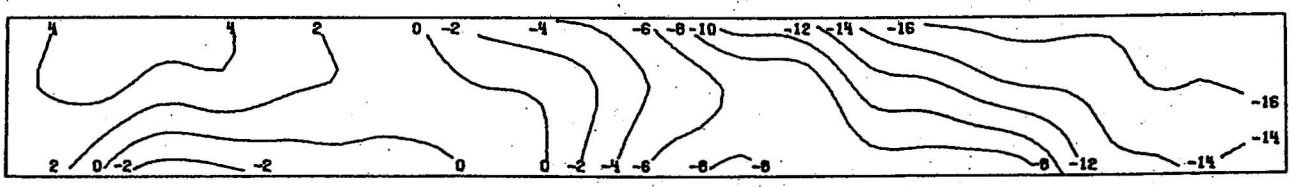

RELATIVE WIND SPEED, COMPONENT NORMAL TO FRONT

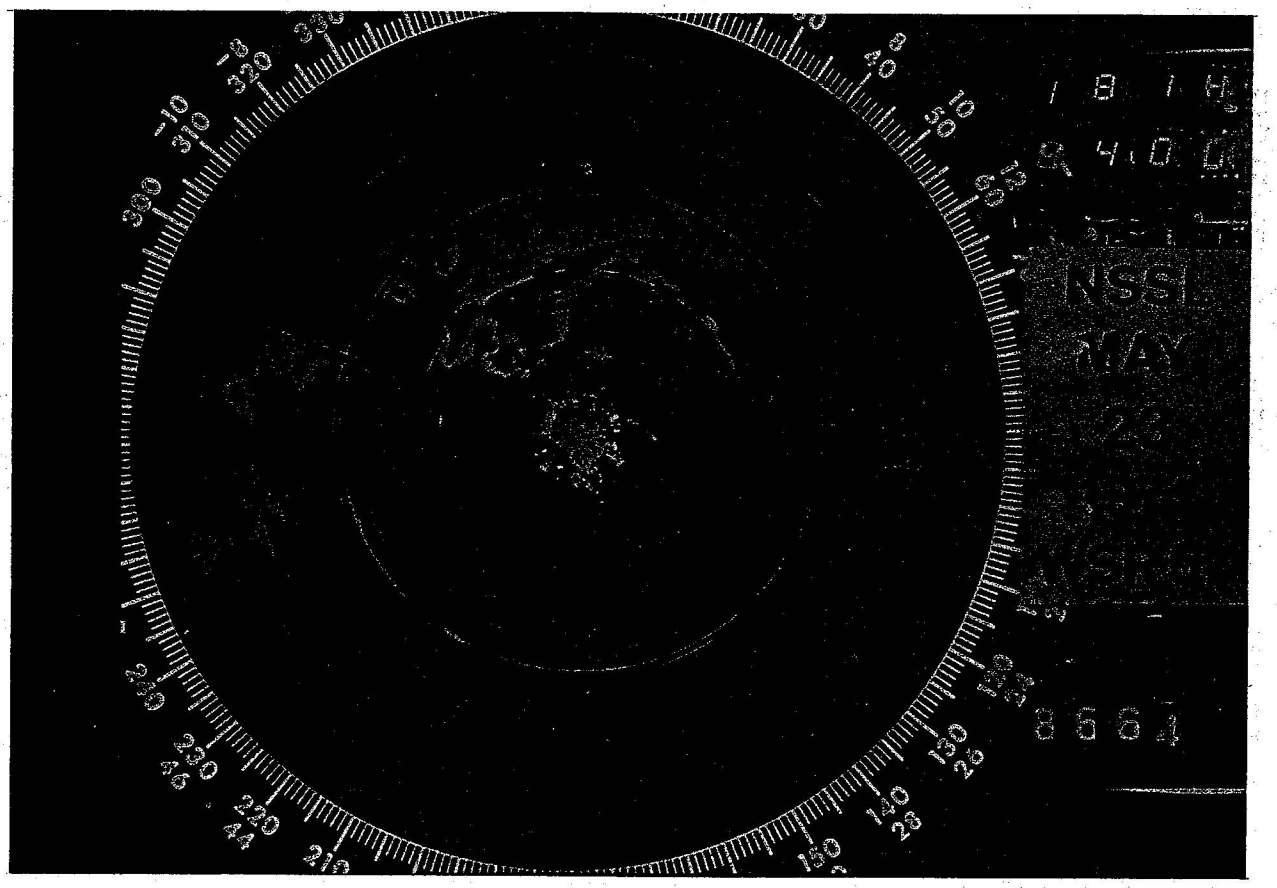

Case Q

Date: 23 May 74 B

Time of gust front: 1844 CST

Speed: 17.5 m s^{-1}

Orientation: 50°

Speed and orientation error about 10%

Pressure jump: 3.9 mb 1816 - 1844 CST

Rain began: 1836 CST ended: about 1920 CST

Total rainfall: 2.19 in

Maximum intensity: 7.20 in hr^{-1} 1859 CST

Remarks: Telemetry equipment failures produced several gaps in data; tornado 30 km west of tower, funnel at Tinker Air Force Base 21 km southeast of tower.

19APR72 1651

1 KM

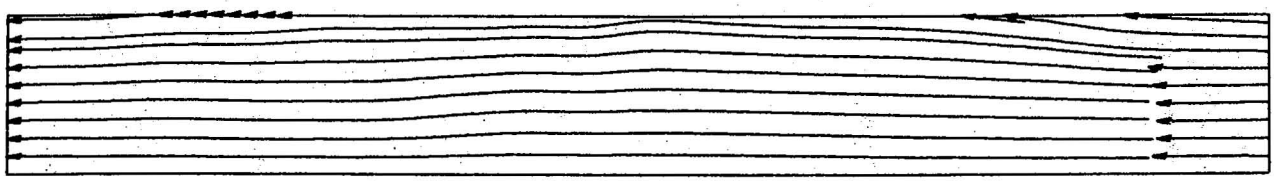

STREAMLINE ANALYSIS

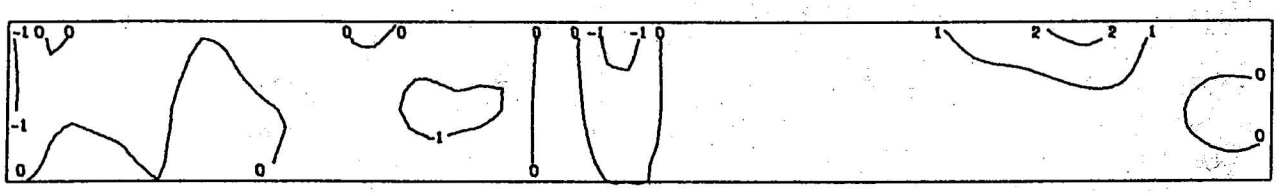

VERTICAL VELOCITY

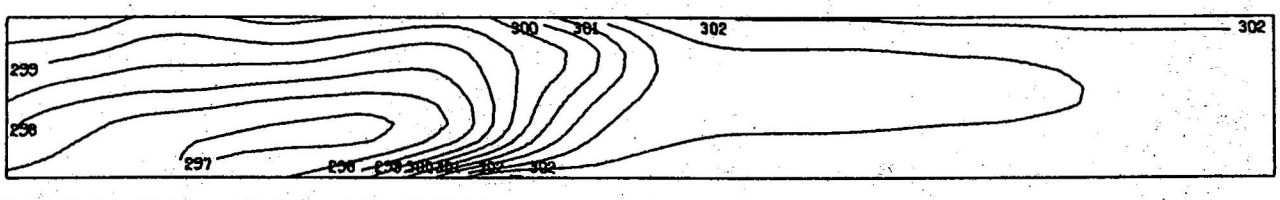

POTENTIAL TEMPERATURE

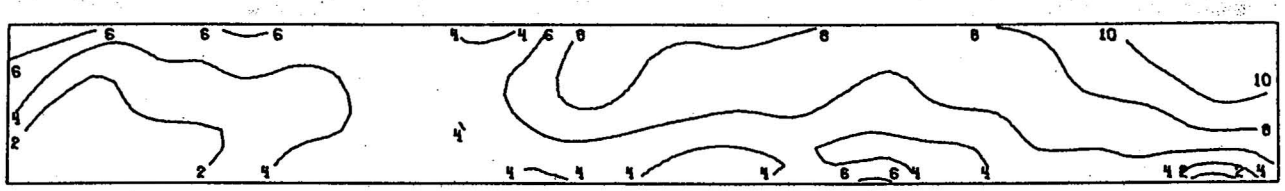

WIND SPEED PARALLEL TO FRONT

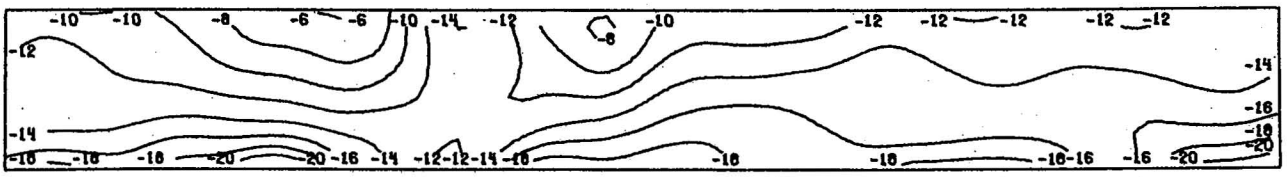

RELATIVE WIND SPEED, COMPONENT NORMAL TO FRONT

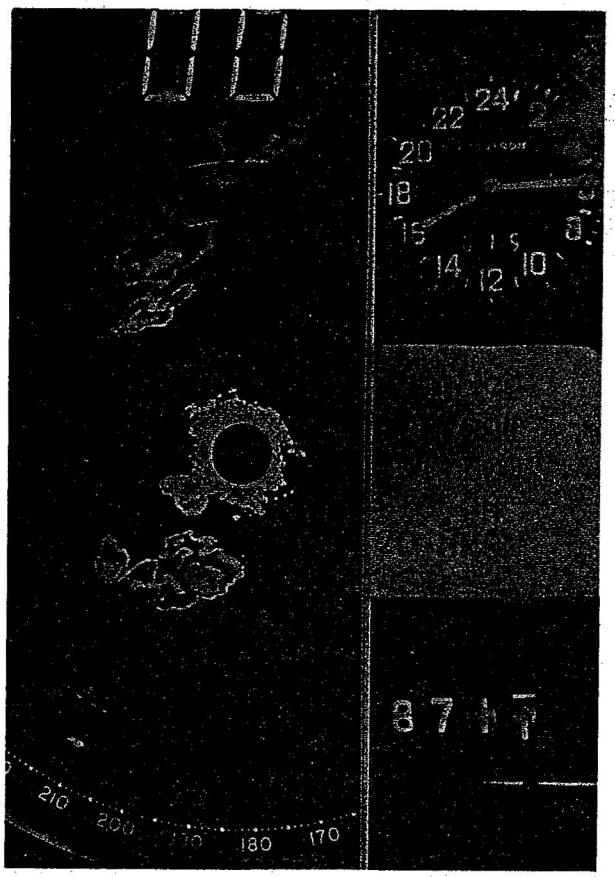

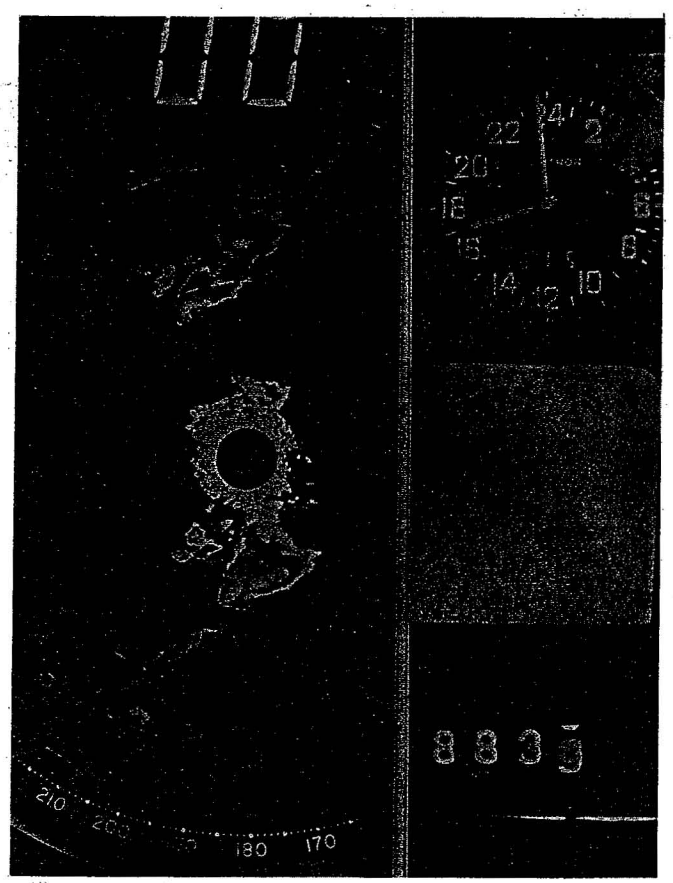

Case R

Date: 19 Apr 72

Time of gust front: 1656 CST

Speed: 25.0 m s^{-1}

Orientation: 290°

Speed and orientation error less than 10%

Pressure jump: 0.8 mb 1643 - 1651 CST

Total rainfall: Trace

Remarks: 1 inch hail at Oklahoma City; tornado associated with parent storm killed 5 people, 60 n mi south of tower.

26MAY71 1904

1 KM

STREAMLINE ANALYSIS

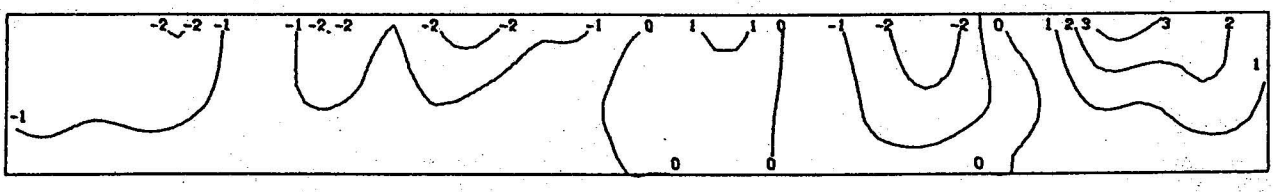

VERTICAL VELOCITY

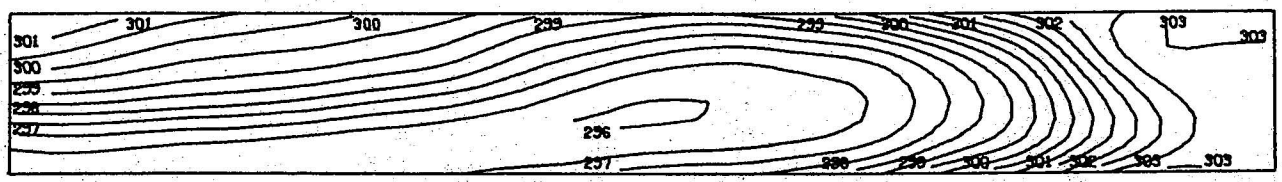

POTENTIAL TEMPERATURE

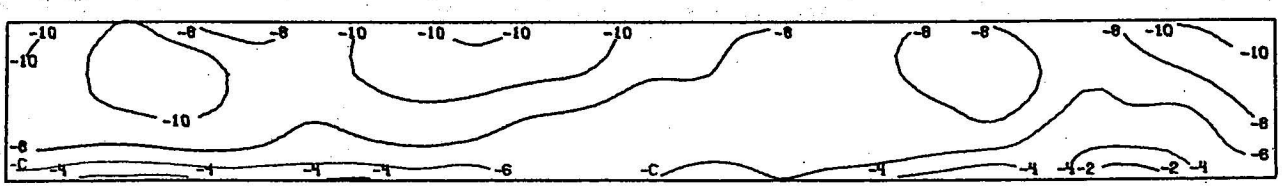

WIND SPEED PARALLEL TO FRONT

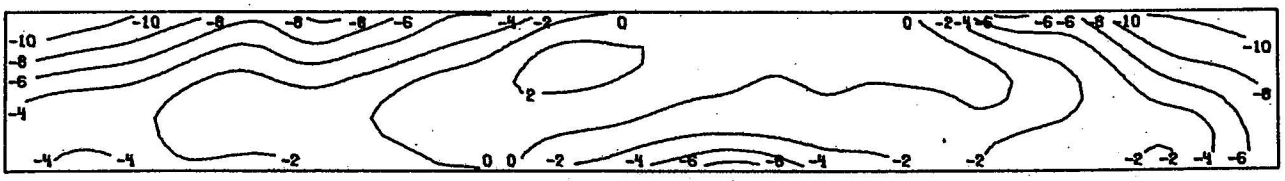

RELATIVE WIND SPEED, COMPONENT NORMAL TO FRONT

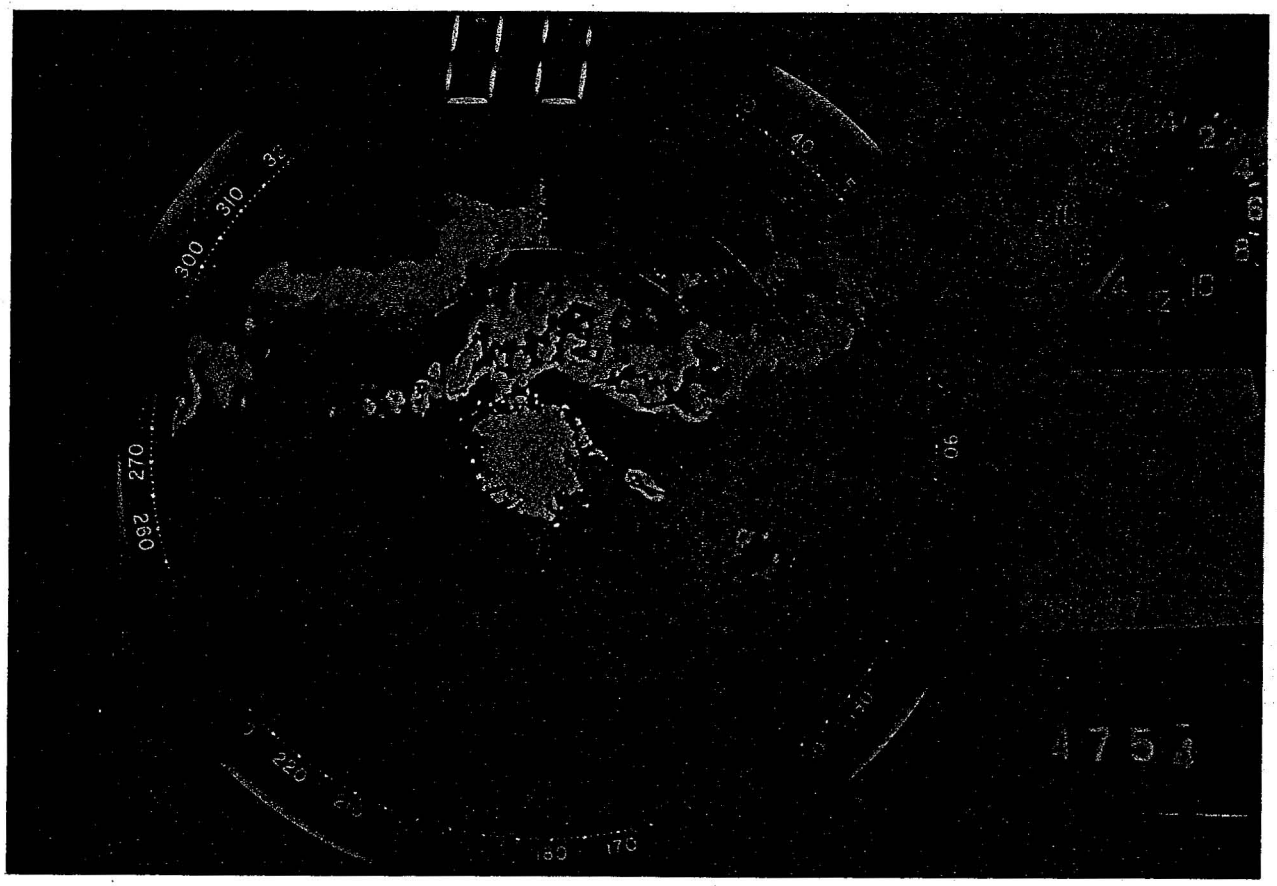

Case S

Date: 26 May 71

Time of gust front: 1906 CST

Speed: 11.0 m s^{-1}

Orientation: 120°

Speed and orientation error about 10%

Pressure jump: 1.9 mb 1819 - 1910 CST

Rain began: 1942 CST ended: unknown time

Total rainfall: 0.50 in

Maximum intensity: Unknown

Remarks: Winds up to 75 mph in Oklahoma City; funnel 10 n mi east southeast of tower; 1/4 inch hail in Oklahoma City; wind caused considerable damage in Norman, 20 n mi south of tower; tower records incomplete because of power failure.

21APR72 0029

1 KM

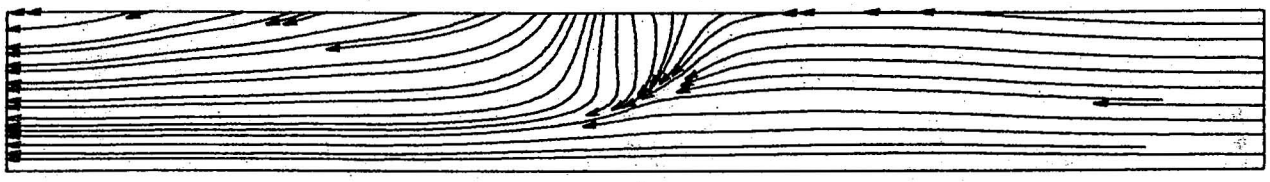

STREAMLINE ANALYSIS

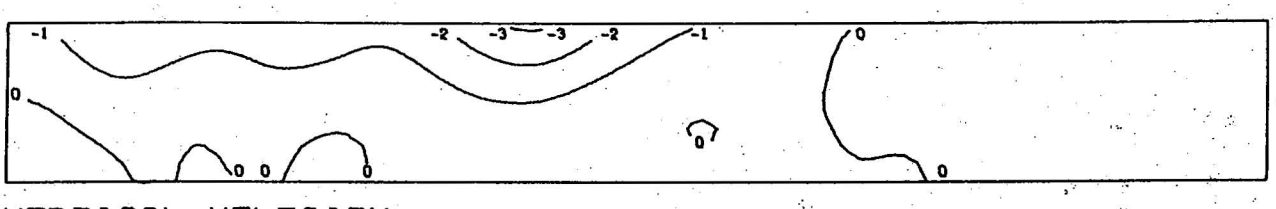

VERTICAL VELOCITY

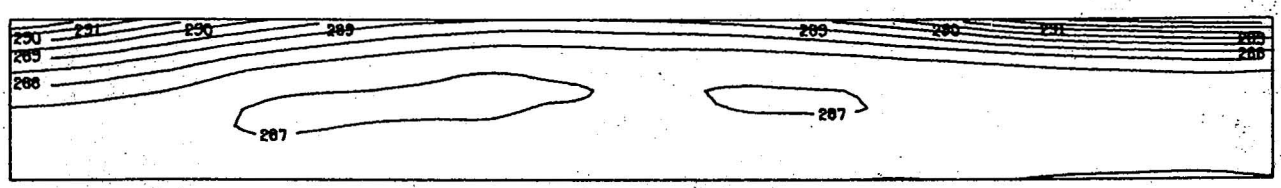

POTENTIAL TEMPERATURE

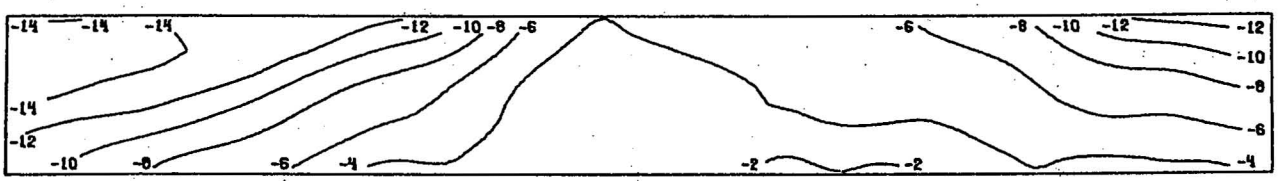

WIND SPEED PARALLEL TO FRONT

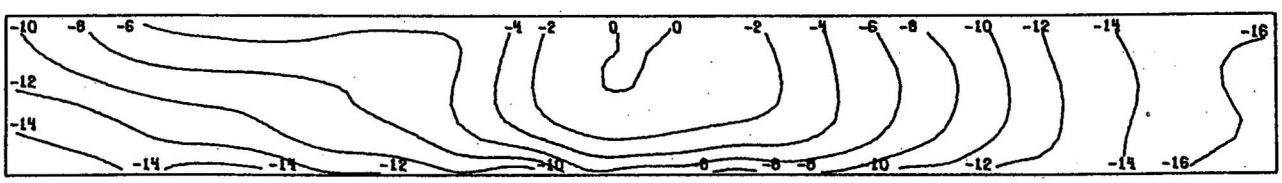

RELATIVE WIND SPEED, COMPONENT NORMAL TO FRONT

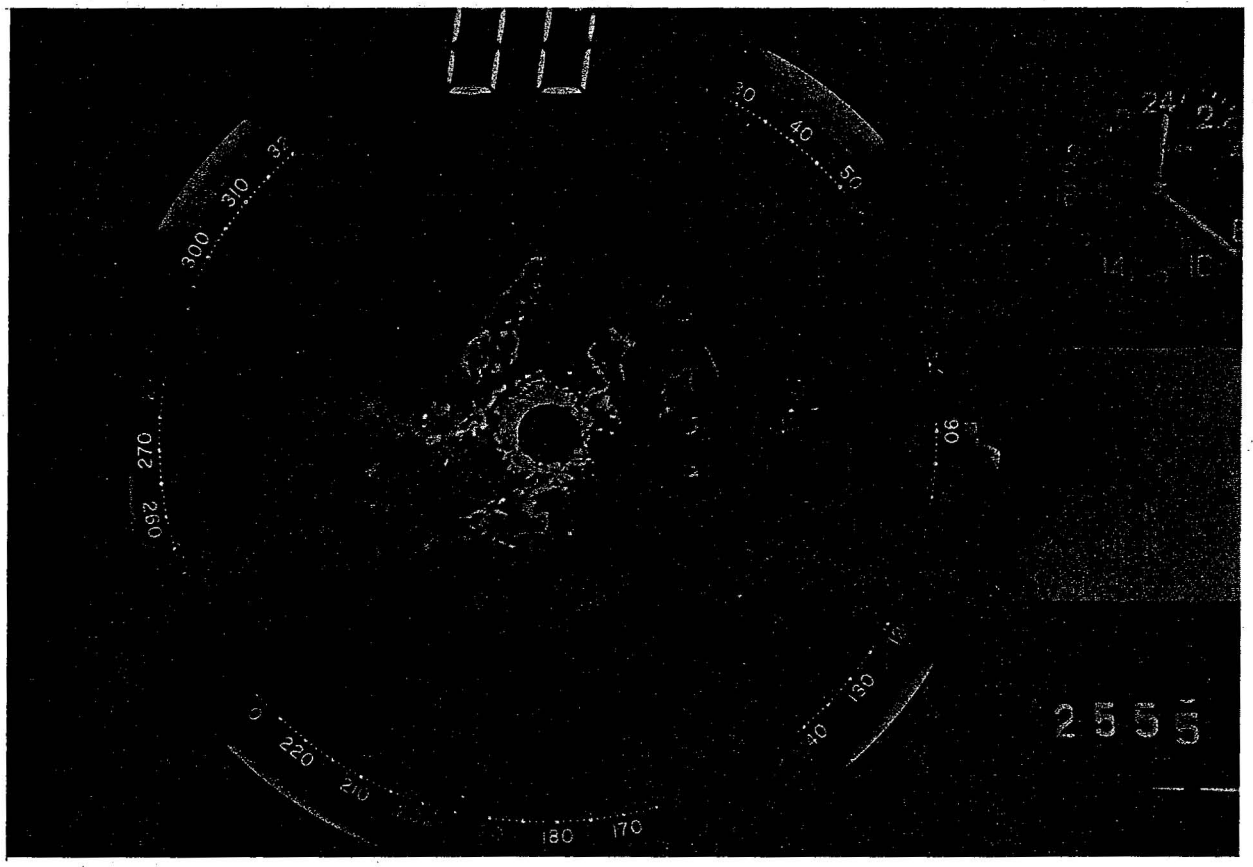

Case T

Date: 21 Apr 72

Time of gust front: 0034 CST

Speed: 19.9 m s^{-1}

Orientation: 5°

Speed and orientation error about 10%

Pressure jump: 3.0 mb 0028 - 0035 CST

Rain began: 0033 CST ended: 0044 CST

Total rainfall: 0.13 in

Maximum intensity: 2.40 in hr^{-1}

Remarks: No severe weather.

NATIONAL SEVERE STORMS LABORATORY

The NSSL Technical Memoranda, beginning with No. 28, continue the sequence established by the U. S. Weather Bureau National Severe Storms Project, Kansas City, Missouri. Numbers 1-22 were designated NSSP Reports. Numbers 23-27 were NSSL Reports, and 24-27 appeared as subseries of Weather Bureau Technical Notes. These reports are available from the National Technical Information Service, Operations Division, Springfield, Virginia 22151, for $3.00, and a microfiche version for $0.95. NTIS numbers are given below in parentheses.

No. 1 National Severe Storms Project Objectives and Basic Design. Staff, NSSP. March 1961. (PB-168207)

No. 2 The Development of Aircraft Investigations of Squall Lines from 1956-1960. B. B. Goddard. (PB-168208)

No. 3 Instability Lines and Their Environments as Shown by Aircraft Soundings and Quasi-Horizontal Traverses. D. T. Williams. February 1962. (PB-168209)

No. 4 On the Mechanics of the Tornado. J. R. Fulks. February 1962. (PB-168210)

No. 5 A Summary of Field Operations and Data Collection by the National Severe Storms Project in Spring 1961. J. T. Lee, March 1962. (PB-165095)

No. 6 Index to the NSSP Surface Network. T. Fujita. April 1962. (PB-168212)

No. 7 The Vertical Structure of Three Dry Lines as Revealed by Aircraft Traverses. E. L. McGuire. April 1962. (PB-168213)

No. 8 Radar Observations of a Tornado Thunderstorm in Vertical Section. Ralph J. Donaldson, Jr. April 1962. (PB-174859)

No. 9 Dynamics of Severe Convective Storms. Chester W. Newton. July 1962. (PB-163319)

No. 10 Some Measured Characteristics of Severe Storms Turbulence. Roy Steiner and Richard H. Rhyne. July 1962. (N62-16401)

No. 11 A Study of the Kinematic Properties of Certain Small-Scale Systems. D. T. Williams. October 1962. (PB-168216)

No. 12 Analysis of the Severe Weather Factor in Automatic Control of Air Route Traffic. W. Boynton Beckwith. December 1962. (PB-168217)

No. 13 500-Kc./Sec. Sferics Studies in Severe Storms. Douglas A. Kohl and John E. Miller. April 1963. (PB-168218)

No. 14 Field Operations of the National Severe Stoms Project in Spring 1962. L. D. Sanders. May 1963. (PB-168219)

No. 15 Penetrations of Thunderstorms by an Aircraft Flying at Supersonic Speeds. G. P. Roys. Radar Photographs and Gust Loads in Three Storms of 1961 Rough Rider. Paul W. J. Schumacher. May 1963. (PB-168220)

No. 16 Analysis of Selected Aircraft Data from NSSP Operations, 1962. T. Fujita. May 1963. (PB-168221)

No. 17 Analysis of Methods for Small-Scale Surface Network Data. D. T. Williams. August 1963. (PB-168222)

No. 18 The Thunderstorm Wake of May 4, 1961. D. T. Williams. August 1963. (PB-168223)

No. 19 Measurements by Aircraft of Condensed Water in Great Plains Thunderstorms. George P. Roys and Edwin Kessler. July 1966. (PB-173048)

No. 20 Field Operations of the National Severe Storms Project in Spring 1963. J. T. Lee, L. D. Sanders and D. T. Williams. January 1964. (PB-168224)

No. 21 On the Motion and Predictability of Convective Systems as Related to the Upper Winds in a Case of Small Turning of Wind with Height. James C. Fankhauser. January 1964. (PB168225)

No. 22 Movement and Development Patterns of Convective Storms and Forecasting the Probability of Storm Passage at a Given Location. Chester W. Newton and James C. Fankhauser. January 1964. (PB-168226)

No. 23 Purposes and Programs of the National Severe Storms Laboratory, Norman, Oklahoma. Edwin Kessler. December 1964. (PB-166675)

No. 24 Papers on Weather Radar, Atmospheric Turbulence, Sferics, and Data Processing. August 1965. (AD-621586)

No. 25 A Comparison of Kinematically Computed Precipitation with Observed Convective Rainfall. James C. Fankhauser. September 1965. (PB-168445).

No. 26 Probing Air Motion by Doppler Analysis of Radar Clear Air Returns. Roger M. Lhermitte. May 1966. (PB-170636)

No. 27 Statistical Properties of Radar Echo Patterns and the Radar Echo Process. Larry Armijo. May 1966. The Role of the Kutta-Joukowski Force in Cloud Systems with Circulation. J. L. Goldman. May 1966. (PB-170756)

No. 28 Movement and Predictablity of Radar Echoes. James Warren Wilson. November 1966. (PB-173972)

No. 29 Notes on Thunderstorm Motions, Heights, and Circulations. T. W. Harrold, W. T. Roach, and Kenneth E. Wilk. November 1966. (AD-644899)

No. 30 Turbulence in Clear Air Near Thunderstorms. Anne Burns, Terence W. Harrold, Jack Burnham, and Clifford S. Spavins. December 1966. (PB-173992)

No. 31 Study of a Left-Moving Thunderstorm of 23 April 1964. George R. Hammond. April 1967. (PB-174681)

No. 32 Thunderstorm Circulations and Turbulence from Aircraft and Radar Data. James C. Fankhauser and J. T. Lee. April 1967. (PB-174860)

No. 33 On the Continuity of Water Substance. Edwin Kessler. April 1967. (PB-175840)

No. 34 Note on the Probing Balloon Motion by Doppler Radar. Roger M. Lhermitte. July 1967. (PB-175930)

No. 35 A Theory for the Determination of Wind and Precipitation Velocities with Doppler Radars. Larry Armijo. August 1967. (PB-176376)

No. 36 A Preliminary Evaluation of the F-100 Rough Rider Turbulence Measurement System. U. O. Lappe. October 1967. (PB-177037)

No. 37 Preliminary Quantitative Analysis of Airborne Weather Radar. Lester P. Merritt. December 1967. (PB-177188)

No. 38 On the Source of Thunderstorm Rotation. Stanley L. Barnes. March 1968. (PB-178990)

No. 39 Thunderstorm - Environment Interactions Revealed by Chaff Trajectories in the Mid-Troposphere. James C. Fankhauser. June 1968. (PB-179659)

No. 40 Objective Detection and Correction of Errors in Radiosonde Data. Rex L. Inman. June 1968. (PB-180284)

No. 41 Structure and Movement of the Severe Thunderstorms of 3 April 1964 as Revealed from Radar and Surface Mesonetwork Data Analysis. Jess Charba and Yoshikazu Sasaki. October 1968. (PB-183310)

No. 42 A Rainfall Rate Sensor. Brian E. Morgan. November 1968. (PB-183979)

No. 43 Detection and Presentation of Severe Thunderstorms by Airborne and Ground-Based Radars: A Comparative Study. Kenneth E. Wilk, John K. Carter, and J. T. Dooley. February 1969. (PB-183572)

No. 44 A Study of a Severe Local Storm of 16 April 1967. George Thomas Haglund. May 1969. (PB-184-970)

No. 45 On the Relationship Between Horizontal Moisture Convergence and Convective Cloud Formation. Horace R. Hudson. March 1970. (PB-191720)

No. 46 Severe Thunderstorm Radar Echo Motion and Related Weather Events Hazardous to Aviation Operations. Peter A. Barclay and Kenneth E. Wilk. June 1970. (PB-192498)

No. 47 Evaluation of Roughness Lengths at the NSSL-WKY Meteorological Tower. Leslie D. Sanders and Allen H. Weber. August 1970. (PB-194587)

No. 48 Behavior of Winds in the Lowest 1500 ft in Central Oklahoma: June 1966 - May 1967. Kenneth C. Crawford and Horace R. Hudson. August 1970.

No. 49 Tornado Incidence Maps. Arnold Court. August 1970. (COM-71-00019)

No. 50 The Meteorologically Instrumented WKY-TV Tower Facility. John K. Carter. September 1970. (COM-71-00108)

No. 51 Papers on Operational Objective Analysis Schemes at the National Severe Storms Forecast Center. Rex L. Inman. November 1970. (COM-71-00136)

No. 52 The Exploration of Certain Features of Tornado Dynamics Using a Laboratory Model. Neil B. Ward. November 1970. (COM-71-00139)

No. 53 Rawinsonde Observation and Processing Techniques at the National Severe Storms Laboratory. Stanley L. Barnes, James H. Henderson and Robert J. Ketchum. April 1971. (COM-71-00707)

No. 54 Model of Precipitation and Vertical Air Currents. Edwin Kessler and William C. Bumgarner. June 1971. (COM-71-00911)

No. 55 The NSSL Surface Network and Observations of Hazardous Wind Gusts. Operations Staff. June 1971. (COM-71-00910)

No. 56 Pilot Chaff Project at the National Severe Storms Laboratory. Edward A. Jessup. November 1971. (COM-72-10106)

No. 57 Numerical Simulation of Convective Vortices. Robert P. Davies-Jones and Glenn T. Vickers. November 1971. (COM-72-10269)

No. 58 The Thermal Structure of the Lowest Half Kilometer in Central Oklahoma: December 9, 1966 - May 31, 1967. R. Craig Goff and Horace R. Hudson. July 1972. (COM-72-11281)

No. 59 Cloud-to-Ground Lightning Versus Radar Reflectivity in Oklahoma Thunderstorms. Gilbert D. Kinzer. September 1972. (COM-73-10050)

No. 60 Simulated Real Time Displays of Velocity Fields by Doppler Radar. L. D. Hennington and G. B. Walker. November 1972. (COM-73-10515)

No. 61 Gravity Current Model Applied to Analysis of Squall-Line Gust Front. Jess Charba. November 1972. (COM-73-10410)

No. 62 Mesoscale Objective Map Analysis Using Weighted Time-Series Observations. Stanley L. Barnes. March 1973. (COM-73-10781)

No. 63 Observations of Severe Storms on 26 and 28 April 1971. Charles L. Vlcek. April 1973. (COM-73-11200)

No. 64 Meteorological Radar Signal Intensity Estimation. Dale Sirmans and R. J. Doviak. September 1973. (COM-73-11923/2AS)

No. 65 Radiosonde Altitude Measurement Using Double Radiotheodolite Techniques. Stephan P. Nelson. September 1973. (COM-73-11934/9AS)

No. 66 The Motion and Morphology of the Dryline. Joseph T. Schaefer. September 1973. (COM-74-10043)

No. 67 Radar Rainfall Pattern Optimizing Technique. Edward A. Brandes. March 1974.

No. 68 The NSSL/WKY-TV Tower Data Collection Program: April - July 1972. R. Craig Goff and W. David Zittel. May 1974.

No. 69 Papers on Oklahoma Thunderstorms, April 29-30, 1970. Stanley L. Barnes, et al. May 1974.

No. 70 Life Cycle of Florida Key's Waterspouts. Joseph H. Golden. June 1974.

No. 71 Interaction of Two Convective Scales Within a Severe Thunderstorm: A Case Study and Thunderstorm Wake Vortex Structure and Thunderstorm Wake Vortex Structure and Aerodynamic Origin. Leslie R. Lemon. June 1974.

No. 72 Updraft Properties Deduced from Rawinsoundings. Robert P. Davies-Jones and James H. Henderson. October 1974.

No. 73 Severe Rainstorm at Enid, Oklahoma - October 10, 1973. L.P. Merritt, K.E. Wilk, and M.L. Weible. November 1974.

No. 74 Mesonetwork Array: Its Effect on Thunderstorm Flow Resolution. Stanley L. Barnes. October 1974.

☆ U.S. GOVERNMENT PRINTING OFFICE: 1975 — 677-347 / 1238 REGION NO. 8